ANALYSIS OF WAVELENGTH SELECTIVE DIRECTIONAL COUPLER WITH AIR GROOVES

BY

MOHAMMAD SAMEER

A Thesis Presented to the

DEANSHIP OF GRADUATE STUDIES

KING FAHD UNIVERSITY OF PETROLEUM & MINERALS

DHAHRAN, SAUDI ARABIA

In Partial Fulfillment of the
Requirements for the Degree of

MASTER OF SCIENCE

In

ELECTRICAL ENGINEERING

January 2008

KING FAHD UNIVERSITY OF PETROLEUM & MINERALS
DHAHRAN 31261, SAUDI ARABIA

DEANSHIP OF GRADUATE STUDIES

This thesis, written by **MOHAMMAD SAMEER** under the supervision of his thesis advisor and approved by his thesis committee, has been presented to and accepted by the Dean of Graduate Studies, in partial fulfillment of the requirements for the degree of

MASTER OF SCIENCE IN ELECTRICAL ENGINEERING

Thesis Committee

Dr. Hussain Ali Al-Jamid
(Committee Chairman)

Dr. Mohammad A. Al-Sunaidi
(Member)

Dr. Sheikh Sharif Iqbal
(Member)

Dr. Ibrahim O. Habiballah
Department Chairman

Dr. Mohammad S. Al-Homoud
Dean of Graduate Studies (A)

30
January 2008

Dedicated to my parents and my only brother

ACKNOWLEDGEMENTS

In the name of Allah, the Most Beneficent, the Most Merciful

All praises are due to Allah (SWT) for his kindest blessings on me and all the members of my family. I feel privileged to glorify his name in sincerest way through this small accomplishment. I ask for his blessings, mercy and forgiveness all the time. I sincerely ask him to accept this meager effort as an act of worship. May the peace and blessings of Allah be upon his dearest prophet, Muhammad (Peace Be upon Him).

I would like to express my profound gratitude and appreciation to my advisor Dr. Hussain Ali Al-Jamid, for his consistent help, guidance and attention that he devoted throughout the course of this work. He was always kind, understanding and sympathetic to me. His valuable suggestions and useful discussions made this work interesting to me. I am also very grateful to my thesis committee members Dr. Mohammad A. Al-Sunaidi and Dr. Sheikh Sharif Iqbal for their interest, cooperation and constructive advice.

I am grateful to the chairman of Electrical Engineering department, Dr. Ibrahim O. Habiballah for his kind help and cooperation. I would also like to thank our former chairman, Dr. Jamil M. Bakhashwain for his timely advice and guidance. I am also thankful to all faculty and staff members for their kind support and continuous cooperation. I would like to acknowledge the support and facilities provided by King Fahd University of Petroleum and Minerals.

I would like to thank my seniors and friends Fareed, Azhar, Omer, Feroz, Aamir, Iliyas, Rizwan Farooq, Waseem, Aamir Baig, Riyaz, Baber, Rauf, Misbhauddin, Mumtaz, Masihullah, Misbah, Kashif Paracha, Murtuza, Asad, Imran, Nizam, Mujahid, Asrar, Mujahid Faiz, Ashik, Shiraz and Sheharyar for their concern and help. I also acknowledge entire Indian Community at KFUPM for their friendly guidance and support; special thanks are due to all 903 building friends.

Last but not least, I humbly offer my sincere thanks to my parents for their incessant inspiration, blessings and prayers. I owe a lot to my brother Mohammad Zabir for his unrequited support, encouragement, and prayers.

(Mohammad Sameer)

CONTENTS

LIST OF TABLES

LIST OF FIGURES

ABSTRACT (English)

NAME: **MOHAMMAD SAMEER**

TITLE: **ANALYSIS OF WAVELENGTH SELECTIVE DIRECTIONAL COUPLER WITH AIR GROOVES.**

MAJOR: **ELECTRICAL ENGINEERING**

DATE: **JANUARY 2008**

In this thesis, we investigate both the coupling and filtering characteristics of a Wavelength Selective Directional Coupler with air grooves. The structure consists of two parallel and identical coupled slab waveguides with periodic air grooves in the space separating them. The spectral response of the structure is investigated by calculating the modal reflectivity and transmissivity. Optical power is launched in one of the four ports of this structure, and the output modal power at the remaining three ports as well as the reflected power at the input port is calculated. The influence of the length, width and the number of periodic air grooves on the coupling and filtering characteristics of the structure are highlighted.

The Method of Lines is used in the analysis of this device. The cascading and doubling approach is utilized for this purpose. A three point non-uniform mesh is used in the MOL. In addition, a perfectly matched layer (PML) is incorporated into the MOL to absorb the radiated field.

MASTER OF SCIENCE DEGREE

KING FAHD UNIVERSITY OF PETROLEUM AND MINERALS, DHAHRAN.

January 2008

ABSTRACT (Arabic)

ملخص الرسالة

الاسم: محمد سمير

عنوان الرسالة: تحليل مرشح طول موجة يتحوي على ثقوب هوائية

الدرجة: الماجستير في العلوم

تاريخ التخرج: 1- 2008م

في هذه الرسالة قمنا بتحليل مرشح طول موجة يحتوي ثقوب هوائية، كما تمت دراسة انتقال الطاقة الضوئية بين اطراف هذا المرشح. يتكون هذا المرشح من موجها موجة متطابقان و مترابطان مع تواجد صف دوري من الثقوب الهوائية في الفضاء الفاصل بين هذان الموجهان. تم حساب طيف الارتداد الطوري وطيف الارسال الطوري للاطراف الأربعة لهذا المرشح وذلك لدراسة تأثير عدد وأبعاد الثقوب الهوائية المستطيلة الشكل على الخواص المختلفة لهذا المرشح.

وقد قمنا باستخدام طريقة الخطوط في جميع الحسابات المتعلقة بهذا المرشح، وذلك تم استعمال شبكة حسابات متكونة من ثلاث نقاط غير متجاسنة البعد. كما تم استعمال طريقة التوصيل والمضاعفة لتسريع هذه الحسابات بالإضافة الى طبقة ماصة مثالية.

درجة الماجستير في العلوم
جامعة الملك فهد للبترول والمعادن
الظهران، المملكة العربية السعودية

CHAPTER 1

INTRODUCTION

1.1 Integrated Optics

Integrated optics [1-5] is a key technology in many advanced industrial applications. The optical communications industry has been the major driving force for progress in integrated optics to increase the reliability, compactness and reduce the cost of optical components used in optical fiber links. Other industries such as optical information storage, optical signal processing and optical computing also benefit from compact Integrated Optics modules in the manipulation of optical beams and signals.

In 1969 Stewart E. Miller [1-2] for the first time proposed that complex patterns of optical circuits, whose communication function might be somewhat analogous to that of lower frequency integrated circuits, could be fabricated in a sheet of dielectric using photolithographic techniques. The principal motivation for these studies is to combine miniaturized individual optical devices through waveguides or other means into a functional optical system incorporated into a small substrate. The resulting system is called an integrated optical circuit (IOC) by analogy with the semiconductor type of integrated circuit.

Technological innovations in long haul fiber optic communication networks have generated a need for these circuits. IOCs are more compact, have lower drive voltages,

lower optical losses and higher modulation frequency than discrete component systems and as a result they are finding increasing applications in a number of communication systems.

An IOC is a thin-film type optical circuit designed to have a certain desired function by integrating a source (such as a laser diode or LED), conventional opto-electronic devices (such as phase modulators, intensity modulators, switches, etc), interconnecting optical waveguide devices (such as directional couplers, beam splitters, polarizers, etc) and detectors (photodiodes) on a single substrate. It has advantages such as reduced weight, higher bandwidth and multiplexing capacity, low transmission loss, higher thermal and mechanical stabilities, low power consumption, etc.

The advantages of having an optical system in the form of an IOC rather than a conventional series of components include (apart from miniaturization) reduced sensitivity to air currents and to mechanical vibrations of the separately mounted parts, low driving voltages and high efficiency, robustness, and (potentially) reproducibility and economy.

As in the case of semiconductor integrated circuits, an IOC can be fabricated on the surface of one material (the substrate), in which case it is called monolithic IOC. If the substrate is doped or additional layers are deposited on the substrate it is called Hybrid IOC.

1.2 Optical Waveguide

The optical waveguide is a structure which can confine light waves and propagate them over a distance with considerably low transmission losses due to the phenomenon of total internal reflection (TIR). To obtain TIR, the refractive index of the cladding material is always kept lower than that of the waveguide core materials. TIR occurs when the angle of incidence between the propagation direction of the light and the normal or perpendicular direction, to the material interface is greater than the critical angle. The critical angle depends on the index of refraction of the materials, which may vary depending on the wavelength of the light.

Optical waveguides are used as components in IOCs or as the transmission medium in local and long haul optical communication systems. Optical waveguides can be classified according to their geometry (planar, strip, or fiber waveguides), mode structure (single-mode, multi-mode), refractive index distribution (step or gradient index) and material (glass, polymer, semiconductor).

A dielectric slab waveguide consists of three layers of materials with different dielectric constants, extending infinitely in the directions parallel to their interfaces. This structure confines electromagnetic waves only in the direction normal to the interface (planar). A rectangular optical waveguide is formed when the guiding layer of the slab waveguide is restricted in both transverse directions rather than just one (strip).

An optical fiber is typically a circular cross-section dielectric waveguide

consisting of a dielectric material surrounded by another dielectric material with a lower refractive index. Optical fibers are most commonly made from silica glass, however other glass materials are used for certain applications and plastic optical fibers can be used for short-distance applications.

Due to the theoretical and computational difficulties in modeling waveguides having a two dimensional confinement, this thesis work will only address waveguide structures with one dimensional confinement.

1.3 Directional Coupler

The capability of transferring power between waveguides is a key function for many applications of integrated optics. Directional couplers are considered building blocks of several systems, especially in optical networks, where they are deployed in devices such as switches, modulators and filters. The standard directional coupler is made of two identical waveguides that are coupled through the evanescent field and its qualitative behavior is well described by coupled mode theory [6]. Such a component exhibits considerable wavelength dependency which often limits the operational bandwidth. Directional Couplers can be of many types. For example there are diffusion couplers, area-splitting couplers, beam splitter couplers and Wavelength Selective couplers.

In its simplest form, a directional coupler consists of two parallel and identical dielectric waveguides in close proximity as shown in Figure 1.1. In this case, the power

coupling is based on optical interference between the evanescent fields of the two waveguides, such that a light wave launched into one of the waveguides can be coupled completely into the other waveguide.

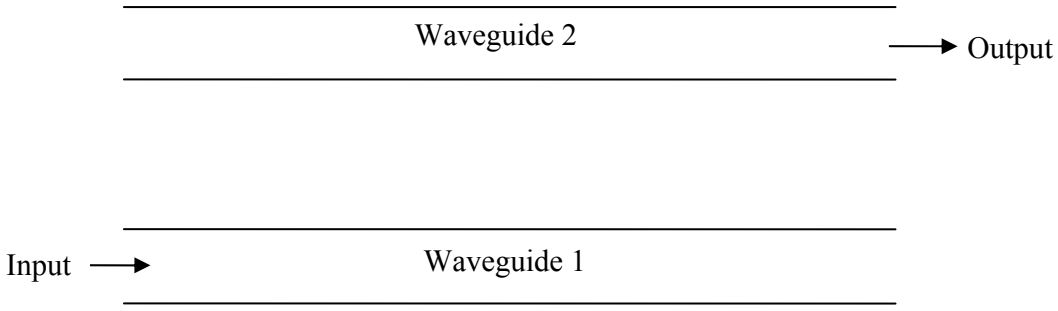

Figure1.1 Directional Coupler

1.4 Grating Assisted Directional Coupler

Periodic patterns i.e. gratings fabricated in optical waveguide structures are one of the most important elements of optical integrated circuits. They have many applications to functional devices for optical wave control. The operation of devices based on gratings depends on electromagnetic wave coupling through phase matching of different propagating modes by the grating region. Each period causes a small reflection of the field and the total reflected field is the phasor sum of the individual reflections.

Researchers have analyzed various Grating Assisted Directional Coupler (GADC) structures, as shown in Figure 1.2, to achieve good coupling efficiency and to investigate

their filtering characteristics. A number of methods have been proposed in the literature [7-15] for the analysis and design of GADC. These devices are fundamental guided-wave components for many applications including contra-directional coupling, distributed Bragg reflector sources, optical wavelength filtering and wavelength-division multiplexing (WDM).

A new approach [7] to the analysis and design of GADC was proposed, in which the power exchange between the waveguides has been maximized through phase matching of two power-orthogonal modes of the parallel waveguide coupler. A GADC with a periodic grating fabricated on the lower slab waveguide shown in Figure 1.2(a) was examined.

A rigorous leaky mode propagation method [10] has been used to investigate the influence of the grating period and grating index profile on the design of GADC shown in Figure 1.2(b). The Floquet–Bloch theorem [11] is used to develop a theory for GADC shown in figure 1.2(c) which predicts the coupled power and coupling lengths and is applicable to lossy waveguides.

A novel dual grating-assisted directional coupler (DGADC) shown in Figure 1.2(d) for coupling an optical fiber with a thin semiconductor waveguide has been developed [12]. Wavelength Selective Directional Coupling (WSDC) that utilized a grating for wavelength selectivity has been reported in the literature [16-19].

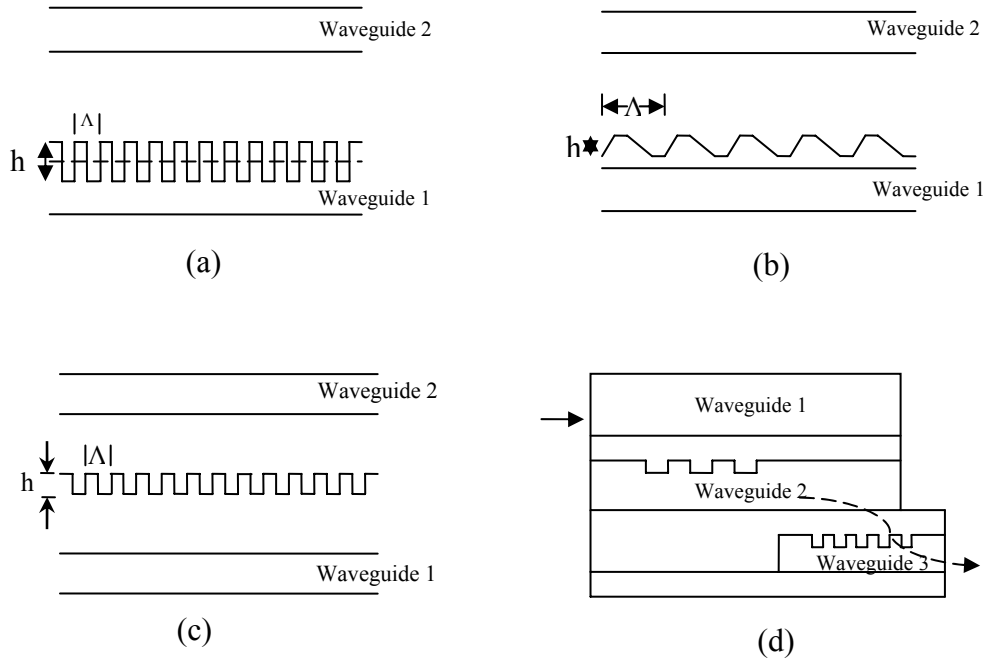

Figure 1.2 GADCs with different types of gratings

A Bragg grating-assisted WDM filter for the three-wavelength multiplexing on a planar-light wave-circuit platform was designed [19]. The 1310-nm and 1550-nm lights were designed to be separated after passing the directional coupler by a half-cycle and a full-cycle coupling actions with losses of 0.07 and 0.19 dB, respectively. The 1492-nm light was reflected back by a Bragg grating fabricated on the directional coupler and its loss was less than 2.0 dB.

Figure 1.3 shows the structure of a three-wavelength multiplexer and its design parameters. L_c is the coupling length of the directional coupler. L_1 is the location

parameter for the Bragg grating and L_g is the length of the Bragg grating.

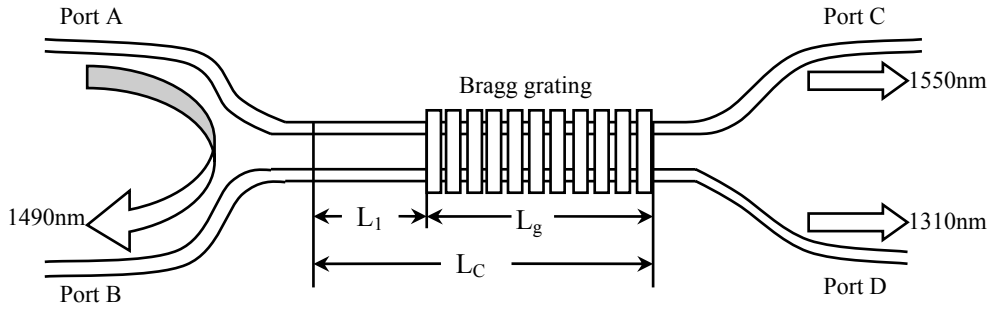

Figure 1.3 Schematic view of a Bragg grating-assisted WDM filter

1.5 Proposed Thesis Work

In this thesis work, a Wavelength Selective Directional Coupler (WSDC) which consists of two identical and parallel slab waveguides with periodic air grooves is analyzed. A schematic diagram of the structure is shown in Figure 1.4(a). The coupling and wavelength filtering characteristics of the device are investigated by varying the air groove length (L), width (w) and number of periods.

Moreover, a variation of the structure shown in Figure 1.4(a) is also analyzed. This other structure consists of two rows of periodic air grooves as shown in Figure 1.4(b).

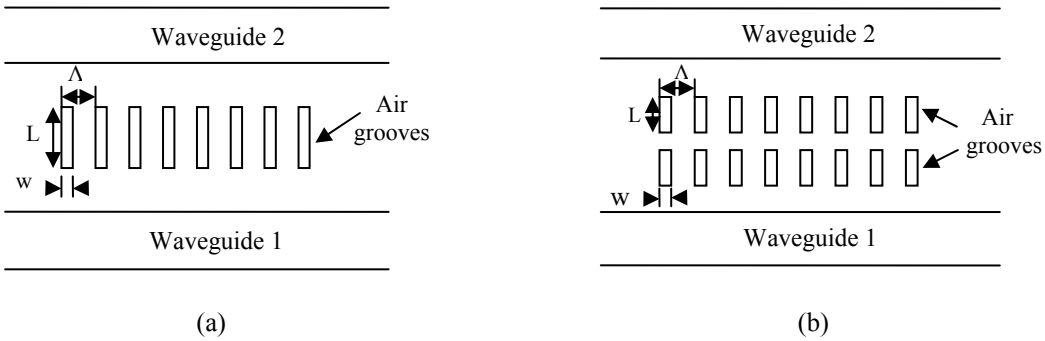

Figure 1.4 WSDC with air grooves

For these structures the spectral modal reflectivity and transmissivity are calculated. Optical power is launched in one of the four ports of the WSDC, and the output power at the remaining three ports as well as the reflected power at the input port is calculated. These calculations are repeated for a number of wavelengths in order to obtain the spectral response of the device.

1.6 Computational Numerical Techniques

Several real-world electromagnetic problems like scattering, radiation, wave guiding etc, are not analytically calculable, for the multitude of irregular geometries designed and used. The inability to derive closed form solutions of Maxwell's equations under various boundary conditions is overcome by computational numerical techniques.

Computational numerical techniques can be used to model the domain generally by discretizing the space in terms of grids, and then solve Maxwell's equations at each

point in the grid. Naturally, such discretization of the computational space consumes computer memory. Large scale electromagnetic problems place computational limitations in terms of memory space, and CPU time on the computer.

Several numerical tools have been developed to model waveguide structures. Among these methods are the Beam Propagation Method (BPM) [20, 21], the Finite Difference Time Domain (FDTD) Method [21-24], the Collection Method [25], Finite-element method (FEM) [26-29] and the Method of Lines (MOL) [30-32].

The Beam Propagation Method solves the Helmholtz equation under conditions of a time-harmonic wave. It is an approximation technique for simulating the propagation of light in slowly varying optical waveguides. It is typically used only in solving for intensity and modes within shaped (bent, tapered, terminated) waveguide structures, as opposed to scattering problems. It is not suited as a generalized solution to Maxwell equations, like the FDTD or FEM methods.

The FDTD method belongs to the general class of grid-based differential time-domain numerical modeling methods. The time-dependent Maxwell's equations (in partial differential form) are discretized using central-difference approximations to the space and time partial derivatives. Since FDTD requires that the entire computational domain be gridded, and the grid spatial discretization must be sufficiently fine to resolve both the smallest electromagnetic wavelength and the smallest geometrical feature in the model, very large computational domains should be developed, which results in very long

solution times.

The MOL is an established and efficient numerical procedure for the analysis of a variety of optical waveguides. Its advantages stem from the fact that it is an analytical approach that leads to comparatively small numerical effort and high accuracy. The MOL is a technique for solving partial differential equations (PDEs) where all but one dimension is discretized. The resulting semi-discrete problem is a set of ordinary differential equations (ODEs).

The MOL can easily account for the backward and forward fields as well as its ability to account for optical structures with large refractive index contrast. This is an important advantage leading to the popularity of the MOL in analyzing longitudinally inhomogeneous structures.

The MOL is used in this thesis to analyze the Wavelength Selective Directional Coupler (WSDC) structures with periodic air grooves.

1.7 Thesis Organization

The introductory chapter, chapter one, gives an overview of this thesis. In this chapter integrated optics, IOCs, optical waveguides, directional couplers, Grating Assisted Directional Couplers and Wavelength Selective Directional Couplers are introduced. The computational numerical techniques used for modeling optical waveguide structures are also discussed in brief.

Chapter two introduces the MOL, which is used in the solution of the wave equation in this thesis. It describes how the eigenpairs are utilized in the field calculations. Chapter three details the analysis of longitudinal waveguide discontinuities using MOL. The cascading and doubling algorithm is introduced in this chapter which is then applied for the simulation of multiple longitudinal waveguide discontinuities. Chapter four introduces the directional coupler. The basic principles of coupling between two identical and parallel waveguides are discussed here using the MOL.

Chapter five is devoted to the analysis of the Wavelength Selective Directional Coupler structures with a single and two rows of periodic air grooves placed exactly in between the two identical and parallel waveguides. The coupling and wavelength filtering characteristics of the devices are investigated by varying the air groove length (L), width (w) and number of periods. For these structures the spectral modal reflectivity and transmissivity are calculated.

The final chapter, chapter six, concludes this thesis work and recommends future extensions.

CHAPTER 2

THE METHOD OF LINES

2.1 Introduction

The Method of Lines (MOL) [30-32] is well established as a versatile numerical tool for the analysis of electromagnetic field problems in microwave, millimeter wave and integrated optical circuits. Due to its semi-analytical approach the computational effort is much less than other methods applied to the same problem. The MOL is a technique for solving partial differential equations (PDEs) where all but one dimension is discretized. The resulting semi-discrete problem is a set of ordinary differential equations (ODEs) which can be solved analytically. This results in a higher numerical accuracy, less computational time, and smaller memory requirements as compared to fully-discretizing finite-difference techniques. This method can account for the backward-reflected field from longitudinally inhomogeneous structures such as waveguide junctions and gratings. It has been applied to model integrated optical and microwave waveguide problems for stationary analysis, as well as for beam propagation [33].

The MOL usually involves partitioning the solution region into layers, discretization of the differential equation in one coordinate direction, transformation to obtain ordinary differential equations, inverse transformation and introduction of the boundary conditions and finally the solution of the equations. This numerical method has been applied to numerous planer longitudinal uniform and nonuniform waveguide

problems, including guided wave problems with abrupt longitudinal discontinuities [34-37] and multiple longitudinal discontinuities [38-42].

This procedure guarantees a high numerical precision with an acceptable computational expense. It relies on the computation of eigenvalues and eigenvectors of the system matrix. If the size of the problem is exceedingly large, the computation of the eigenpairs becomes computationally demanding.

2.2 Basic MOL Algorithm

The planar dielectric slab waveguide is one of the simplest waveguide structures. A simple planar three-layer step-index dielectric slab waveguide structure is illustrated in Figure 2.1. The core refractive index is assumed to be n_1, the superstrate and substrate with refractive indices n_2 and n_3 respectively where $n_1 > (n_2, n_3)$ so that total internal reflection takes place at the top and bottom interfaces. In the case of $n_2 = n_3$ it is called a symmetric slab waveguide.

The symmetric slab waveguide is assumed to be uniform and infinitely long along the y-axis so as to simplify the computational analysis. This allows us to assume that the field does not vary along the y-axis and hence $\frac{\partial}{\partial y} = 0$.

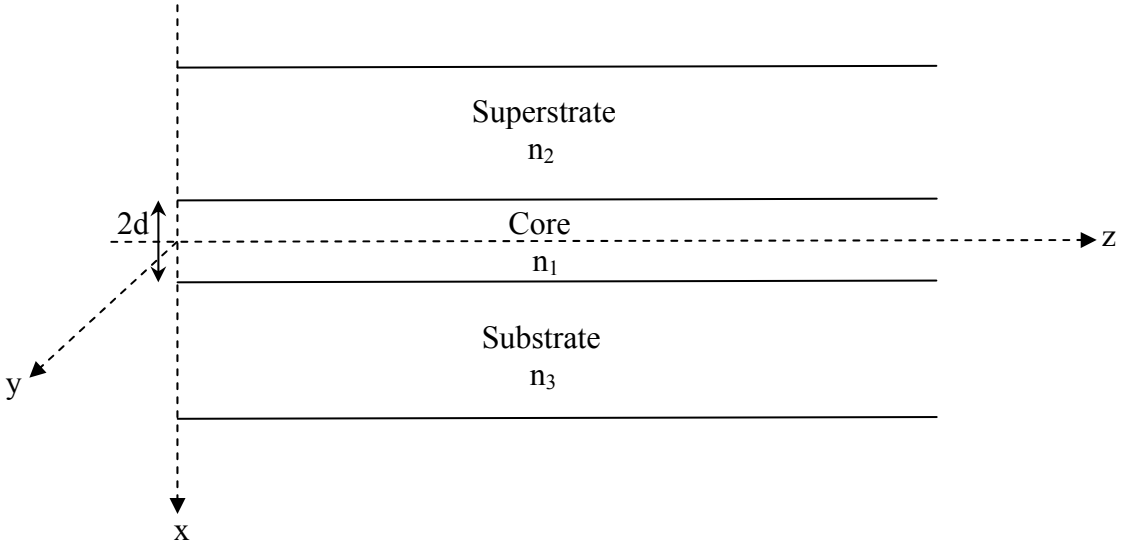

Figure 2.1 A planar dielectric slab waveguide

In this case, the electromagnetic field is governed by a two dimensional wave equation. In order to solve the resulting two dimensional wave equation using the MOL, the field is discretized in one dimension and solved analytically in the direction of wave propagation [43, 44]. The waveguide's interfaces are kept parallel to the direction of propagation (z-axis) and the field is discretized along the transverse direction (x-axis) as shown in Figure 2.2. The field will be calculated along these discretized lines called the mesh lines. The structure is considered to be bounded by an electric wall where $E_y = 0$ or a magnetic wall where $H_y = 0$ in order to terminate the problem space [45, 46].

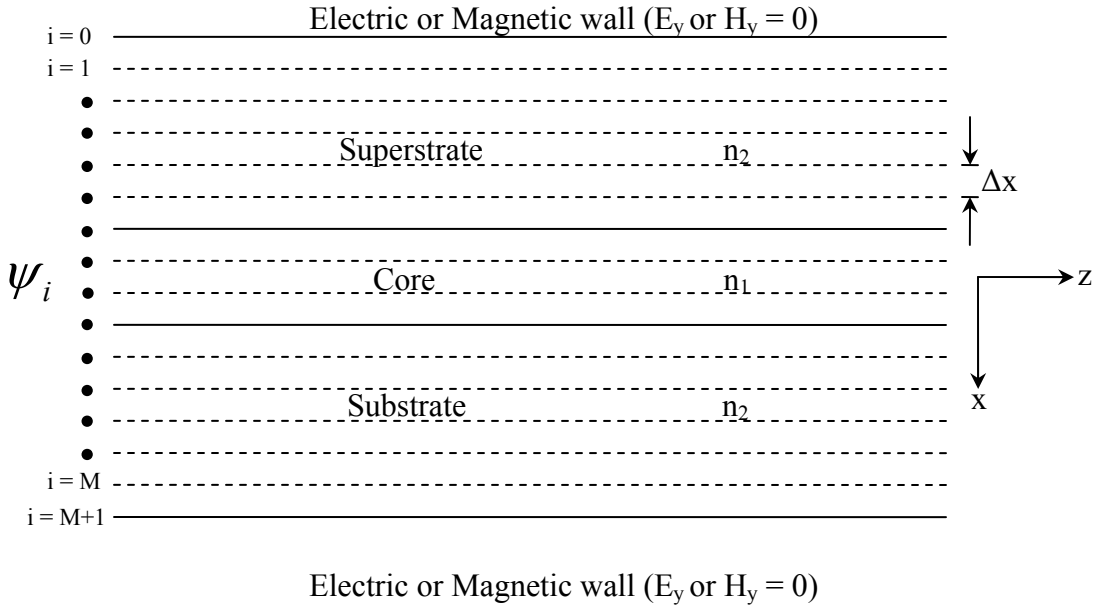

Figure 2.2 Discretization of space in the x-direction

Non-uniform discretization will be used in this thesis in order to decrease the total number of mesh lines and hence reduce the computational effort. The number of mesh lines is decreased by increasing the mesh size (Δx) in the regions where the field does not exhibit extreme differences [47].

Consider the two dimensional wave equation

$$\frac{\partial^2}{\partial z^2}\psi(x,z)+\frac{\partial^2}{\partial x^2}\psi(x,z)+k_0^2 n^2\psi(x,z)=0 \tag{2.1}$$

where ψ is the electric field E_y for TE waves or the magnetic field H_y for TM waves, $k_0 = 2\pi/\lambda_0$ is the free space wave number, λ_0 is the free space wavelength and n is refractive index of the medium.

The refractive index is assumed to be uniform along the z-direction. The electro-magnetic field $\psi(x,z)$ and the refractive index $n(x)$ are discretized along the x-axis. The field $\psi(x,z)$ is calculated analytically on the mesh lines in the direction of wave propagation (z-axis). To calculate the field in discrete form, an expression for its second derivative with respect to x in discrete form is needed. This can be accomplished using the well-known three-point central difference approximation.

2.3 Discretizing the Wave Equation

The second derivative operator $\frac{\partial^2}{\partial x^2}\psi(x,z)$ in the 2-D wave equation 2.1 is replaced by the well known three point central difference approximation given by,

$$\psi^{(2)}(0) \cong \frac{\psi_1 - 2\psi(0) + \psi_{-1}}{(\Delta x)^2} \tag{2.2}$$

At the i^{th} mesh line we get

$$\frac{d^2}{dz^2}\psi_i(z) + \frac{\psi_{i+1}(z) - 2\psi_i(z) + \psi_{i-1}(z)}{(\Delta x)^2} + k_0^2 n_i^2 \psi_i(z) = 0 \tag{2.3}$$

The field is discretized into M points in the x-direction excluding the electric or magnetic walls, i.e. i = 1, 2, 3, …, M

i = 1: $$\frac{d^2}{dz^2}[\psi_1] + \frac{1}{(\Delta x)^2}[\psi_2 - 2\psi_1 + \psi_0] + k_0^2 n_1^2 [\psi_1] = 0 \tag{2.4}$$

i = 2: $$\frac{d^2}{dz^2}[\psi_2] + \frac{1}{(\Delta x)^2}[\psi_3 - 2\psi_2 + \psi_1] + k_0^2 n_2^2 [\psi_2] = 0 \tag{2.5}$$

i = 3: $$\frac{d^2}{dz^2}\left[\psi_3\right]+\frac{1}{(\Delta x)^2}\left[\psi_4-2\psi_3+\psi_2\right]+k_0^2 n_3^2\left[\psi_3\right]=0 \tag{2.6}$$

---

i = M: $$\frac{d^2}{dz^2}\left[\psi_{\mathrm{M}}\right]+\frac{1}{(\Delta x)^2}\left[\psi_{\mathrm{M+1}}-2\psi_{\mathrm{M}}+\psi_{\mathrm{M\text{-}1}}\right]+k_0^2 n_{\mathrm{M}}^2\left[\psi_{\mathrm{M}}\right]=0 \tag{2.7}$$

Representing the above equations in matrix form we get,

$$\frac{d^2}{dz^2}\begin{bmatrix}\psi_1(z)\\ \psi_2(z)\\ \psi_3(z)\\ .\\ .\\ .\\ .\\ \psi_{\mathrm{M}}(z)\end{bmatrix}+\frac{1}{(\Delta x)^2}\begin{bmatrix}-2 & 1 & & & & & & & \\ 1 & -2 & 1 & & & & & 0 & \\ & 1 & -2 & 1 & & & & & \\ & & . & . & . & & & & \\ & & & . & . & . & & & \\ & & & & 1 & -2 & 1 & & \\ & 0 & & & & 1 & -2 & 1 & \\ & & & & & & 1 & -2 & \end{bmatrix}\begin{bmatrix}\psi_1(z)\\ \psi_2(z)\\ \psi_3(z)\\ .\\ .\\ .\\ .\\ \psi_{\mathrm{M}}(z)\end{bmatrix}$$

$$+k_0^2\begin{bmatrix}n_1^2 & & & & & & & \\ & n_2^2 & & & & & 0 & \\ & & n_3^2 & & & & & \\ & & & . & & & & \\ & & & & . & & & \\ & & & & & . & & \\ & 0 & & & & & . & \\ & & & & & & & n_{\mathrm{M}}^2\end{bmatrix}\begin{bmatrix}\psi_1(z)\\ \psi_2(z)\\ \psi_3(z)\\ .\\ .\\ .\\ .\\ \psi_{\mathrm{M}}(z)\end{bmatrix}=\begin{bmatrix}0\\ 0\\ 0\\ .\\ .\\ .\\ .\\ 0\end{bmatrix} \tag{2.8}$$

Rewriting the above matrix equations in simple form, we get

$$\frac{d^2}{dz^2}\Psi + \frac{1}{(\Delta x)^2} C\Psi + k_0^2 N\Psi = 0 \tag{2.9}$$

where C is a tri-diagonal matrix, N is a diagonal matrix with elements being the square of the refractive indices $[\, n_1^2 \quad n_2^2 \quad n_3^2 \quad . \quad . \quad . \quad n_M^2\,]$ at the mesh points and $\Psi = [\, \psi_1(z) \quad \psi_2(z) \quad \psi_3(z) \quad . \quad . \quad . \quad \psi_M(z)]^t$ is a column vector that represents the discretized field.

Equation (2.9) can be written in a compact form as

$$\frac{d^2}{dz^2}\Psi + Q\Psi = 0 \tag{2.10}$$

where

$$Q = \frac{1}{(\Delta x)^2} C + k_0^2 N \tag{2.11}$$

The solution of the above second order ordinary matrix differential equation is as follows

$$\Psi = e^{j\sqrt{Q}z} A + e^{-j\sqrt{Q}z} B \tag{2.12}$$

$e^{j\sqrt{Q}z}$ represents wave propagation in the $+z$ direction and $e^{-j\sqrt{Q}z}$ represents wave propagation in the $-z$ direction. A and B represent the $\pm z$ propagating fields at $z = 0$, respectively. Electromagnetic field Ψ, A and B are column vectors of size MX1. The MXM matrices $e^{\pm j\sqrt{Q}z}$ are evaluated by first diagonalizing Q using its eigenvalues and eigenvectors,

$$Q = UVU^{-1} \tag{2.13}$$

where U is the eigenvector matrix and V is a diagonal matrix consisting of the eigenvalues of Q. The exponential matrices $e^{\pm j\sqrt{Q}z}$ are calculated using the following relation

$$e^{\pm j\sqrt{Q}z} = Ue^{\pm j\sqrt{V}z}U^{-1} \tag{2.14}$$

2.4 Interface Conditions

In this thesis we are concerned with structures like WSDC with air grooves which are made-up of multi-layers in which the material properties (refractive index) are constant within each layer and change abruptly from one layer to the next. Hence the interface conditions should be applied so as to correctly model the electric and magnetic fields at the interfaces. The tangential electric field E_y and its first derivative are continuous across an interface whereas the tangential magnetic field H_y is continuous but its first derivative is discontinuous at an interface. All other higher order derivatives of both fields are discontinuous at an interface.

Consider the simple planar symmetric dielectric slab waveguide shown in figure 2.3. Using Maxwell's equations at an interface for TE polarization (whose components are H_x, E_y, H_z)

$$H_z = -\frac{j}{\omega\mu_0}\frac{\partial E_y}{\partial x} \tag{2.15}$$

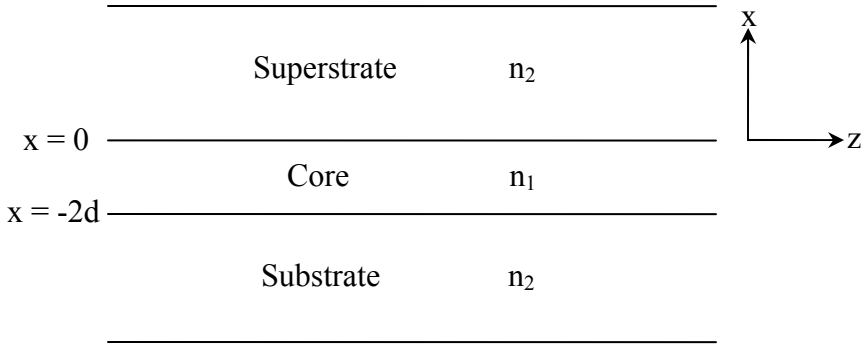

Figure 2.3 Simple three layer slab waveguide

the H_z field is continuous at the interface x = 0, i.e. $H_z^{0+} = H_z^{0-}$, using equation 2.15 we get,

$$-\frac{j}{\omega\mu_0}\frac{\partial E_y^{0+}}{\partial x} = -\frac{j}{\omega\mu_0}\frac{\partial E_y^{0-}}{\partial x} \tag{2.16}$$

which gives

$$\frac{\partial E_y^{0+}}{\partial x} = \frac{\partial E_y^{0-}}{\partial x} \tag{2.17}$$

This shows that the first derivative of the electric field E_y is continuous at the interface.

For TM polarization (whose components are E_x, H_y, E_z) from Maxwell's equations we have

$$E_z = -\frac{j}{\omega n_i^2 \varepsilon_0}\frac{\partial H_y}{\partial x} \tag{2.18}$$

E_z is continuous at the interface x = 0, i.e. $E_z^{0+} = E_z^{0-}$, hence

$$-\frac{j}{\omega n_2^2 \varepsilon_0}\frac{\partial H_y^{0+}}{\partial x} = -\frac{j}{\omega n_1^2 \varepsilon_0}\frac{\partial H_y^{0-}}{\partial x} \tag{2.19}$$

which gives

$$\frac{1}{n_2^2}\frac{\partial H_y^{0+}}{\partial x} = \frac{1}{n_1^2}\frac{\partial H_y^{0-}}{\partial x} \tag{2.20}$$

This shows that the first derivative of magnetic field H_y is discontinuous at the interface.

An improved three point central difference approximation of the second derivative operator is developed [43] for non-uniform meshing while accounting for the interface conditions, given by,

$$\psi_{\mathrm{i}}^{(2)}(z) = \frac{\psi_{\mathrm{i+1}} - (\tau_{21}\rho_{21} + 1 + 0.5h_{\mathrm{i+1}}^2\varsigma_{12})\psi_{\mathrm{i}} + \tau_{21}\rho_{21}\psi_{\mathrm{i-1}}}{0.5h_{\mathrm{i+1}}(h_{\mathrm{i}}\rho_{21} + h_{\mathrm{i+1}})} \tag{2.21}$$

where h is the mesh size, n is the refractive index, $\tau_{21} = \frac{h_{\mathrm{i+1}}}{h_{\mathrm{i}}}$, $\varsigma_{12} = k_0^2(n_i^2 - n_{i+1}^2)$ and $\rho_{21} = \frac{n_{i+1}^2}{n_i^2}$ (for TM), $\rho_{21} = 1$ (for TE). The above relation can be used to approximate the $\frac{\partial^2}{\partial x^2}$ operator at any sampling point i in terms of the field values at i+1, i and i-1 sampling points.

2.5 Absorbing Boundary Conditions

To analyze planar waveguide structures numerically, they must be enclosed by walls to limit the computational window. The use of electric/magnetic walls at the edge of the computational window produces errors, since the tangential field components E_y or H_y, are set to zero. These electric or magnetic walls reflect back the radiated field into the computational space producing errors in the computed results. In order to minimize the reflected field appropriate numerical absorbing boundary conditions must be introduced [47-49]. One such effective absorbing boundary condition is a Perfectly Matched Layer (PML).

2.5.1 Perfectly Matched Layer (PML)

The absorption of the radiative wave can be achieved by transforming the distance x from a real to an imaginary quantity. This introduces a numerical attenuation factor in the radiative field and hence causes decay of the radiative field in the PML region. If the PML region is kept sufficiently wide, then only negligible electromagnetic reflections at the extreme edges of the computational space occur. The last mesh point of the PML region is terminated by an electric or magnetic wall boundary condition. The real distance is transformed into a complex distance according to the following transformation,

$$x \rightarrow x(1 + j\sigma) \tag{2.22}$$

In discrete form the transformation is

$$\Delta x \rightarrow \Delta x(1 + j\sigma) \tag{2.23}$$

where σ is the decay factor constant. The wave $e^{+jk\Delta x}$ propagating in the $+x$ direction

in the real space will be transformed into

$$e^{+jk\Delta x(1+j\sigma)} = e^{+jk\Delta x} e^{-k\sigma\Delta x} \tag{2.24}$$

in the complex space. The factor $e^{-k\sigma\Delta x}$ causes the decay of the field in the $+x$ direction in the complex space. The value of σ is chosen arbitrarily [49] and the number of samples in the PML absorber is chosen to cause a significant decay in the field without significant reflection at the PML inner wall or the electric/magnetic wall. This absorbing PML scheme is incorporated into the MOL as illustrated by the following Figure 2.4. The use of a non-uniform mesh size allows the application of a PML region with a non-uniform loss profile [49]. In general

$$(\sigma\Delta x)_i = (\eta/P) f(x_i) \tag{2.25}$$

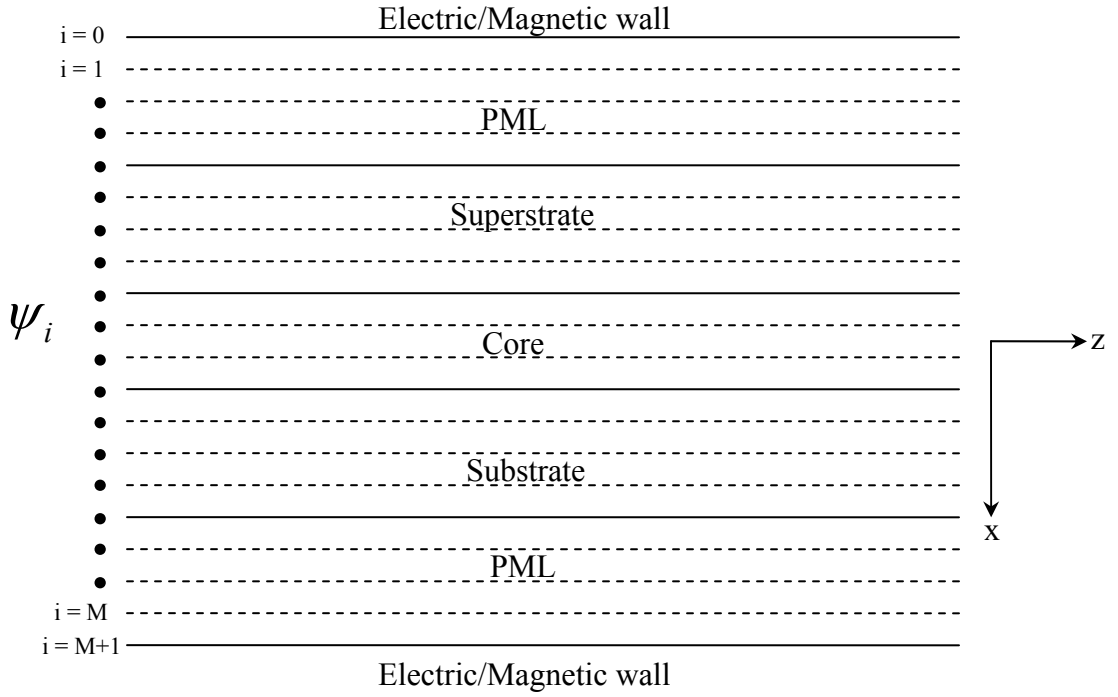

Figure 2.4 PML incorporated in Mesh Discretization.

where $(\sigma\Delta x)_i$ represents the value of the imaginary part of the mesh size σ at the i^{th} mesh point in the PML, η is the PML strength parameter and P represents the number of mesh points in the PML layer. The parameter x_i is chosen as $x_i = {}^{i\pi}\!/_{2(P+1)}$ and $f(x_i)$ is an arbitrary increasing function of x_i. In this thesis work $f(x_i)$ is chosen to be a tangent profile, hence $f(x_i) = \tan(x_i)$

2.5.2 Gaussian Field Propagation in air

In order to assess the performance of the PML, the propagation of a two-dimensional Gaussian beam in air is simulated using the MOL. A Gaussian beam with a spot size of w = 0.5 μm and the operating wavelength λ = 0.86μm is launched at z = 0. The computational window is chosen to be 5 μm wide with 60 mesh lines in the air and 10 in the PML. The propagated Gaussian beam is calculated at different distances with the PML layers and without the PML layers. If correct boundary conditions are applied the Gaussian beam maintains its basic shape but expands as it propagates. As shown in Figure 2.5 the Gaussian beam expands maintaining its basic shape, when it is propagated in air with the PML layers, hence the PML is correctly applied.

Its clear from the Figure 2.5 that in the absence of the PML layer, the Gaussian beam reflects strongly from the electric walls. The reflection manifests itself by the formation of oscillatory field along the x direction. The ripples from the top and the bottom electric walls are not symmetric because of the inability to launch the Gaussian beam exactly at the center of the computational window. The presence of the PML layer

is seen to inhibit reflections from the electric walls and the Gaussian beam propagates without any interference of the reflected field. The absence of the oscillatory field confirms this assertion.

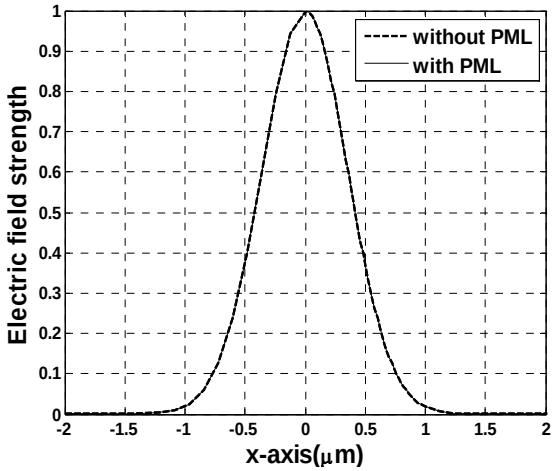

(a) Gaussian beam at the input

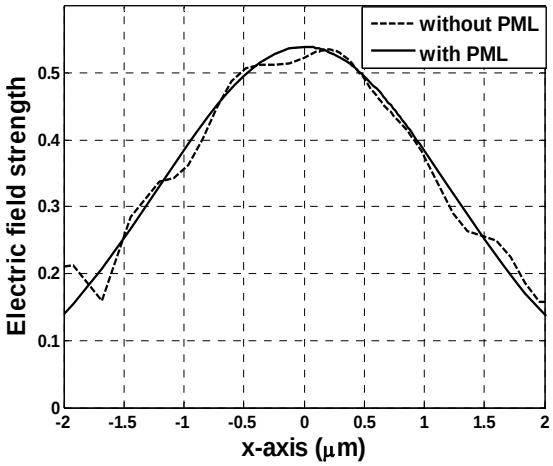

(b) Gaussian beam after 10 μm

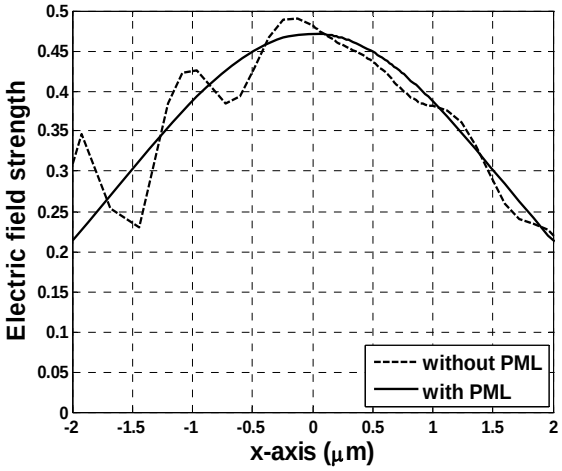

(c) Gaussian beam after 20 μm

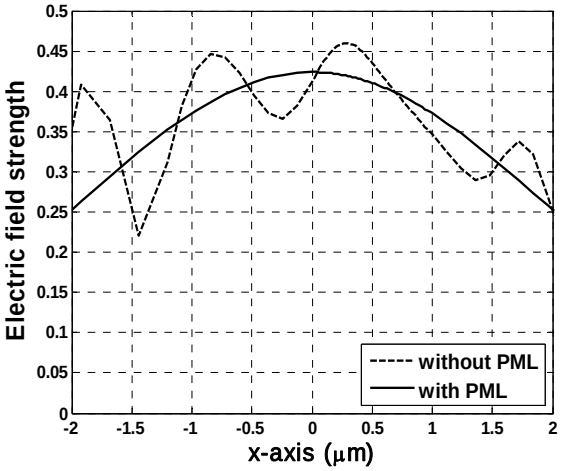

(d) Gaussian beam after 30 μm

Figure 2.5 Gaussian Beam Propagation with and without PML

CHAPTER 3

MOL ANALYSIS OF WAVEGUIDES WITH LONGITUDINAL DISCONTINUITIES

3.1 Introduction

Longitudinal discontinuities occur in many guided optical devices. They play an important role in designing optical devices such as tapers, couplers, mode converters, wavelength filters etc. A lot of effort has been done in understanding the reflection and transmission phenomena at a longitudinal discontinuity. A number of numerical techniques have been developed to simulate waveguide structures with longitudinal discontinuities [50-52].

In this thesis we will simulate a Wavelength Selective Directional Coupler with air grooves. This device consists of a large number of abrupt and periodic longitudinal discontinuities. The MOL is suited in this case because it can easily account for the backward and forward fields, as well as its inherent ability to account for optical structures with large refractive index contrast.

3.2 Analysis of a Single Longitudinal Waveguide Discontinuity

Consider the simple case of a waveguide with a single longitudinal discontinuity as shown in Figure 3.1. The discontinuity is assumed to be located at $z = 0$. The problem space is divided into two regions namely region 0 and region 1. The field is assumed to be incident from region 0. Due to the presence of this discontinuity, part of the field is reflected back into region 0 and the remaining part of the field is transmitted to region 1.

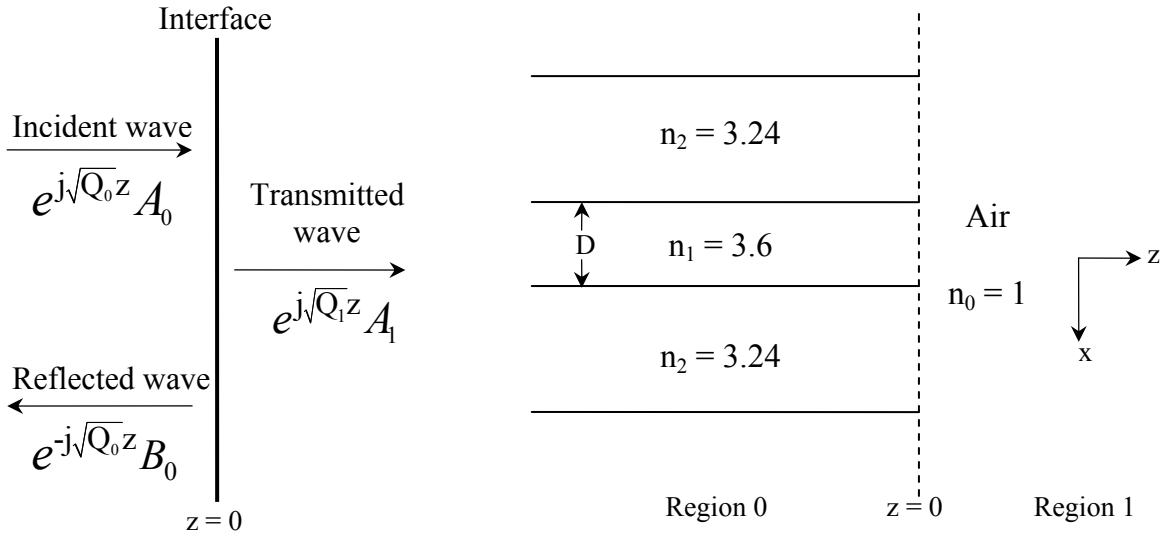

(a) Single Longitudinal Discontinuity

(b) Waveguide Structure

Figure 3.1 A single longitudinal waveguide discontinuity

The total field Ψ_0 in region 0 is the sum of the incident and the reflected fields,

$$\Psi_0 = e^{+jS_0z}A_0 + e^{-jS_0z}B_0 \tag{3.1}$$

The total field, Ψ_1, in region 1 consists only of the transmitted field

$$\Psi_1 = e^{+jS_1z}A_1 \tag{3.2}$$

where Ψ is a column vector containing the descritized fields. A_0, B_0 and A_1 are constant vectors. A_0, B_0 are the incident and the reflected field in region 0 at z = 0. A_1 is the transmitted field in region 1 at z = 0. $S = \sqrt{Q}$ and Q is defined in chapter 2. By applying the appropriate boundary conditions at the longitudinal interface z=0, it is possible to express the reflected field B_0 and the transmitted field A_1 in terms of the incident field A_0.

For the TM polarization the resulting relations are [53],

$$A_1 = 2(I + S_0^{-1}N_0N_1^{-1}S_1)^{-1}A_0 = TA_0 \tag{3.3}$$

$$B_0 = (I - S_0^{-1}N_0N_1^{-1}S_1)(I + S_0^{-1}N_0N_1^{-1}S_1)^{-1}A_0 = RA_0 \tag{3.4}$$

where I is the identity matrix, T is the transmission matrix and R is the reflection matrix. N_0 and N_1 are the diagonal matrices of refractive indices squared n_i^2 at each sample point of region 0 and region 1 respectively.

For TE polarized waves, both the field Ψ and its first derivative with respect to z are continuous across the interface, which is equivalent to replacing the matrix $N_0 N_1^{-1}$ appearing in equations 3.3 and 3.4 by the identity matrix I. The resulting relations for TE polarized waves are as follows,

$$A_1 = 2(I + S_0^{-1} S_1)^{-1} A_0 = T A_0 \tag{3.5}$$

$$B_0 = (I - S_0^{-1} S_1)(I + S_0^{-1} S_1)^{-1} A_0 = R A_0 \tag{3.6}$$

The transmission and reflection matrices at a single longitudinal discontinuity are related by

$$A_1 = A_0 + B_0 = (R + I) A_0 = T A_0 \tag{3.7}$$

i.e.,
$$T = I + R \tag{3.8}$$

which is applicable to both TE and TM polarized waves.

3.2.1 Modal Reflectivity and Modal Transmissivity

The expression for the calculation of the incident power is given by [53],

$$P_z = \frac{1}{2\omega \in_0} \mathrm{Re}[N_0^{-1} S_0 A_0 A_0^*] \Delta x \tag{3.9}$$

The above equation can be used for the calculation of the reflected and transmitted power of the waveguide. The modal field amplitude can also be obtained by calculating the modal expansion coefficient α_m of the waveguide given by

$$\alpha_m = \frac{A^t N_0^{-1} F_m}{F_m^t N_0^{-1} F_m} \tag{3.10}$$

where F_m represents the discretized modal field distribution of the mth mode and A is the discretized general field. The above formulae are for TM modes and they can be used for TE modes by replacing the matrix N with the identity matrix. On squaring the modal expansion coefficient one can obtain the required mode power. Since this thesis is emphasized on obtaining the modal reflectivity and transmissivity of the WSDC structure, the definitions of these terms are given below.

Modal Reflectivity (R) is defined as the ratio of the modal reflected power to the modal incident power and modal transmissivity (T) is defined as the ratio of the modal transmitted power to the modal incident power.

3.2.2 Numerical Results for a single waveguide discontinuity

A single waveguide discontinuity shown in Figure 3.2 is modeled at $\lambda = 0.86$ μm. The waveguide core width, D is varied from 0.05 to 1.0 μm. The fundamental TE_0 mode is incident from left on the waveguide. The computational window is kept large enough so that the field is negligible at the electric walls, and it is terminated by the PML layers. The variation of the fundamental modal reflectivity of the TE wave is shown in Figure 3.3 as a function of the core width, D. The same structure has been treated in reference [54]. Figure 3.3 shows good agreement between our results and those of the reference [54].

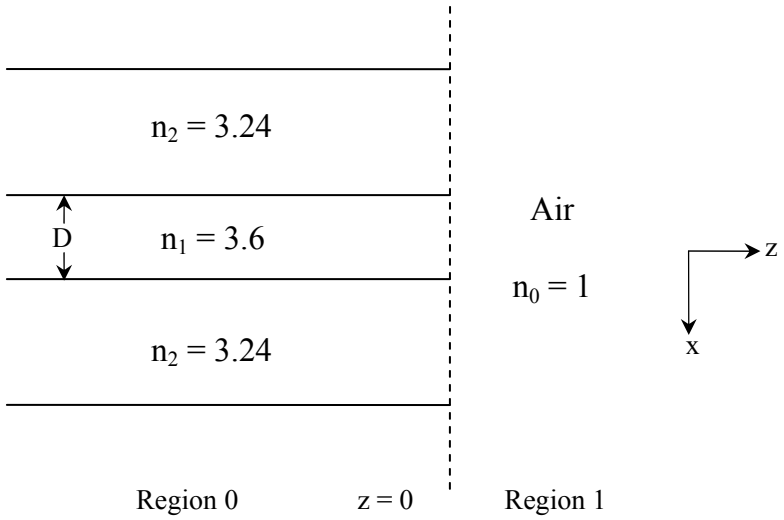

Figure 3.2 A single longitudinal waveguide discontinuity

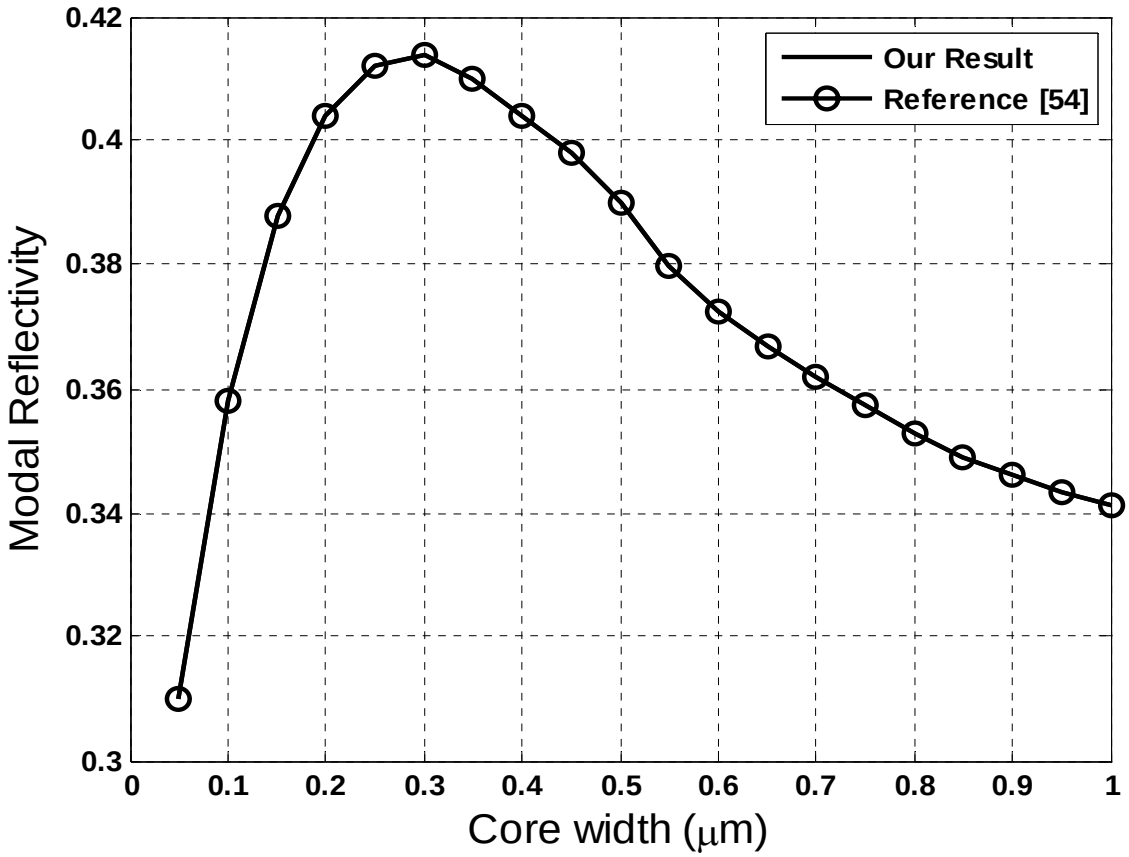

Figure 3.3 Fundamental TE mode Reflectivity

3.3 The Cascading and Doubling Algorithm

The structure of interest in this thesis, the Wavelength Selective Directional Coupler, consists of thousands of longitudinal discontinuities. To analyze such a structure we need an efficient algorithm which can correctly model the electromagnetic fields.

The Cascading and Doubling algorithm [55] offers an efficient way of calculating the transmitted and the reflected fields of waveguides with multiple discontinuities. This algorithm can be applied if knowledge of the field in the intermediate regions is not required. Two waveguide regions 'A' and 'B' in Figure 3.4 represent generally asymmetric distributed discontinuities. These waveguide regions are attached together with a uniform region of width d. The field reflection and transmission matrices of both regions are assumed to be known. In Figure 3.4, R_A and T_A are assumed, respectively, to be the reflection and transmission matrices of the isolated structure A.

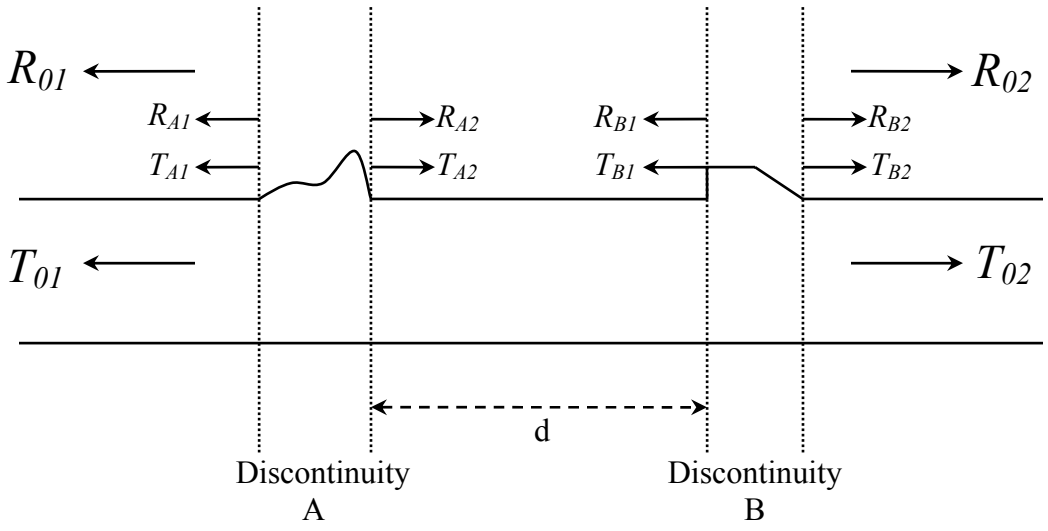

Figure 3.4 Two Waveguide Discontinuities Cascaded Together

[R_{A1}, T_{A2} (R_{A2}, T_{A1})] are, the reflection and transmission matrices of discontinuity A when the field is incident from the left (right) of the discontinuity, respectively. Similarly [R_{B1}, T_{B2} (R_{B2}, T_{B1})] are, the corresponding reflection and transmission matrices of the discontinuity B.

The field propagation in the waveguide section of length d is described by $e^{\pm jSz}$ .The field vector a_0 is assumed to be incident from the left on the first discontinuity. When both discontinuities are joined together then, the reflection and transmission matrices [R_{01}, T_{02}, (R_{02}, T_{01})] of the combined structure when the field is incident from left (right) are given by [55],

$$R_{01} = R_{A1} + T_{A1} e^{jSd} R_{B1} (I - e^{jSd} R_{A2} e^{jSd} R_{B1})^{-1} e^{jSd} T_{A2} \qquad (3.11)$$

$$T_{02} = T_{B2} (I - e^{jSd} R_{A2} e^{jSd} R_{B1})^{-1} e^{jSd} T_{A2} \qquad (3.12)$$

Equations 3.11 and 3.12 are very similar with a common quotient factor $(I - e^{jSd} R_{A2} e^{jSd} R_{B1})^{-1} e^{jSd} T_{A2}$. These formulae give net reflection and transmission matrices of a cascaded structure composed of two substructures in terms of their individual reflection and transmission matrices. The relations for R_{02} and $T_{01,}$ as seen from the right, can be easily obtained from equations 3.11 and 3.12 by interchanging $A \rightleftharpoons B$ and $1 \rightleftharpoons 2$ [55]. If each of the discontinuities A and B are symmetrical, i.e., $R_1 = R_2 = R$ and $T_1 = T_2 = T$ and identical i.e., $R_A = R_B$ and $T_A = T_B$, then the equations 3.11 and 3.12 reduce to

$$R_{01} = R + Te^{jSd}R(I - e^{jSd}Re^{jSd}R)^{-1}e^{jSd}T \tag{3.13}$$

$$T_{02} = T(I - e^{jSd}Re^{jSd}R)^{-1}e^{jSd}T \tag{3.14}$$

Finally, in the important special case, in which the above two identical and symmetric discontinuities, are attached directly to each other, such that $d = 0$ as shown in Figure 3.5,

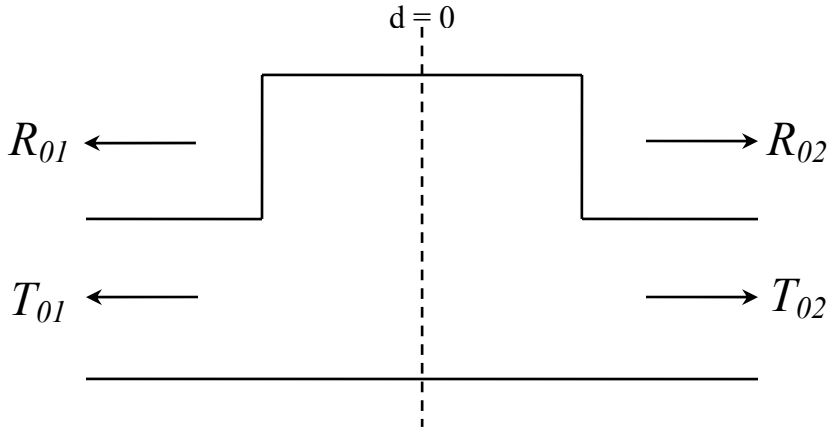

Figure 3.5 Two identical and symmetric discontinuities attached directly (d = 0)

then we end up with the very simplified relationship,

$$R_{01} = R + TR(I - R^2)^{-1}T = R_{02} \tag{3.15}$$

$$T_{02} = T(I - R^2)^{-1}T = T_{01} \tag{3.16}$$

The above equations 3.15 and 3.16 can be used to model waveguides with a large number of periodic gratings in an efficient manner. This can be done by combining two

periods using the above equations, then the two periods can again be combined using the same equation to find the reflection and transmission matrices of four periods. The same process is continued for the whole structure. Therefore, as can be seen, this algorithm works in a power of 2. For 2^N periods, it requires repeated use of equations 3.15 and 3.16, N times only, thus improving the efficiency of the procedure.

This algorithm works in the power of 2 only, but we can model any number of periods by attaching the appropriate number of sections each having periods expressed as power of 2. For example, we can model twenty periods by attaching sixteen and four periods.

3.3.1 Numerical Results

We applied the cascading and doubling algorithm in the MOL to simulate a waveguide with multiple periodic gratings as shown in Figure 3.6. The refractive indices of the superstrate, core and substrate are 1, 1.53 and 1.52, respectively. The depth of the periodic grating is taken to be 0.5 μm. The period consists of the widths, L_A = 0.106553 μm and L_B = 0.106456 μm. These are the same specifications used in the reference [55]. The TE_0 wave is assumed to be incident on the left of the waveguide and the TE_0 modal reflectivity is calculated.

The cascading and doubling algorithm has been used to calculate the TE_0 modal reflectivity. The following Figure 3.7 shows the modal reflectivity versus wavelength for 5000 grating periods. Figure 3.7 shows good agreement between our results and those of the reference [55].

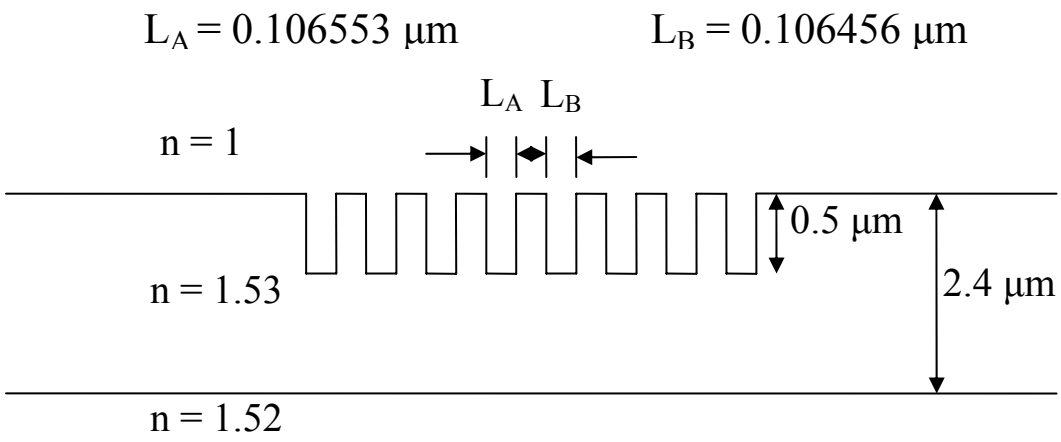

Figure 3.6 Waveguide Grating Structure.

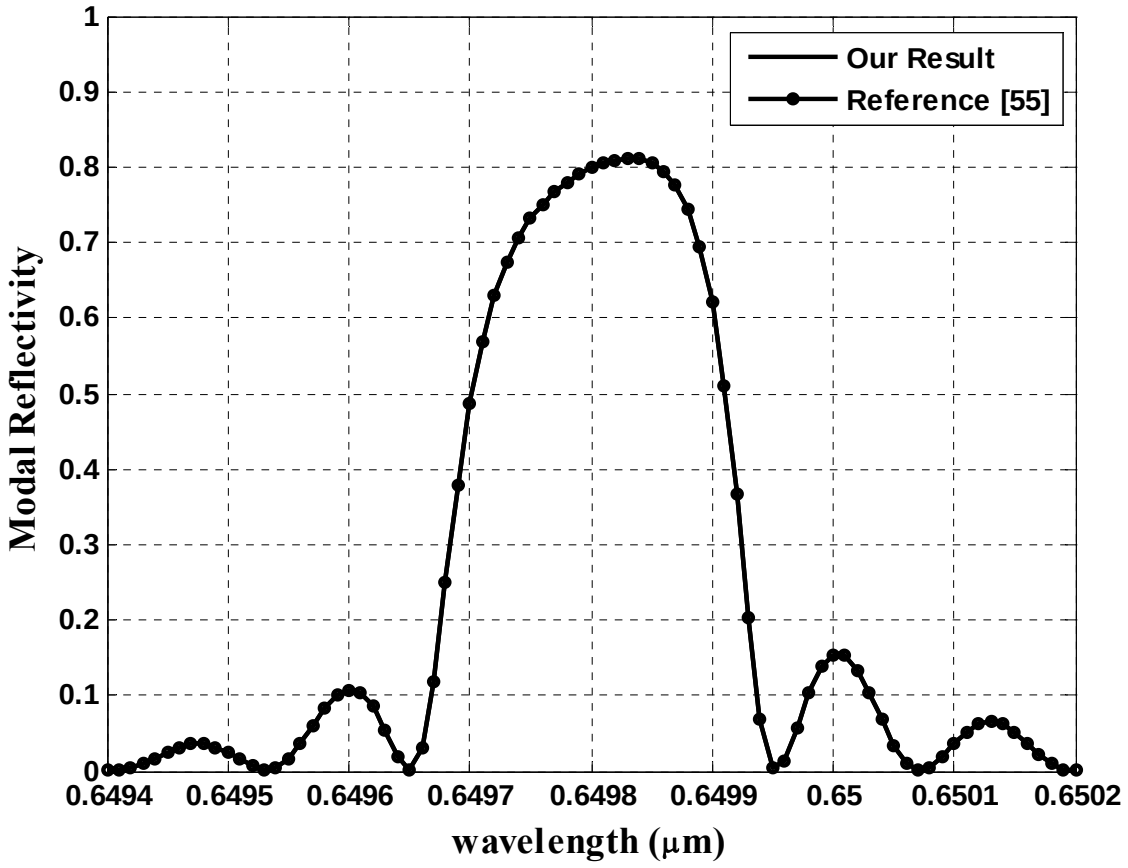

Figure 3.7 Modal Reflectivity versus wavelength for a Periodic Grating with 5000 periods

CHAPTER 4

ANALYSIS OF DIRECTIONAL COUPLER

4.1 Introduction

The importance of guided waves in the domain of optics has stimulated great interests in the development of related components. These components are needed to perform some of the basic functions required in any integrated optical system. One of the most important functions that was first considered was the transfer, or coupling of signal power from one waveguide to another. In fact, whether in microwave technology, integrated or fiber optics, the design of couplers has always been a primary concern from early days of these technologies.

Although a large variety of coupler geometries [56-58] has been investigated, they mostly rely on the mechanism of evanescent wave interaction. Recent advances in single-mode waveguide couplers, at least in the case of dielectric media, are based on this mechanism. This mechanism requires that the two waveguides to be coupled be brought close to each other to make possible the interaction of the evanescent fields which extend just outside of the waveguides.

Bracey [59] used this principle very early in 1959 to demonstrate coupling between two Teflon rods at microwave frequencies. In integrated optics, directional

couplers are now routinely fabricated in which light transfer occurs between adjacent channel waveguides placed on a common substrate.

4.2 The concept of waveguide coupling

The introduction of a perturbation to an otherwise perfect guide can cause an interchange of energy amongst the modes of that guide. In fact, one individual mode can be converted into another with close to 100 percent efficiency in many cases. This principle, known as mode coupling, occurs in many branches of physics other than guided wave optics.

The Directional Coupler works by coupling together two modes traveling in the same direction. In its simplest form it acts as a beam splitter, but more complicated devices can be used as two way switches or modulators, further variants can be used as filters or polarizers.

In its simplest form, a directional coupler consists of two parallel and identical dielectric waveguides in close proximity as shown in Figure 4.1. In this case, the power coupling is based on optical interference between the evanescent fields of the two waveguides, such that a light wave launched into one of the waveguides can be coupled completely into the other waveguide.

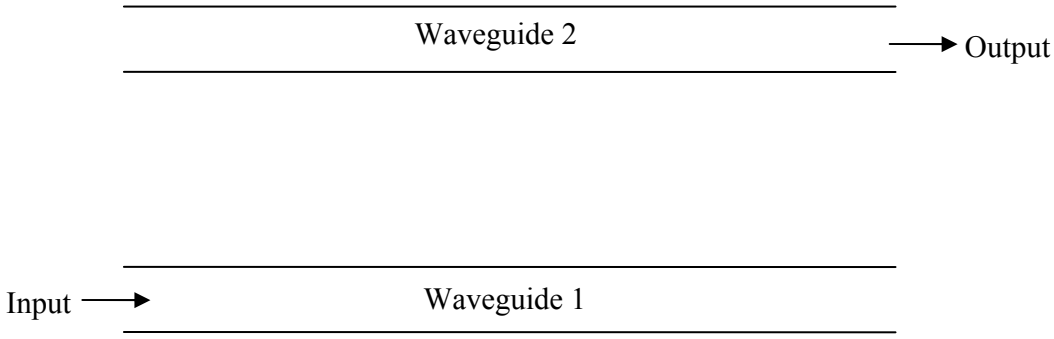

Figure 4.1 Directional Coupler

In the coupled mode theory [60] the mode of each individual waveguide is assumed to be unchanged by the presence of the other waveguide. Part of the evanescent field of the waveguide mode reaches the other waveguide, causing evanescent wave coupling between the two guiding structures. If at z = 0 only waveguide 1 is excited, one expects its evanescent field to excite the mode of waveguide 2 and energy transfer to occur. The strength of this coupling mechanism is clearly a function of the magnitude of this evanescent field. When the waveguides are far apart, the evanescent field of one waveguide at the other waveguide is weak, and significant energy transfer occurs over a long interaction distance (weak coupling). Conversely, when the waveguides are close to each other the evanescent field is strong and transfer occurs over a short distance (strong coupling).

4.3 Basic Principles

When the two single mode dielectric waveguides are brought in close proximity to each other, the combined coupled structure supports two modes. One of these modes has an even transverse electric field variation, while the other is characterized by an odd transverse field. The even and the odd modes of the coupled structure are shown in Figure 4.2(a) and (b) respectively. The refractive index of the waveguide core is 3.5 whereas the refractive index of the substrate is 3.4. These modes are known to have almost similar values of the effective index with the even mode having a slightly larger effective refractive index than that of the odd mode.

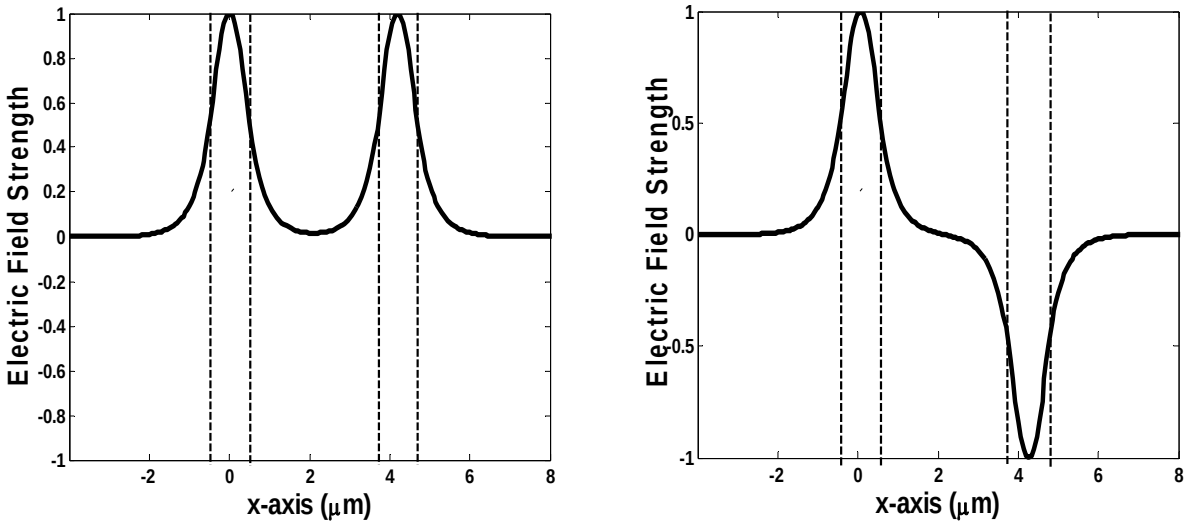

(a) Even TE_0 mode (b) Odd TE_0 mode

Figure 4.2 Fundamental Modes of the Directional Coupler

The length at which the power is transferred completely from one waveguide to another is called the coupling length. The coupling length of a directional coupler can be theoretically obtained using the relation [61],

$$L_c = \frac{\pi}{\Delta\beta} \tag{4.1}$$

where $\Delta\beta$ is the propagation constant difference of the even and odd modes of the structure given by

$$\Delta\beta = \beta_0 - \beta_1 \tag{4.2}$$

β_0 and β_1 are the phase constants of the TE_0 and the TE_1 modes respectively of the coupled structure.

We start with two identical single-mode guides, and choose the length of the coupling region so that the device runs from z = 0 to z = L. Under normal circumstances an input to guide 1 will then be coupled across and emerge as an output from guide 2. And for another coupling distance, power is transferred back to guide 1 and this process continues. In fact the process is a continuous, bidirectional one. The condition the guides must satisfy for 100 percent power transfer is that they should be synchronous (i.e. have the same propagation constants). This usually requires them to be identical.

4.4 MOL Analysis of Directional Coupler

The simple directional coupler shown in Figure 4.3 which consists of two identical parallel dielectric slab waveguides will be analyzed. The refractive index of the

core is 3.5 and that of the substrate is 3.4. The waveguide cores are 0.8 μm wide and the gap between them is fixed at 2.8 μm. The computational window is 13 μm wide including the PML layers. 200 non-uniform mesh lines are used in the analysis.

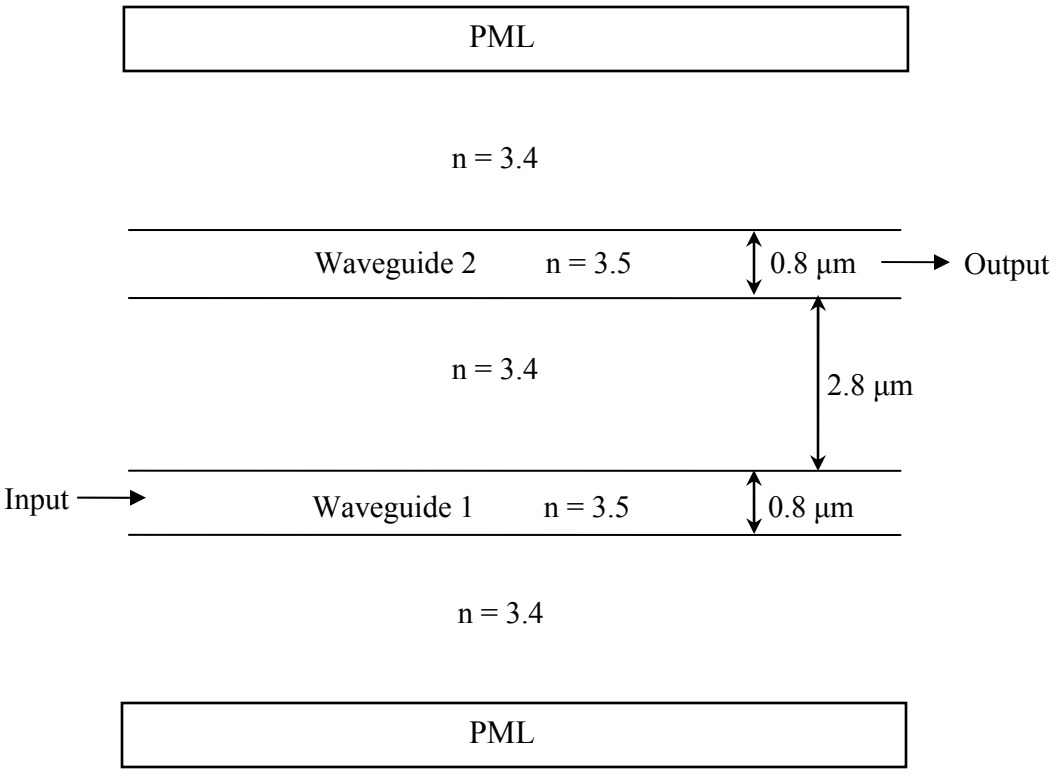

Figure 4.3 Directional Coupler used in the MOL simulation

The fundamental TE mode of an isolated waveguide is used as input for this device which is illustrated in Figure 4.4. The same input field configuration is used throughout this thesis.

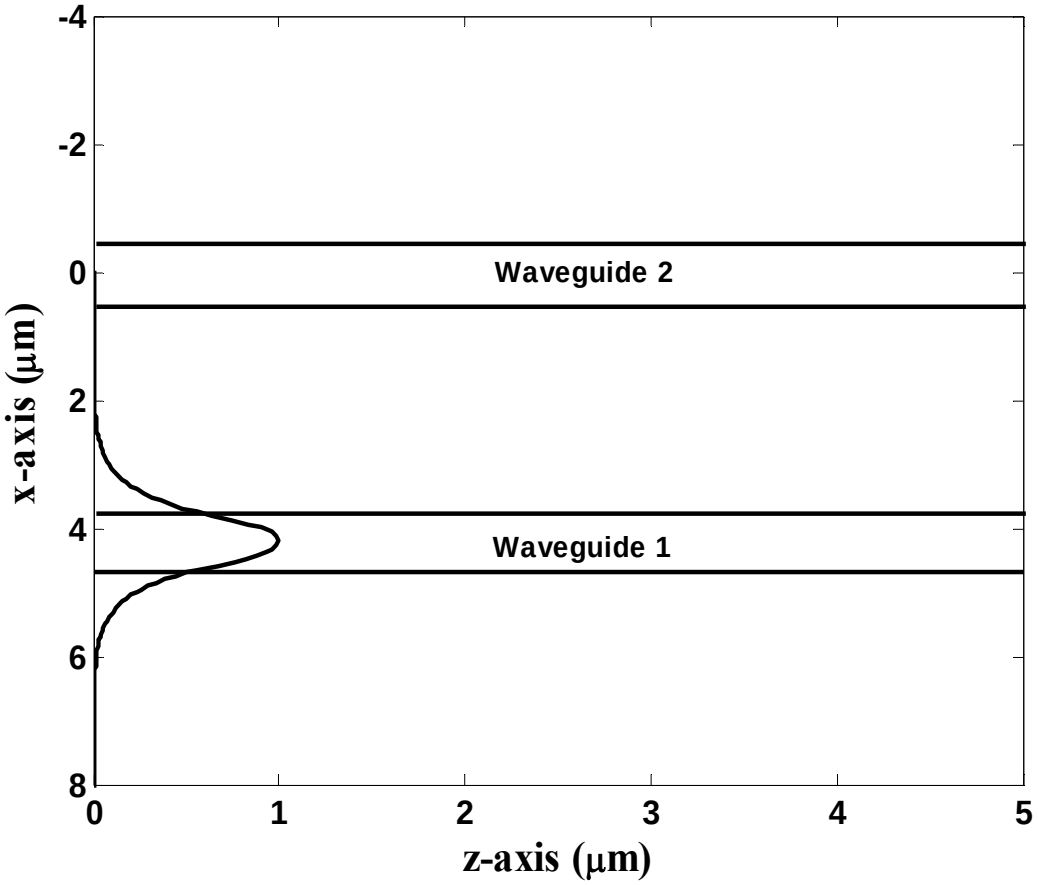

Figure 4.4 Incident field of the Directional Coupler

The waveguide 1 of the directional coupler is excited using the fundamental TE_0 field of the isolated waveguide and the field is propagated in the direction of propagation (z-axis). The coupling length of the directional coupler is calculated to be $L_c = 2.1507$ cm (using equation 4.1). The following Figure 4.5 shows the field propagation in the directional coupler. The input field is incident at z = 0. From the simulation results it can be seen that the field traveling through the waveguide 1 is coupled to the other waveguide completely after a distance 2.1507 cm, and again coupled back to the input waveguide after the same distance.

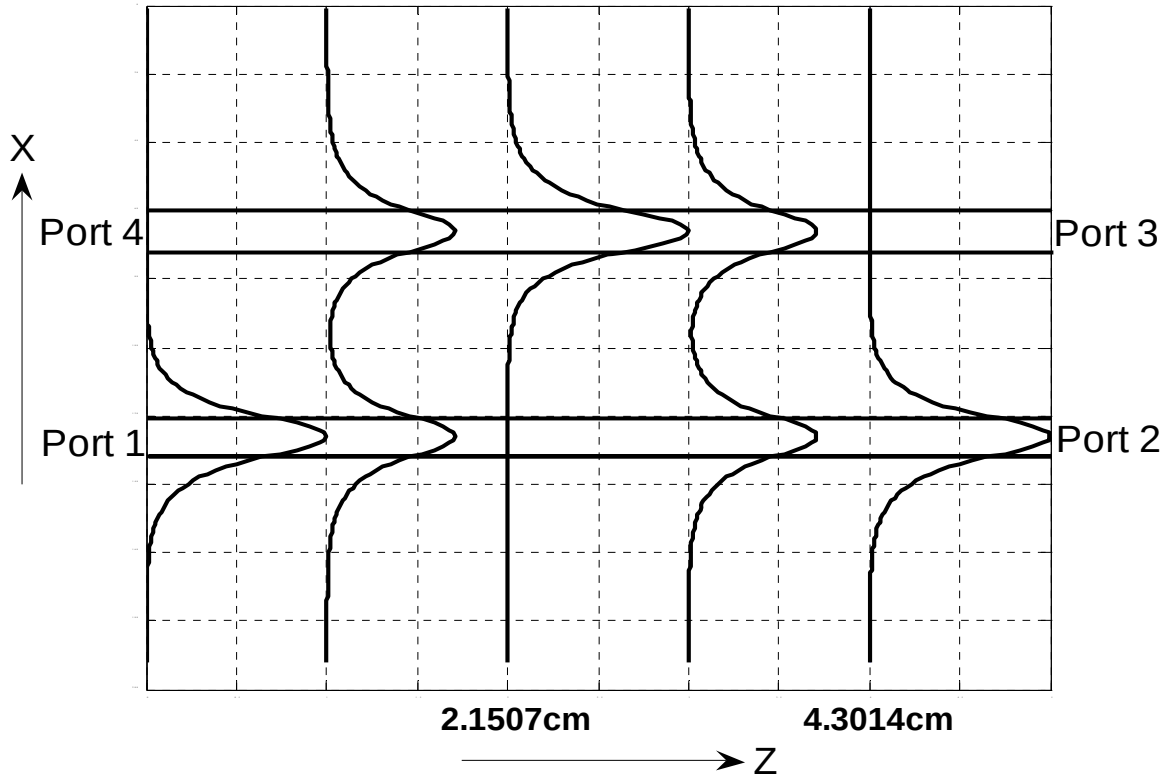

Figure 4.5 The TE_0 Mode at different points of the Directional Coupler calculated using the Method of Lines

CHAPTER 5

ANALYSIS OF WAVELENGTH SELECTIVE DIRECTIONAL COUPLER WITH AIR GROOVES

5.1 Introduction

A Wavelength Selective Directional Coupler (WSDC) which consists of two identical and parallel slab waveguides with periodic air grooves is considered. A schematic diagram of the structure is shown in Figure 5.1. The air grooves are etched into the substrate that separates the two waveguides. L, w and Λ represent the length, width and the period of the air grooves. The coupling and wavelength filtering characteristics of the device are investigated by varying the air groove length (L), width (w) and total number of periods.

For this structure the spectral modal reflectivity and transmissivity are calculated. The fundamental TE_0 mode field of an isolated waveguide is launched in port 1 of the WSDC, and the output power at the remaining three ports as well as the reflected power at the input port 1 is calculated. These calculations are repeated for a number of wavelengths in order to obtain the spectral response of the device. R_1 and R_4 are the modal reflectivities of port 1 and port 4 respectively; T_2 and T_3 are the modal transmissivities of port 3 and port 4 respectively (see Figure 5.1).

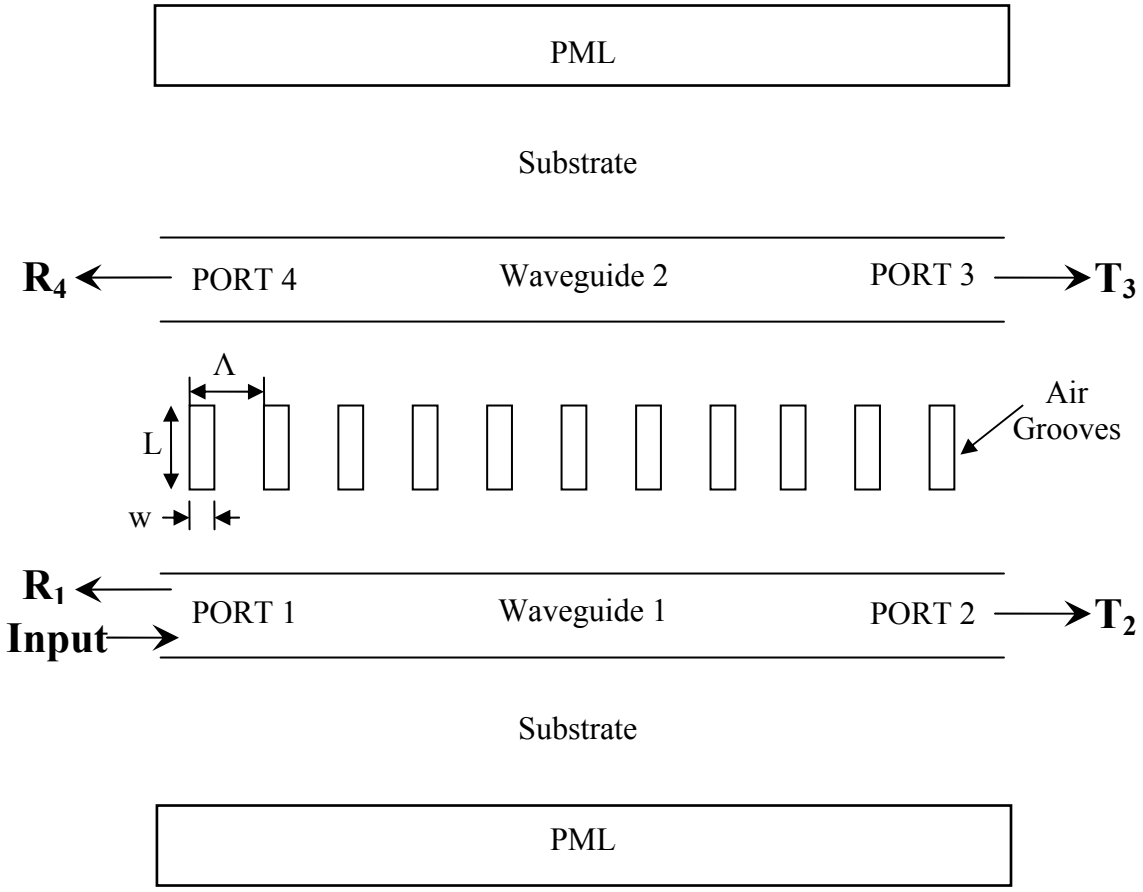

Figure 5.1 WSDC with air grooves

5.2 Numerical analysis of the WSDC with air grooves

The WSDC with periodic air grooves is simulated using the previously developed MOL code. The waveguide cores have a refractive index of 3.5. The surrounding media is chosen to have a refractive index of 3.4. The core width of both the waveguides is taken to be 0.8 μm which insures single mode operation. The waveguides separation is fixed at 2.8 μm. The computational window is 11.4 μm wide and the mesh size along x-axis is taken as 50 nm.

A PML layer with a tangent loss profile is used at both ends of the computational window to prevent reflections from the electric walls at the extreme edges of the computational window. The Cascading and doubling algorithm is used to calculate the modal reflectivities R_1 and R_4 and the modal transmissivities T_2 and T_3 at the four ports.

For the waveguide separation of 2.8 μm, the calculated coupling length is L_c = 2.1507 cm (using equation 4.1). In our case the length of the WSDC is considered to be $0.25L_c$ which is equal to 0.537675 cm. The period of the air grooves is calculated using the approximate relationship,

$$\text{Period} = \frac{\pi}{\beta} \tag{5.1}$$

where $\beta = k_0 \times n_{eff}$.

Using equation 5.1 the calculated period is 0.224079 μm. The length of the WSDC considered, $0.25L_c$, is divided by the period to obtain the total number of periods which is equal to 23995. All these parameters are fixed and the effect of the air groove width (w), length (L) and the number of periods on the response of the WSDC is studied in the following sections.

5.3 Effect of the air groove width (w)

The length of the air groove is fixed at 1.4 μm and the air groove width (w) is varied to find its effect on the response of the WSDC at all the four ports. Figure 5.2 shows the modal reflectivity R_1 versus wavelength of WSDC at port 1 for air groove

widths w = 0.005, 0.03, 0.05, 0.07 and 0.1 μm. The modal reflectivity R_1 at the resonance wavelength initially increases as the air groove width, w is increased from 0.005 μm to 0.03 μm. It rises to unity and remains constant for air groove widths ranging from 0.03 μm to 0.07 μm and then starts to decrease as the air groove width is increased beyond 0.07 μm.

At w = 0.005 μm the modal reflectivity R_1 reaches a maximum of 0.75 at the resonance wavelength of 1.54997 μm. As illustrated in Figure 5.2, the modal reflectivity R_1 has some small side lobes and it is nearly zero at all other wavelengths. The spectral width in this case is approximately 1Å (angstrom). As the air groove width is increased, the modal reflectivity R_1 increases gradually and it attains a maximum value of unity at w = 0.03 μm. Here the spectral width of R_1 increases to 1.5 Å and the resonance wavelength is slightly shifted to a lower value of wavelength which is 1.54992 μm. At all other wavelengths throughout the spectrum of R_1 is zero with some ripples near the resonance wavelength. The modal reflectivity R_1 at the resonance wavelength retains the maximum value of unity as the air groove width is increased from 0.03 μm to 0.07 μm, its spectral width remains constant at 1.5 angstrom, and the resonance wavelength shifts slightly to a lower value but stays around 1.5499 μm.

R_1 at the resonance wavelength starts to decrease when the air groove width is raised above 0.07 μm. As shown in figure 5.2 the maximum value of R_1 is 0.9 at w = 0.1 μm and its spectral width is reduced to 1.2 Å. R_1 decreases further if the air groove width is increased above 0.1 μm. It can be said that the modal reflectivity R_1 acts as a band pass filter with a spectral width of roughly 1Å.

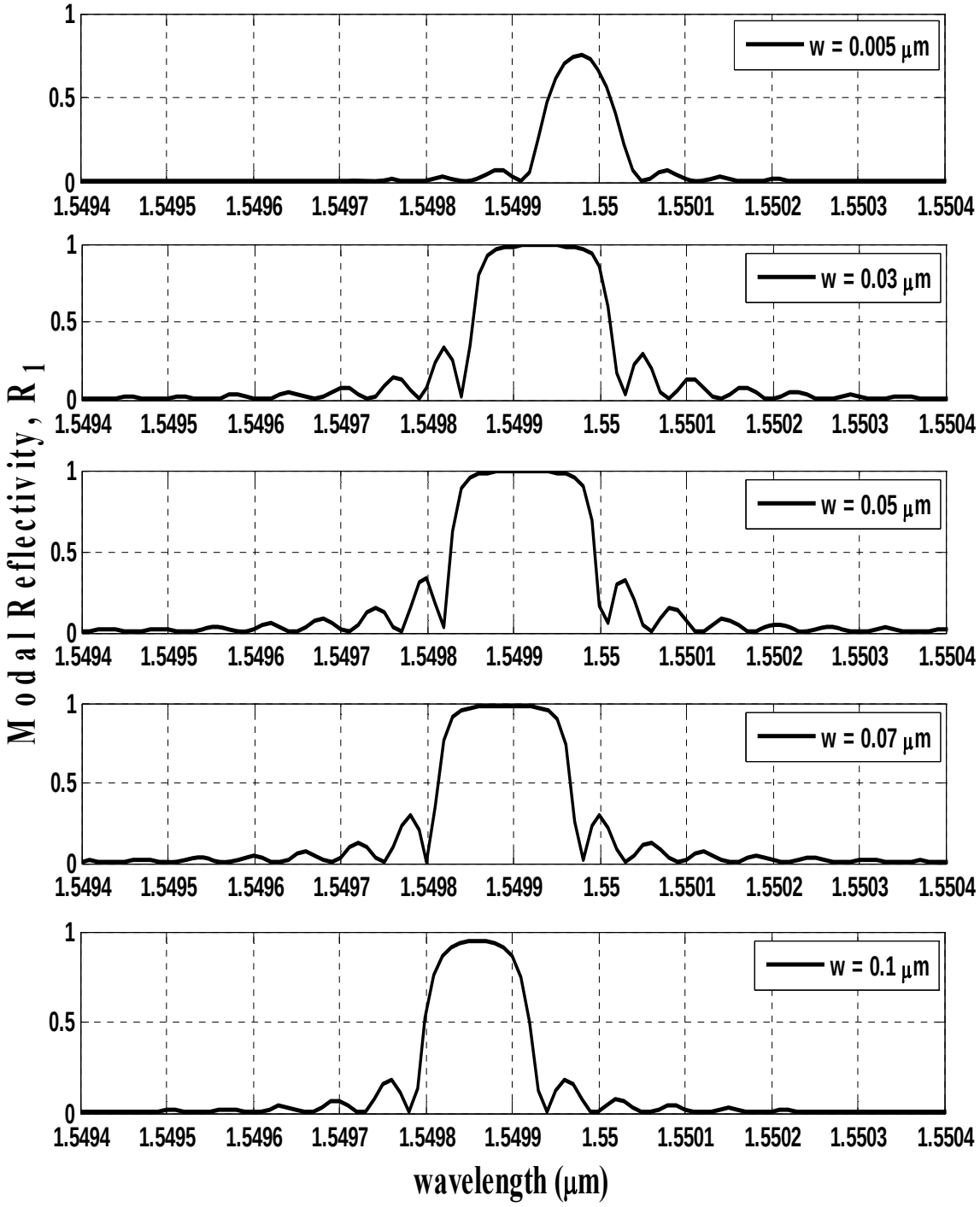

Figure 5.2 Modal Reflectivity R_1 versus wavelength at port 1 for different air groove widths.

The modal transmissivity T_2 at port 2 is illustrated in Figure 5.3 for the same air groove widths w = 0.005, 0.03, 0.05, 0.07 and 0.1 μm. At w = 0.005 μm the modal transmissivity T_2 is about 0.95 throughout the spectrum except within a spectral width of 1Å there is a dip in T_2 . At the resonance wavelength of 1.54997 μm the modal transmissivity T_2 has a minimum value of 0.25. As the air groove width is increased, the modal transmissivity T_2 at the resonance wavelength decreases gradually and it becomes nearly zero at w = 0.03 μm. Here the spectral width of T_2 increases to 1.5 Å and the resonance wavelength is slightly shifted to a lower value of 1.54992 μm. At all other wavelengths throughout the spectrum the modal transmissivity T_2 remains at 0.95 with some ripples near the resonance wavelength.

The modal transmissivity T_2 at the resonance wavelength retains the minimum value of zero as the air groove width is increased from 0.03 μm to 0.07 μm, its spectral width remains almost constant at 1.5 Å, and the resonance wavelength shifts slightly to a lower value but stays around 1.5499 μm. At all other wavelengths the transmissivity T_2 retains the maximum value of unity with small ripples near the resonance wavelength. T_2 at the resonance wavelength starts to increase when the air groove width is raised above 0.07 μm. As shown in Figure 5.2 the minimum value of T_2 is about 0.1 at w = 0.1 μm and its spectral width is approximately 1.2 Å. The minimum value of T_2 increases further if the air groove width is increased above 0.1 μm.

The modal transmissivity spectrum at port 2 exhibits the reverse action of the modal reflectivity spectrum at port 1. It acts as a band-stop filter with the same spectral

width of roughly 1.5 Å as seen in the modal reflectivity response R_1.

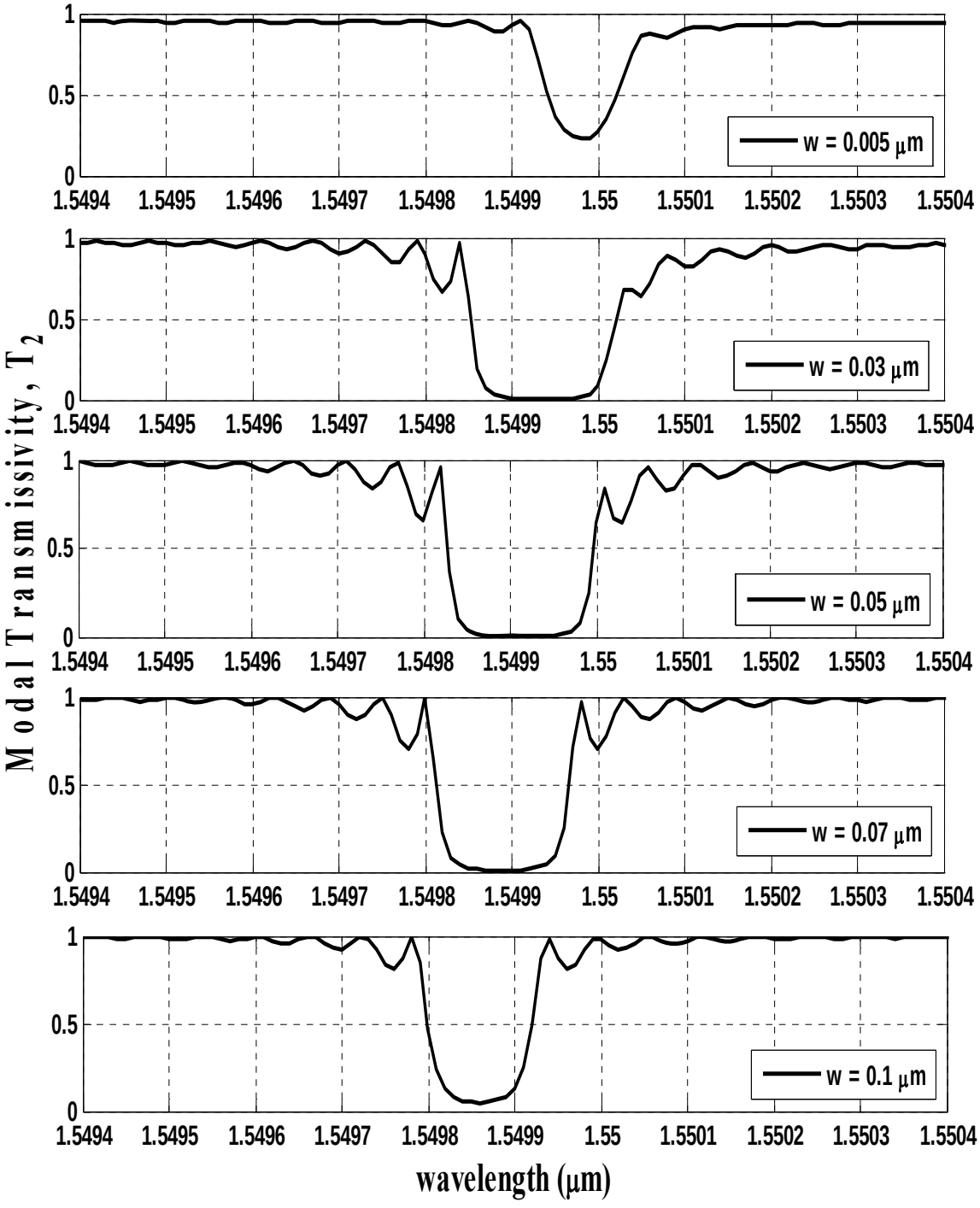

Figure 5.3 Modal Transmissivity T_2 versus wavelength at port 2 for different air groove widths.

The modal transmissivity T_3 at port 3 is illustrated in Figure 5.4 for air groove widths w = 0.005, 0.03, 0.05, 0.07 and 0.1 μm. As seen in the figure, T_3 remains low. This is attributed to the short length of the WSDC which is taken to be $0.25L_c$. At this length only a small amount of power is coupled to the port 3. For w = 0.005 μm, as we move from the left of the spectrum towards the right hand side the modal transmissivity T_3 remains constant at 0.05, it drops to near zero at the wavelength of 1.54995 μm and then it starts to increase reaching a peak value of 0.12 which occurs at 1.55004 μm. It again drops with some ripples and remains constant at 0.06 for wavelengths greater than 1.5502 μm.

Maximum power is coupled to port 3 at resonance when the air groove width w = 0.03 μm. As shown in Figure 5.4, the maximum value of the modal transmissivity T_3 is 0.22 at the resonance wavelength of 1.55002 μm, at all other wavelengths T_3 remains constant at about 0.03. As the air groove width is increased above 0.03 μm the modal transmissivity T_3 starts to decrease. For instance, at w = 0.05 μm, T_3 equals 0.01 throughout the spectrum, drops to nearly zero at 1.5499 μm, and peaks to about 0.1 at 1.55 μm.

At w = 0.07 μm, T_3 decreases further and its highest value of 0.01 which occurs at 1.54997 μm, and at all other wavelengths throughout the spectrum it is substantially small. When the air groove width is increased above 0.07 μm, T_3 becomes almost negligible. For instance, at w = 0.1 μm, the maximum value of T_3 is about 0.0001. The spectrum of T_3 is asymmetric for all the air groove widths.

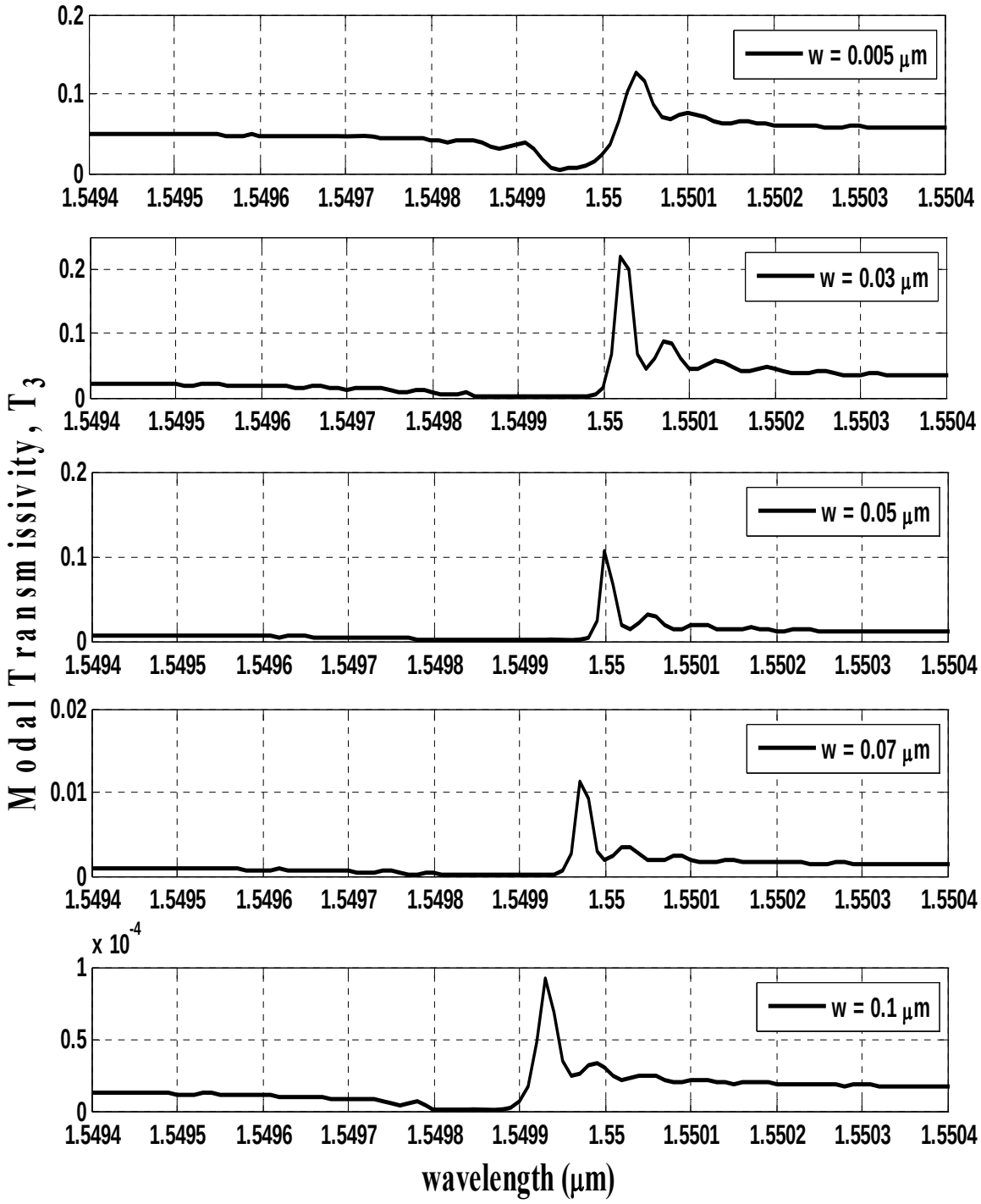

Figure 5.4 Modal Transmissivity T_3 versus wavelength at port 3 for different air groove widths.

The modal Reflectivity R_4 versus the wavelength at port 4 is illustrated in Figure 5.5 for the air groove widths w = 0.005, 0.03, 0.05, 0.07 and 0.1 μm. At w = 0.005 μm, as we move from the left hand side towards the right of the spectrum, the modal reflectivity R_4 is nearly zero continuously until the wavelength of 1.5498 μm, it then starts to increase slowly and the increase is substantial at 1.55 μm, a maximum of 0.06 occurs at 1.55003 μm. R_4 again drops with some ripples and becomes about zero at 1.5502 μm and continues to be near zero throughout the right hand side of the spectrum.

The air groove width is increased above 0.005 μm. Maximum reflection into port 4 occurs when the air groove width is 0.03 μm. At w = 0.03 μm, as shown in Figure 5.5, the modal Reflectivity R_4 is near zero throughout the spectrum except for a spectral width of 0.2 Angstrom. At the resonance wavelength of 1.55002 μm, R_4 peaks to 0.15.

As the air groove width is increased above 0.03 μm, the reflection into port 4 starts to decline. The maximum value of R_4 at w = 0.05 μm is 0.075, at the resonance wavelength of 1.55 μm. It is obvious from the Figure 5.5 that the resonance wavelength is slightly shifted to the left as the air groove width is increased. At w = 0.07 μm, the modal Reflectivity R_4 peaks to 0.009 at 1.54997 μm. And as the air groove width is increased further R_4 becomes negligible. In fact at w = 0.1 μm, its peak has a low value of 0.6×10^{-4} at 1.54992 μm.

Sum of R_1, T_2, T_3, R_4 at any wavelength is almost equal to unity, indicating negligible loss due to radiation.

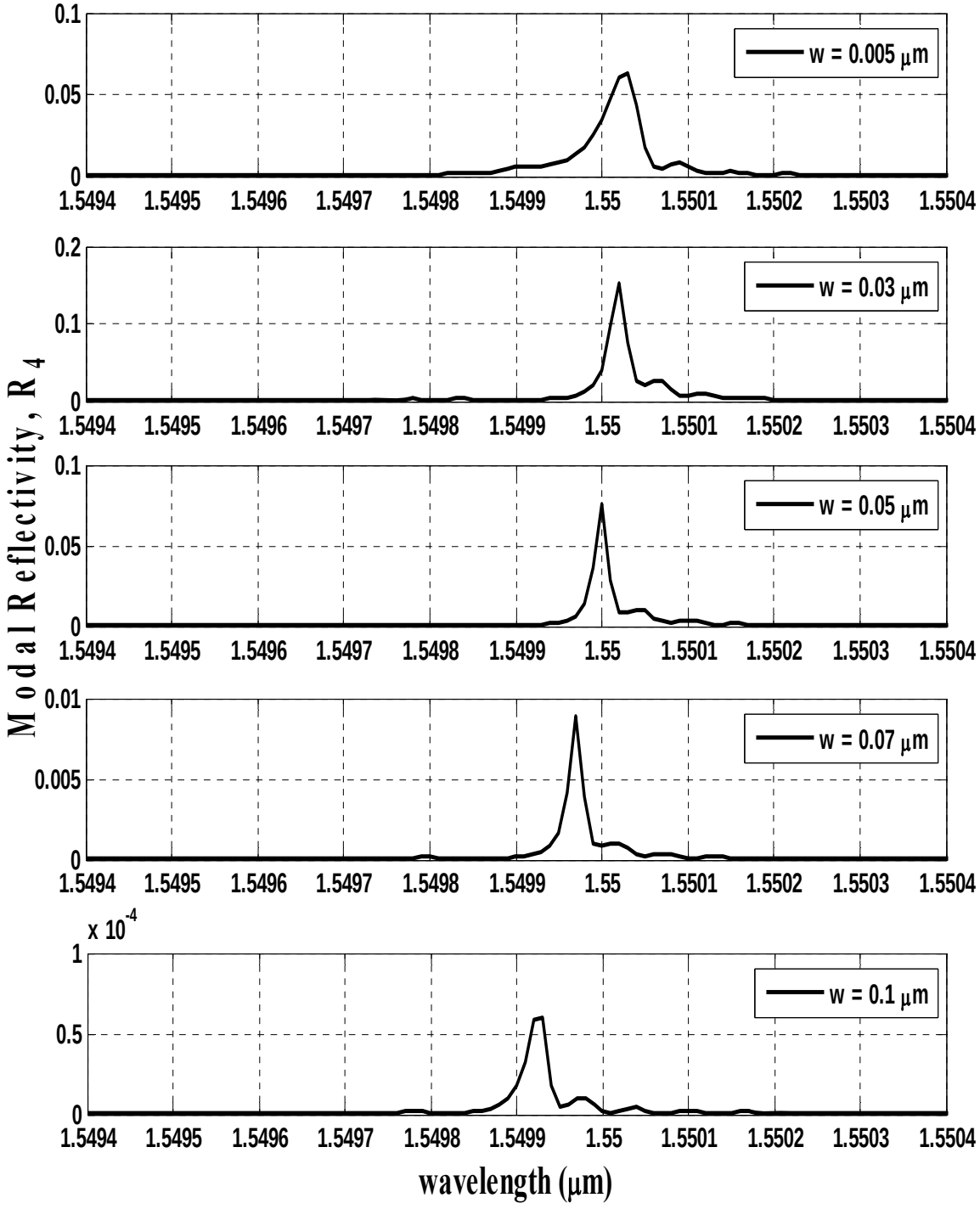

Figure 5.5 Modal Reflectivity R_4 versus wavelength at port 4 for different air groove widths.

5.4 Effect of the air groove length (L)

The width of the air groove is next fixed at 0.03 μm and the response of the WSDC for various air groove lengths is analyzed. Figure 5.6 shows the modal reflectivity R_1 versus wavelength at port 1 for different air groove lengths L = 1, 1.4, 1.6, 1.8 and 2 μm. Initially as the air groove length is increased from 1μm to 1.4 μm the reflectivity R_1 increases and attains a maximum of unity at 1.4 μm and maintains this maximum value as we increase the air groove length further.

For L = 1 μm the modal reflectivity R_1 equals 0.65 at the resonance wavelength of 1.54997 μm. As illustrated in Figure 5.6, the modal reflectivity R_1 has some small side lobes near the resonance wavelength and it is approximately zero at all other wavelengths. The spectral width in this case is 1Å. When L is increased from 1 μm to 1.4 μm, the spectral width of R_1 is seen to increase to 1.5 Å and the resonance wavelength is slightly shifted to the lower value of 1.54992 μm. At all other wavelengths throughout the spectrum R_1 is about zero with some ripples near the resonance wavelength. As the air groove length is increased above 1.4 μm, the spectral width of R_1 increases gradually and the resonance wavelength shifts to a lower value.

If we increase L further to 1.6 μm, the spectral width of R_1 increases to 2.2 Å. It increases further to approximately 4Å at L = 1.8 μm. The spectral width of R_1 at L = 2 μm is about 7 Å.

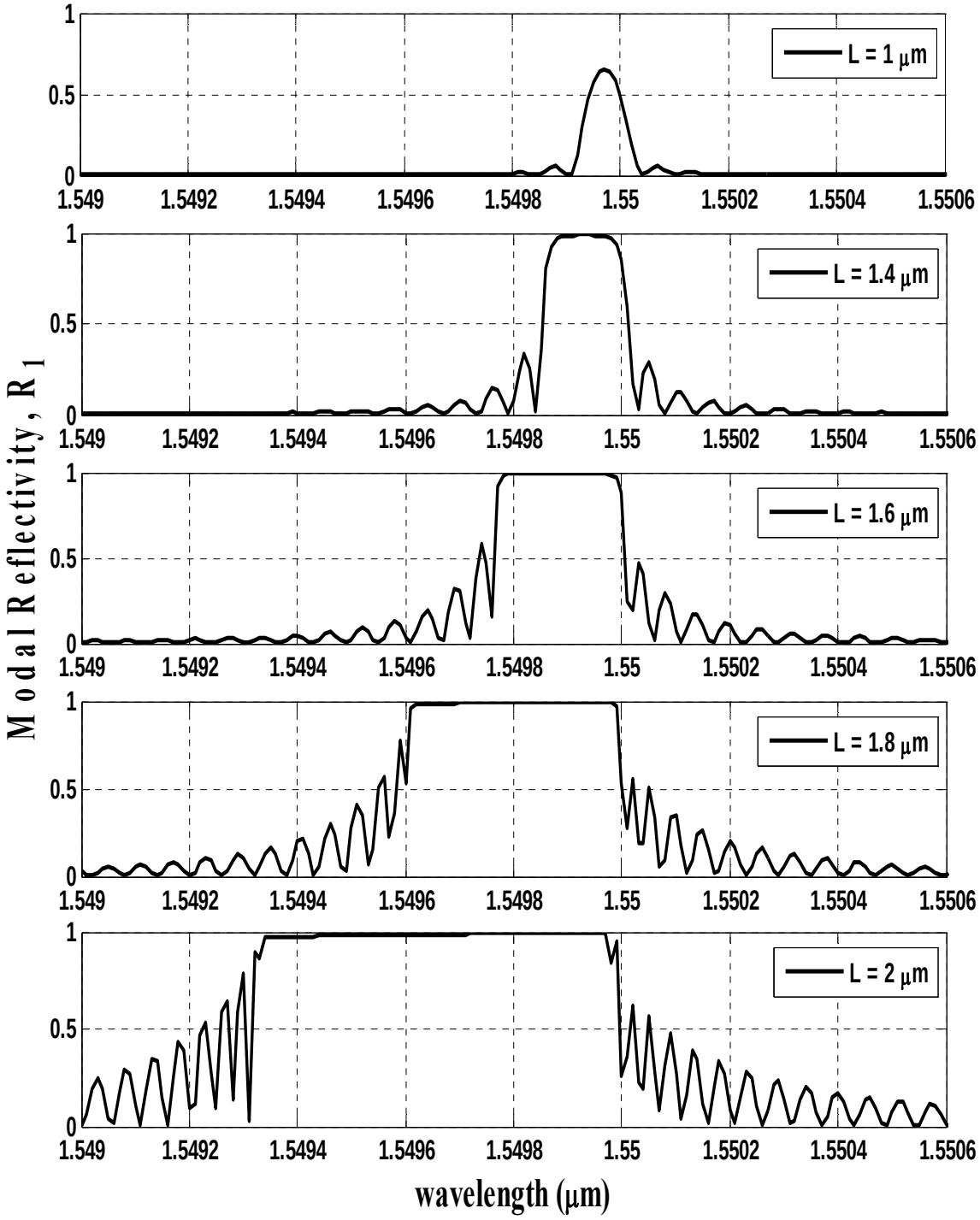

Figure 5.6 Modal Reflectivity R_1 versus wavelength at port 1 for varying air groove lengths.

The modal transmissivity T_2 versus wavelength at port 2 of the WSDC is illustrated in Figure 5.7 for the air groove lengths L = 1, 1.4, 1.6, 1.8 and 2 μm. At L = 1 μm the modal transmissivity T_2 is approximately 0.95 throughout the spectrum except for a spectral width of about 1Å where there is a dip in T_2. At the resonance wavelength of 1.54997 μm the modal transmissivity T_2 is ≈0.3. As the air groove length is increased, T_2 at the resonance wavelength decreases gradually and it becomes ≈zero at L = 1.4 μm. Here the spectral width of T_2 increases to ≈1.5 Å and the resonance wavelength is slightly shifted to the lower value of 1.54992 μm. At all other wavelengths throughout the spectrum, the modal transmissivity T_2 is ≈0.95 with some ripples near the resonance wavelength.

The modal transmissivity T_2 at the resonance wavelength retains the minimum of ≈zero as the air groove height is increased above 1.4 μm, its spectral width increases, and the resonance shifts to a shorter wavelength. At all other wavelengths the modal transmissivity T_2 retains a maximum value of ≈0.95 with small ripples in the neighborhood of the resonance wavelength.

At L = 1.6 μm, the spectral width of T_2 increases to ≈2.2 Å and it is ≈4Å at L = 1.8 μm. The spectral width of T_2 at L = 2 μm is ≈7 Å. The modal transmissivity T_2 at port 2 exhibits opposite behavior when compared with the modal reflectivity R_1 at port 1. As can be seen from Figure 5.7 it acts as a band-stop filter with the same spectral width as the modal reflectivity response R_1.

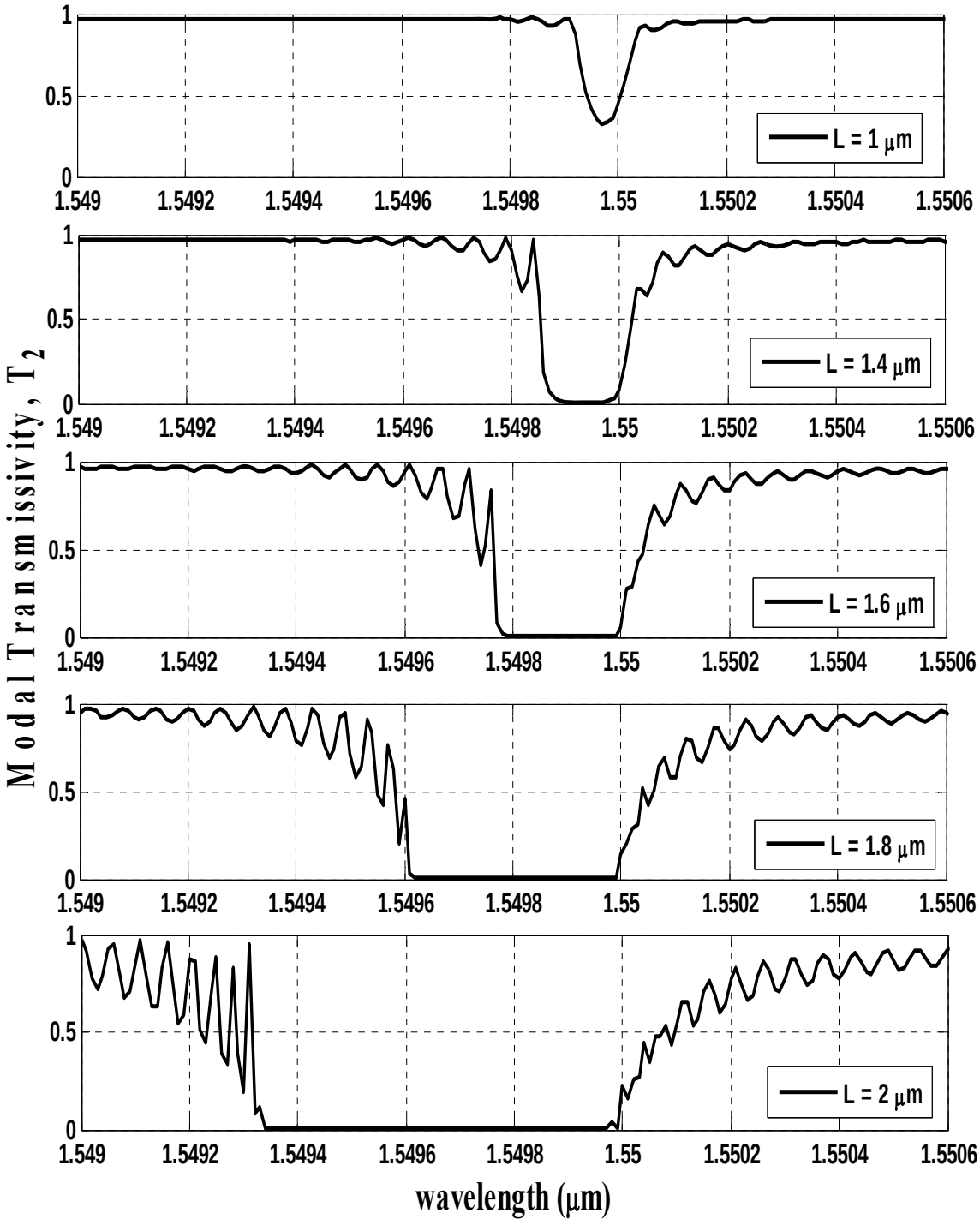

Figure 5.7 Modal Transmissivity T_2 versus wavelength at port 2 for varying air groove lengths.

The modal transmissivity T_3 at port 3 of the WSDC is illustrated in Figure 5.8 for the air groove lengths L = 1, 1.4, 1.6, 1.8 and 2 μm. The modal transmissivity T_3 remains low since the length of the WSDC is considered to be $0.25L_c$, at this length only a small amount of power is coupled to the port 3. For the air groove length L = 1 μm, as we move from the left hand side towards the right of the spectrum the modal transmissivity T_3 remains constant at ≈0.03, it drops to ≈zero at the wavelength of 1.54992 μm and then it starts to increase and the maximum of ≈0.075 occurs at 1.55002 μm, and again it drops with some ripples and remains constant at ≈0.03 for the wavelengths greater than 1.5504 μm.

For L = 1.4 μm, the maximum value of T_3 is ≈0.22 which occurs at 1.55002 μm. Maximum power is coupled to port 3 when the air groove length is L = 1.6 μm. As shown in Figure 5.8, the maximum value of modal transmissivity T_3 is ≈0.32 at the wavelength of 1.55002 μm, at all other wavelengths T_3 remains constant at ≈0.02. T_3 maintains the asymmetric spectrum for all the air groove lengths.

For L = 1.6, 1.8 and 2 μm, T_3 is very low as we move from the left of the spectrum, then it drops to ≈zero and then it peaks to ≈0.32 and continues with some lower peaks and slowly drops back with ripples and remains constant at ≈0.02. For L = 2 μm, multiple peaks of the modal transmissivity T_3 are prominent, in fact as illustrated by Figure 5.8, the first two peaks have a maximum value of ≈0.32 and then the peaks start to decrease gradually.

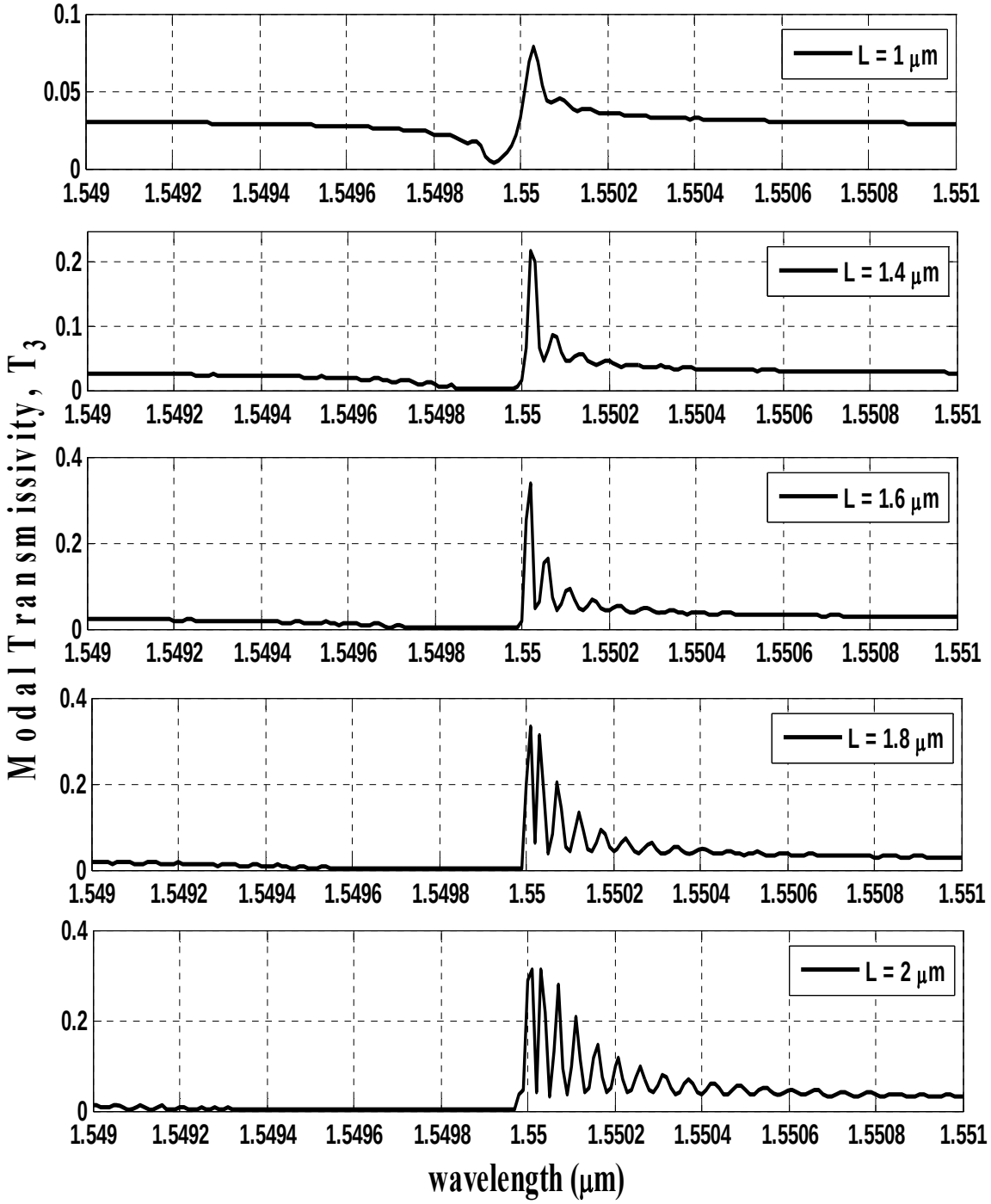

Figure 5.8 Modal Transmissivity T_3 versus wavelength at port 3 for varying air groove lengths.

The modal Reflectivity R_4 versus wavelength at port 4 of the WSDC is illustrated in Figure 5.9 for the air groove lengths L = 1, 1.4, 1.6, 1.8 and 2 μm. For L = 1 μm, as we move from the left hand side towards the right of the spectrum, the modal reflectivity R_4 is ≈zero continuously until the wavelength of 1.5499 μm, then it starts to increase slowly and the increase is substantial at 1.55 μm, it has a maximum of ≈0.04 which occurs at 1.55002 μm, and again it drops with some ripples and becomes ≈zero at 1.5502 μm and continues to be ≈zero throughout the right side of the spectrum.

The air groove length is increased above 1 μm. For L = 1.4 μm, as shown in Figure 5.9, the modal Reflectivity R_4 is ≈zero throughout the spectrum except for a spectral width of 0.2 Å. At the resonance wavelength of 1.55002 μm, the modal Reflectivity R_4 has a maximum of ≈0.15.

Maximum reflection into port 4 occurs when the air groove length is 1.6 μm. The modal Reflectivity R_4 peaks to ≈0.22 at 1.55001 μm. Hence it can be seen that the resonance wavelength is slightly shifting to a lower value. At L = 1.8 μm, R_4 has two equal peaks of ≈0.18 then it drops to ≈zero with some ripples. The spectrum of R_4 is asymmetric for all the air groove lengths. For L = 2 μm, the asymmetric nature of the spectrum of the R_4 is prominent and the maximum value of R_4 is ≈0.2.

Sum of R_1, T_2, T_3, R_4 at any wavelength is almost equal to unity, indicating negligible loss due to radiation.

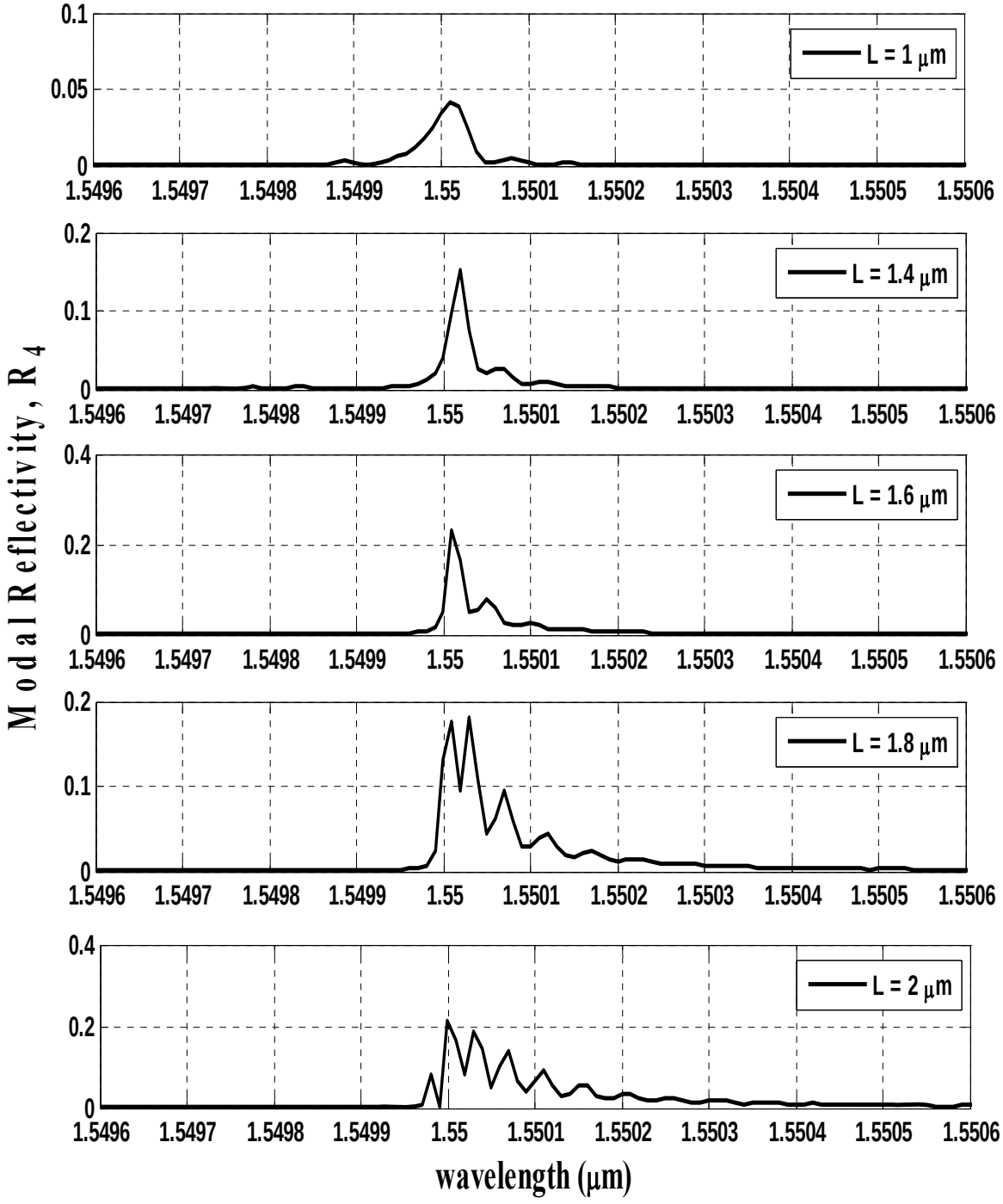

Figure 5.9 Modal Reflectivity R_4 versus wavelength at port 4 for varying air groove lengths.

5.5 Effect of the number of air groove periods

The width and length of the air grooves will be fixed at 0.03 μm and 1.4 μm, respectively. The length of the WSDC will be varied. In other words, the number of the air groove periods will be varied and the response of the WSDC is simulated. The different lengths of the WSDC considered are $0.25L_c$, $0.5L_c$, $0.75L_c$ and L_c. The length of the WSDC considered in the previous sections is $0.25L_c$.

Table 5.1 Different lengths and corresponding number of air groove periods of WSDC

S.No	Notation	Length of the WSDC in cm	Number of Periods
1	0.25 L_c	0.5376	23995
2	0.5 Lc	1.0753	47991
3	0.75 Lc	1.6130	71987
4	Lc	2.1507	95983

Figure 5.10 shows the modal reflectivity R_1 versus wavelength of WSDC at port 1 for four different lengths of the WSDC, $0.25L_c$, $0.5L_c$, $0.75L_c$ and L_c. When the length of the WSDC equals $0.25L_c$, R_1 is ≈zero on the left side of the spectrum and it slowly increases starting at the wavelength of ≈1.5494 μm with small ripples and attains the maximum of ≈unity at the resonance wavelength of ≈1.54992 μm, and again drops back to ≈zero with some ripples. From Figure 5.10 it is clear that the modal reflectivity R_1 exhibits a band- pass filter behavior with a spectral width of ≈1.5 Å.

When the length of the WSDC is increased to $0.5L_c$, the modal reflectivity R_1 is ≈zero on the left side of the spectrum and it slowly increases starting at the wavelength of ≈1.5495 μm with small ripples and attains the maximum of ≈unity around the resonance wavelength of 1.54992 μm. It then slowly drops back to ≈zero with some ripples. The ripples are denser than in the case of $0.25L_c$.

As the length of the WSDC is increased further to $0.75L_c$ and L_c, the modal reflectivity R_1 at the resonance wavelength retains the maximum value of unity, its spectral width remains almost constant at ≈1.5 Å, and its resonance wavelength also stays ≈constant at 1.54992 μm. At all other wavelengths throughout the spectrum it is ≈zero with some small ripples near the resonance wavelength.

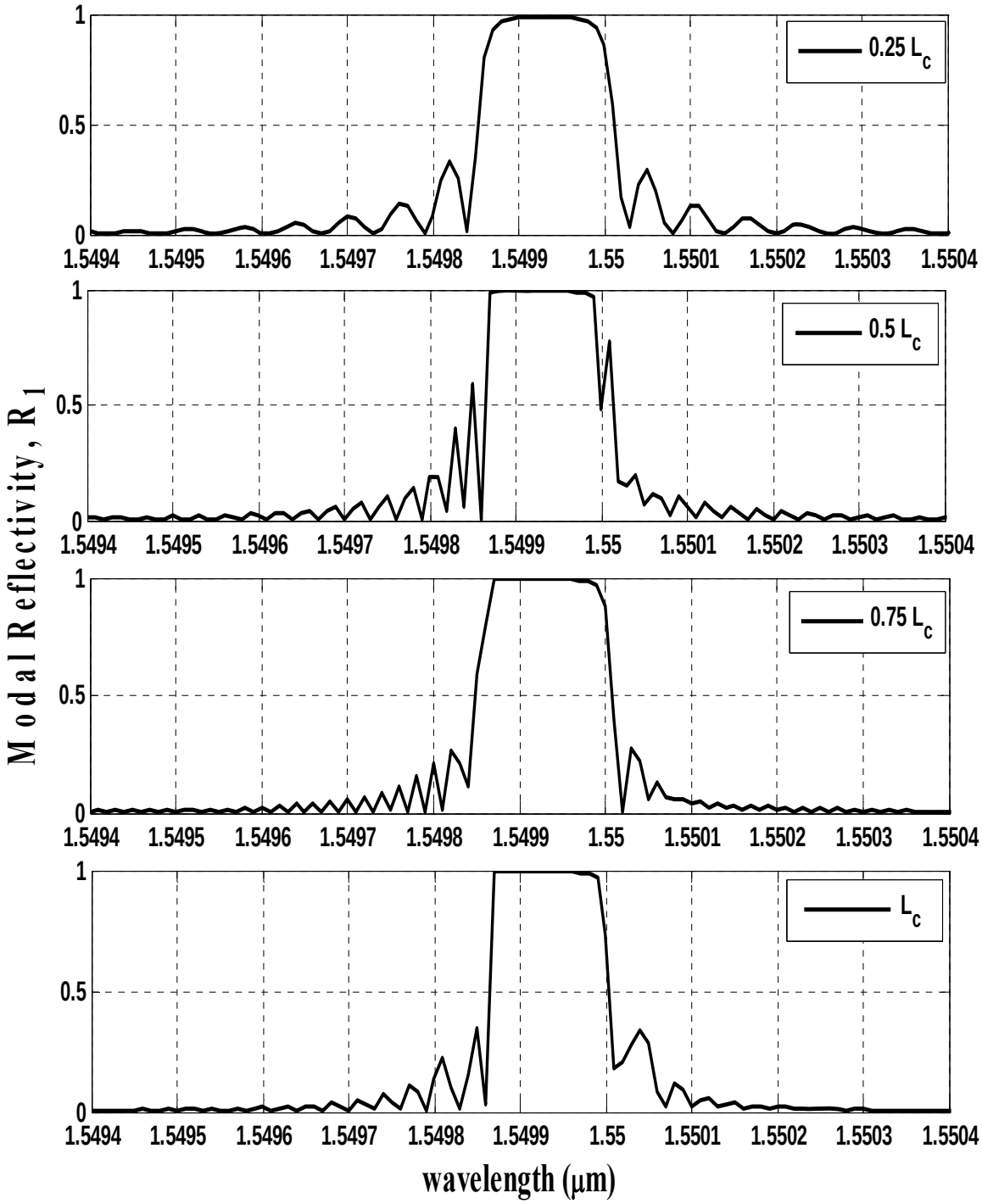

Figure 5.10 Modal Reflectivity R1 versus wavelength at port 1 for varying length of WSDC.

The modal transmissivity T_2 at port 2 of the WSDC is illustrated in Figure 5.11 for four different lengths of the WSDC $0.25L_c$, $0.5L_c$, $0.75L_c$ and L_c. When the length of the WSDC is $0.25L_c$, T_2 is approximately 0.95 throughout the spectrum except for a spectral width of about 1.5Å where there is a dip in T_2. At the resonance wavelength of 1.54992 μm T_2 drops to almost zero. Hence T_2 at port 2 exhibits opposite behavior when compared with the modal reflectivity R_1 at port 1. As can be seen from Figure 5.11 it acts as a band-stop filter with the spectral width of 1.5 Å.

When the length of the WSDC is increased to $0.5L_c$, T_2 is constant at nearly 0.9 at the left side of the spectrum with some ripples and it suddenly drops to almost zero at the wavelength of 1.54985 μm and retains the minimum of nearly zero until 1.55 μm and then it starts to increase slowly and reaches the maximum of approximately 0.9 at 1.5506 μm. The spectrum of T_2 has changed compared to the case of $0.25L_c$, here the drop is sudden but the rise is slow.

When the length of the WSDC is $0.75L_c$, T_2 is constant at almost 0.79 at the left side of the spectrum and increases slightly to approximately 0.82 with some ripples and it drops to near zero at the wavelength of 1.54985 μm and retains the minimum of zero until 1.55 μm and then it peaks to almost 0.3 and drops immediately to 0.1 and starts to increase slowly and reaches the maximum of approximately 0.79 at 1.551 μm. An additional peak appears here in the spectrum of T_2 which was not seen in the previous two cases ($0.25L_c$ and $0.5L_c$). The peak is prominent when the length of the WSDC is L_c. The maximum of the peak is nearly 0.38 and its spectral width is around 0.1Å.

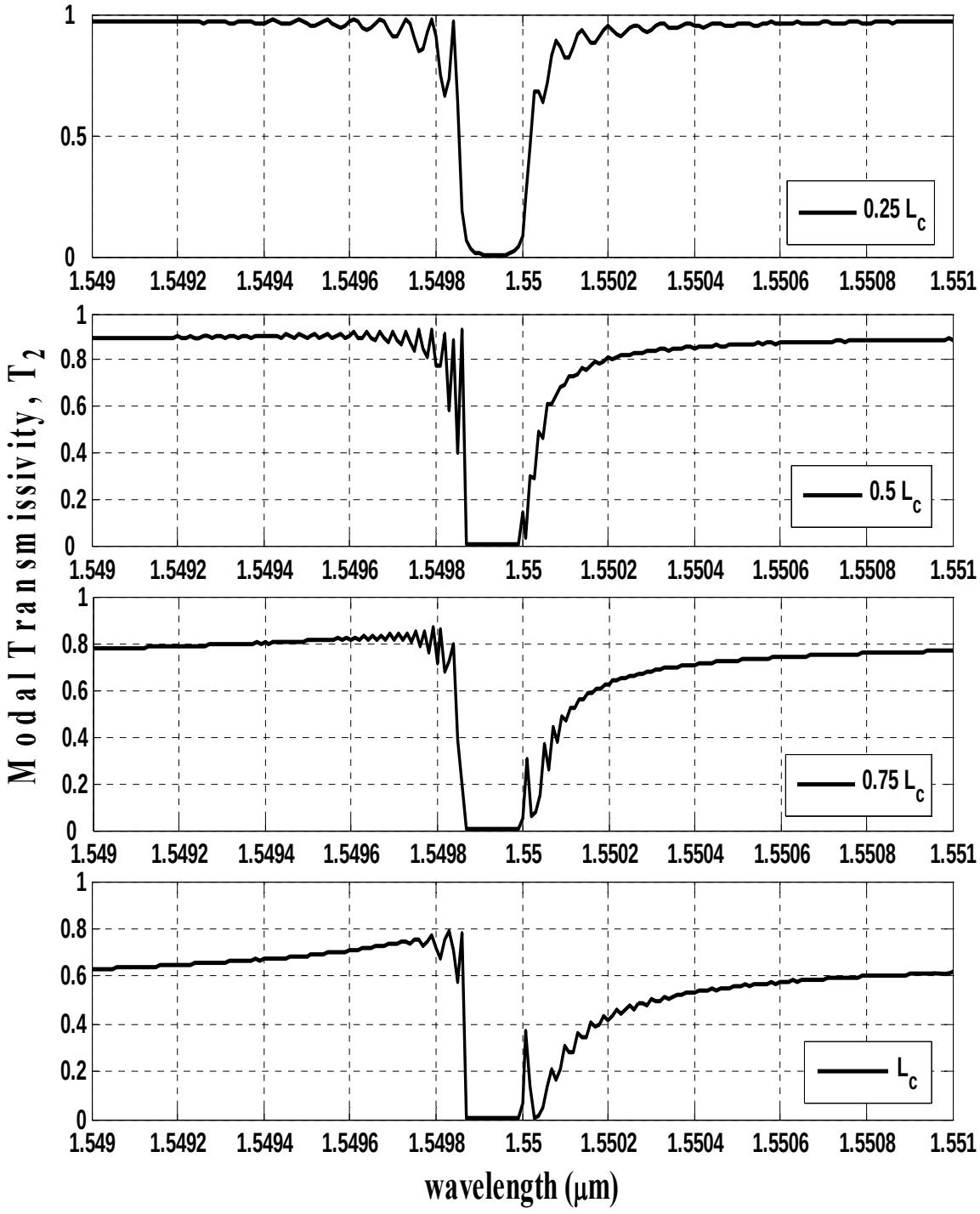

Figure 5.11 Modal Transmissivity T2 versus wavelength at port 2 for varying length of WSDC.

The modal transmissivity T_3 at port 3 of the WSDC is illustrated in Figure 5.12 for four different lengths of the WSDC $0.25L_c$, $0.5L_c$, $0.75L_c$ and L_c. When the length of the WSDC is $0.25L_c$, as we move from the left of the spectrum the modal transmissivity T_3 remains constant at approximately 0.03, it drops to nearly zero at the wavelength of 1.5499 μm and then it starts to increase and a maximum of around 0.22 occurs at 1.55002 μm, and again it drops with some ripples and remains constant at almost 0.03 for the wavelengths greater than 1.5504 μm.

When the length of the WSDC is increased to $0.5L_c$, T_3 peaks to ≈0.42 at the wavelength of 1.55002 μm, it is ≈zero from 1.5499 μm to 1.55 μm and is constant at ≈0.1 through out the spectrum. When the length of the WSDC is $0.75L_c$, T_3 increases and remains constant at ≈0.2 through out the spectrum, but it drops to ≈zero at 1.5499 μm and shoots to ≈0.9 at 1.55002 μm and then slowly drops to ≈0.2 at 1.5506 μm.

When the length of the WSDC is L_c, as we move from the left hand side towards the right of the spectrum the modal transmissivity T_3 remains constant at ≈0.38, it drops to ≈zero at the wavelength of 1.5499 μm and then it starts to increase and a maximum of ≈0.7 occurs at 1.55004 μm, and again it drops with some ripples and remains constant at ≈0.38 for the wavelengths greater than 1.5504 μm. Hence a substantial increase in T_3 through out the spectrum is observed as the length of the WSDC is increased.

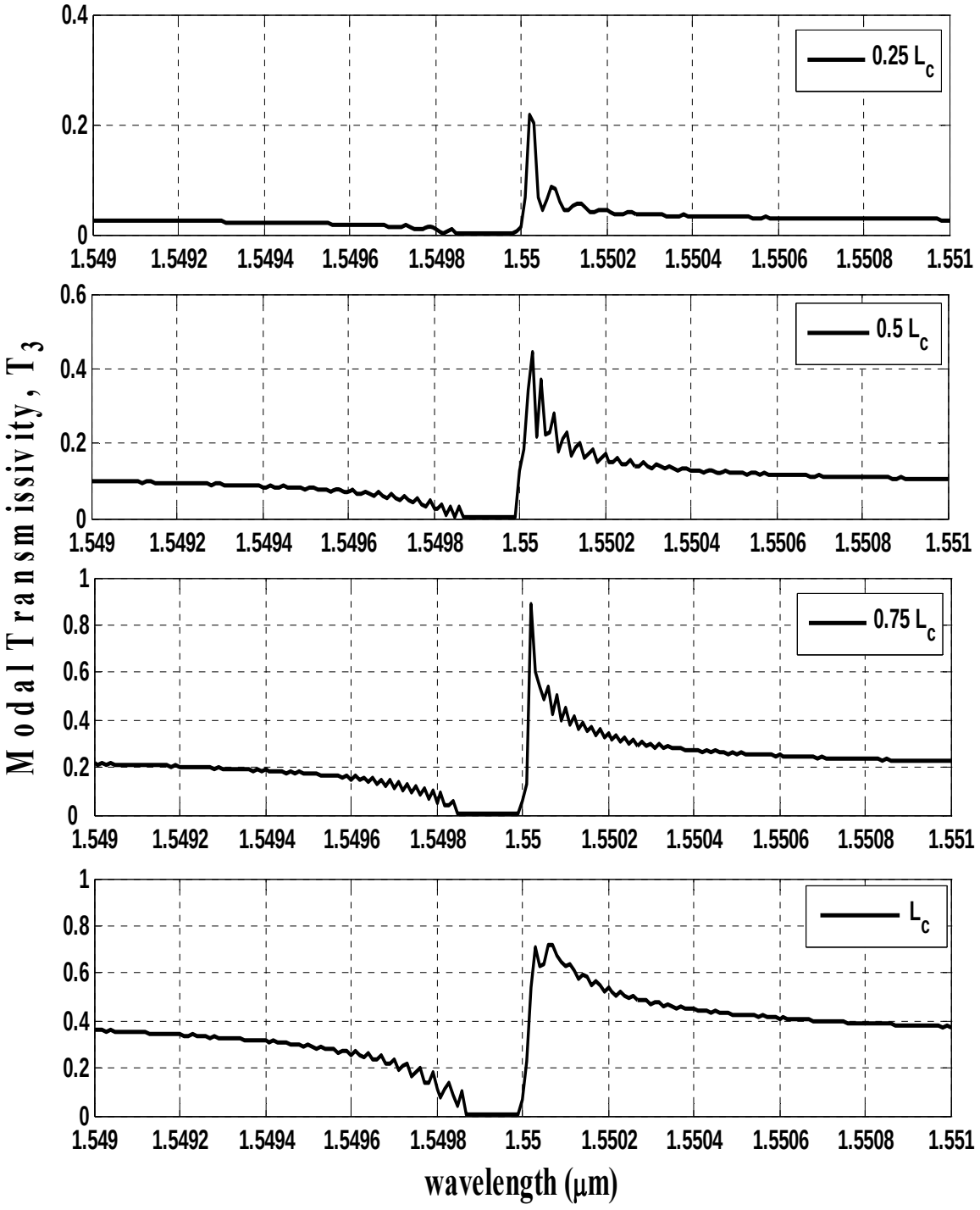

Figure 5.12 Modal Transmissivity T_3 versus wavelength at port 3 for varying length of WSDC.

The modal Reflectivity R_4 versus wavelength at port 4 of the WSDC is shown in Figure 5.13 for four different lengths of the WSDC $0.25L_c$, $0.5L_c$, $0.75L_c$ and L_c. When the length of the WSDC is $0.25L_c$, as we move from the left hand side towards the right of the spectrum, the modal reflectivity R_4 is ≈zero continuously until the wavelength of 1.5499 μm, then it starts to increase slowly and the increase is substantial at 1.55 μm, a maximum of ≈0.15 occurs at 1.55002 μm, and again it drops to ≈zero with some ripples at 1.5502 μm and continues to be ≈zero throughout the right side of the spectrum. The spectral width of R_4 in this case is 0.2 Å.

Maximum reflection into port 4 occurs when the length of the WSDC is $0.5L_c$. The modal Reflectivity R_4 peaks to ≈0.25 at the wavelength of 1.55 μm. Another peak of ≈0.18 occurs immediately at ≈1.55002 μm and then R_4 slowly drops to ≈zero and stays at zero through out the spectrum. The spectrum of R_4 is asymmetric in this case.

When the length of the WSDC is increased to $0.75L_c$, as we move from the left of the spectrum, R_4 is ≈zero until the wavelength of 1.5494 μm, then it starts to increase slowly and drops suddenly to ≈zero at 1.54985 μm, and then it shoots to ≈0.15, and again it drops to ≈zero with some ripples at 1.5506 μm and continues to be ≈zero throughout the right side of the spectrum. A similar response occurs when the length of the WSDC is L_c, a peak of ≈0.2 occurs here.

Sum of R_1, T_2, T_3, R_4 at any wavelength is almost equal to unity, indicating negligible loss due to radiation.

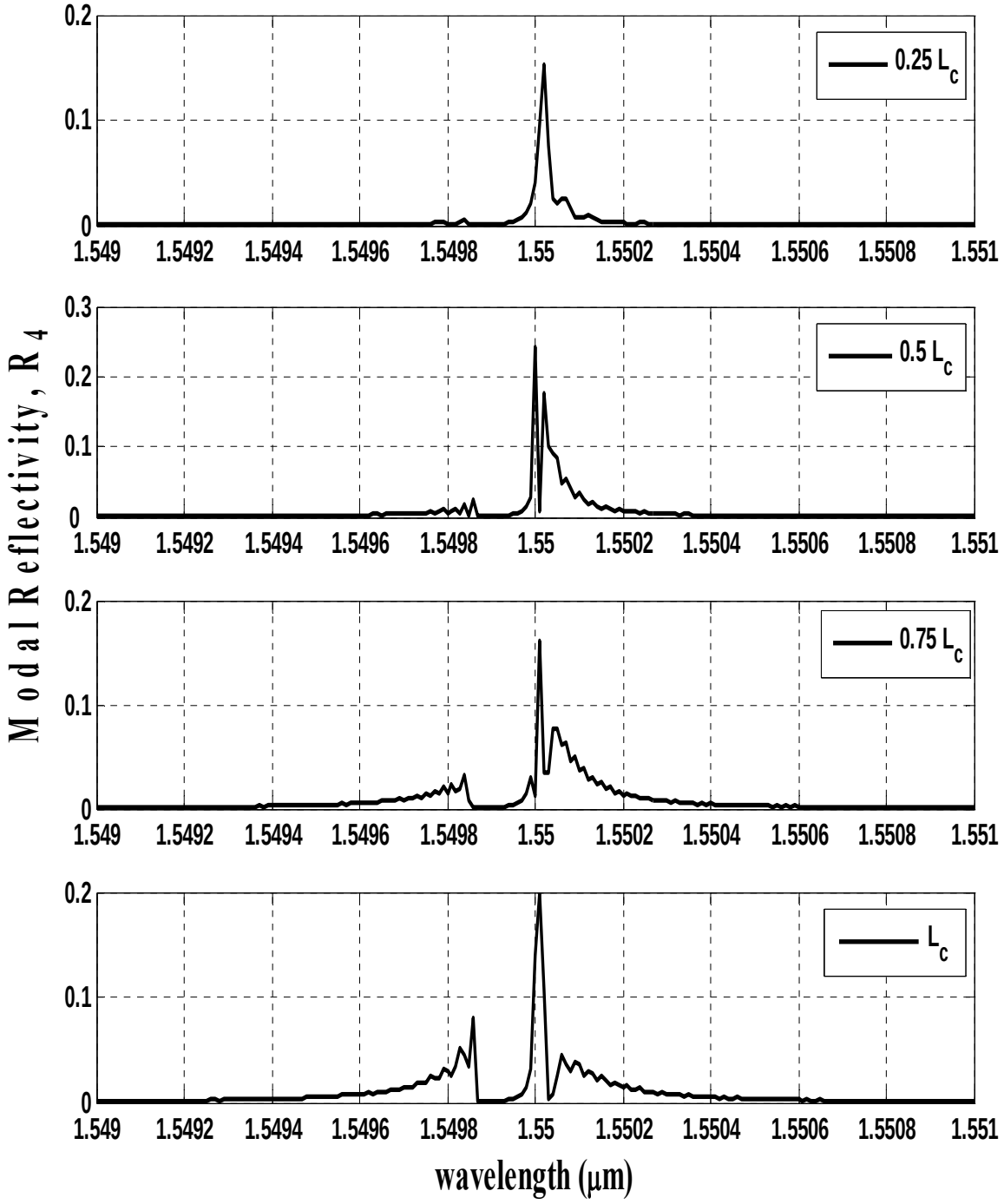

Figure 5.13 Modal Reflectivity R4 versus wavelength at port 4 for varying length of WSDC.

5.6 Power swapping between ports 1 and 4

Figure 5.14 shows the spectral response of the WSDC at all the four ports. Here the air groove width (w) is 0.03 μm and length (L) is 1.4 μm and the length of WSDC is $0.25L_c$. The modal reflectivity R_1 at port 1 of the WSDC attains the maximum of ≈unity at the resonance wavelength of 1.54992 μm. From the Figure 5.14 it is clear that the modal reflectivity R_1 exhibits a band-pass filter behavior with a spectral width of 1.5 Å.

The modal transmissivity T_2 at port 2 of the WSDC is ≈0.95 through out the spectrum except for a spectral width of 1.5 Å there is a dip in T_2. At the resonance wavelength of 1.54992 μm T_2 drops to zero. As we move from the left of the spectrum the modal transmissivity T_3 at port 3 of the WSDC remains constant at ≈0.03, it drops to zero at the wavelength of 1.5499 μm and then it starts to increase and a maximum of ≈0.22 occurs at 1.55002 μm, and again it drops with some ripples and remains constant at ≈0.03 for the wavelengths greater than 1.5504 μm.

The modal reflectivity R_4 at port 4 of the WSDC is ≈zero continuously from the left of the spectrum until the wavelength of 1.5499 μm, then it starts to increase slowly and its maximum of ≈0.15 occurs at 1.55002 μm, and again it drops to ≈zero with some ripples at 1.5502 μm and continues to be ≈zero throughout the right side of the spectrum. The spectral width of R_4 in this case is 0.2 Å.

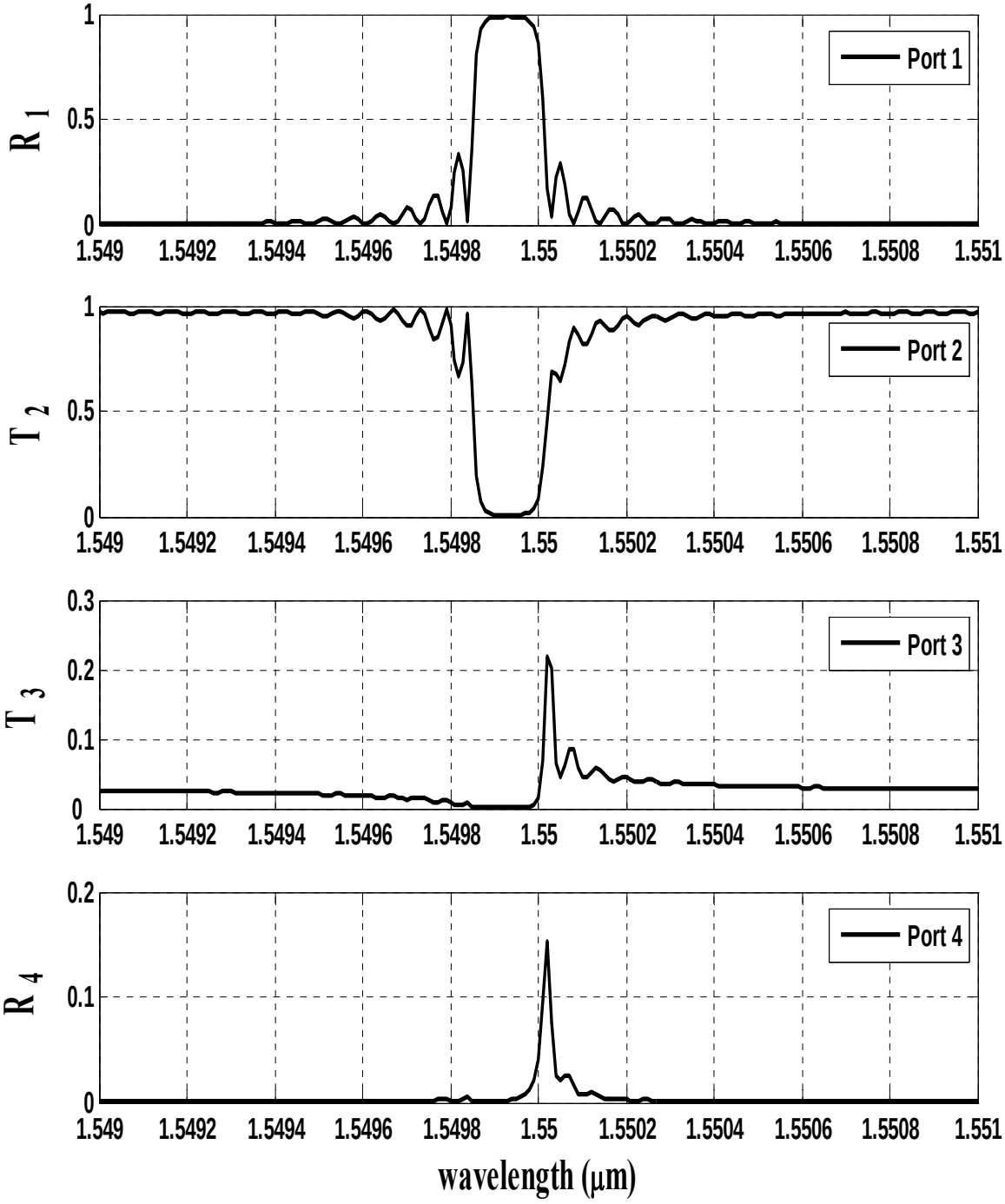

Figure 5.14 Spectral responses of all ports of WSDC

If maximum optical power of unity is desired at port 4 of the WSDC instead of port 1, it is possible to do so by swapping the power spectra between ports 1 and 4. This can be achieved by appending a directional coupler section at the input of the WSDC as shown is Figure 5.15. If the length of the appended directional coupler section is $0.5L_c$, then the power can be completely swapped between ports 1 and 4 as demonstrated in Figure 5.16.

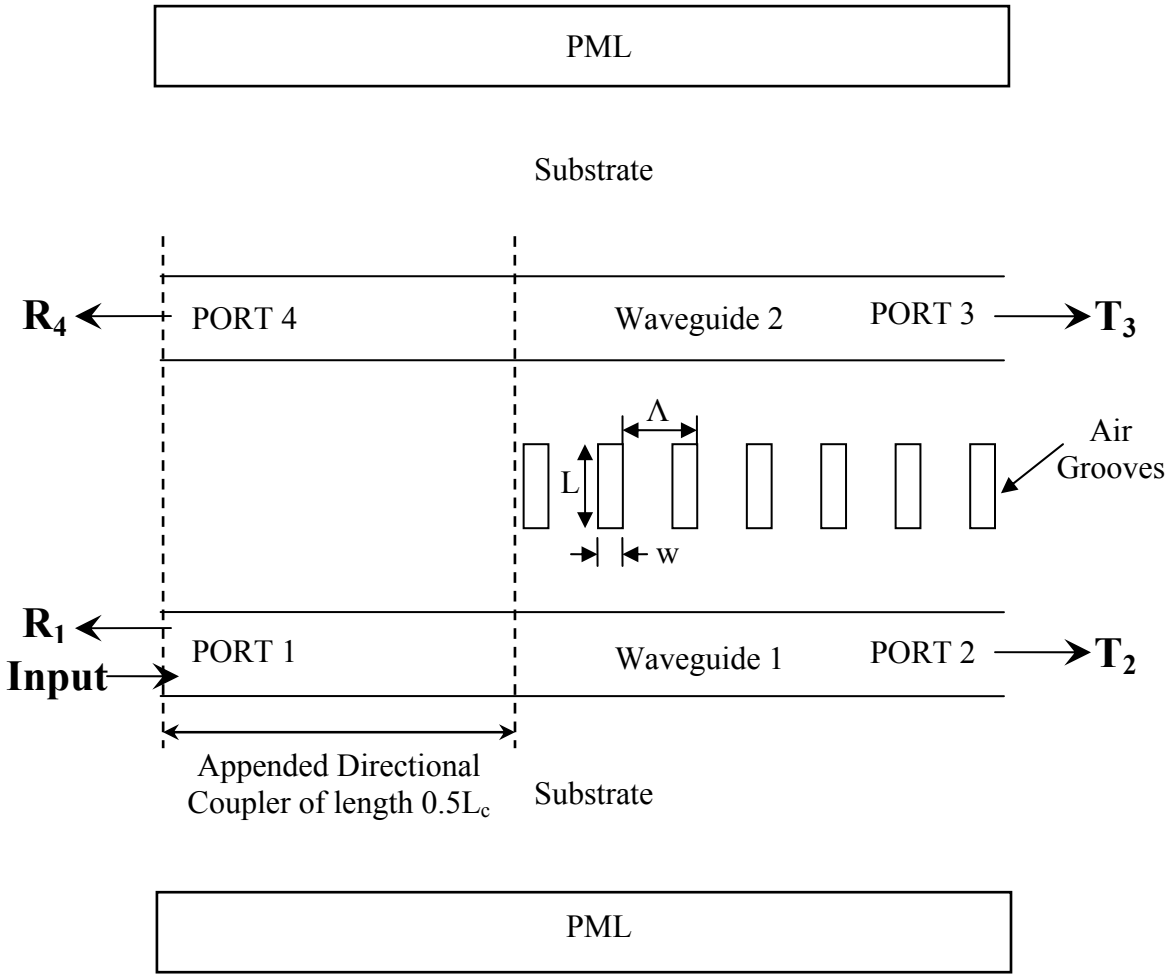

Figure 5.15 Directional Coupler section appended to WSDC at the input.

Since a directional coupler section of length $0.5L_c$ is appended at the input of the WSDC, the incident TE_0 modal field at the input propagates a distance of half of L_c through the added directional coupler section. The field undergoes partial coupling before it is launched into the WSDC. The reflected field is also propagated back through the added directional coupler section and then the reflectivities R_1 and R_4 are calculated. This arrangement causes R_1 and R_4 of ports 1 and 4 respectively to be effectively swapped as illustrated by the following Figure 5.16. The modal reflectivity R_1 now has a peak of 0.15 at the wavelength 1.55002 μm, and the modal reflectivity R_4 exhibits a band-pass filter behavior with a maximum of ≈0.98 and a spectral width of ≈1.5Å.

Since the actual input to the WSDC is no longer a pure TE_0 modal field of the isolated waveguide, the transmissivities T_2 and T_3 differ from those shown in Figure 5.14. The modal transmissivity T_2 at port 2 of the WSDC decreases from ≈0.95 to ≈0.35 throughout the spectrum. The dip to near zero within a spectral width of ≈1.5 Å remains the same.

There is a substantial increase in the modal transmissivity T_3 at port 3 of the WSDC. Previously it was very low at ≈0.03 throughout the spectrum with a peak of ≈0.22 at the wavelength 1.55002 μm (see Figure 5.14). With the addition of the Directional Coupler section at the input of the WSDC the modal transmissivity T_3 has increased to ≈0.65 throughout the spectrum, except for a spectral width of 1.5 Å there is a dip in T_3. Hence the modal transmissivity T_3 behaves as a band-stop filter with a spectral width of 1.5 Å.

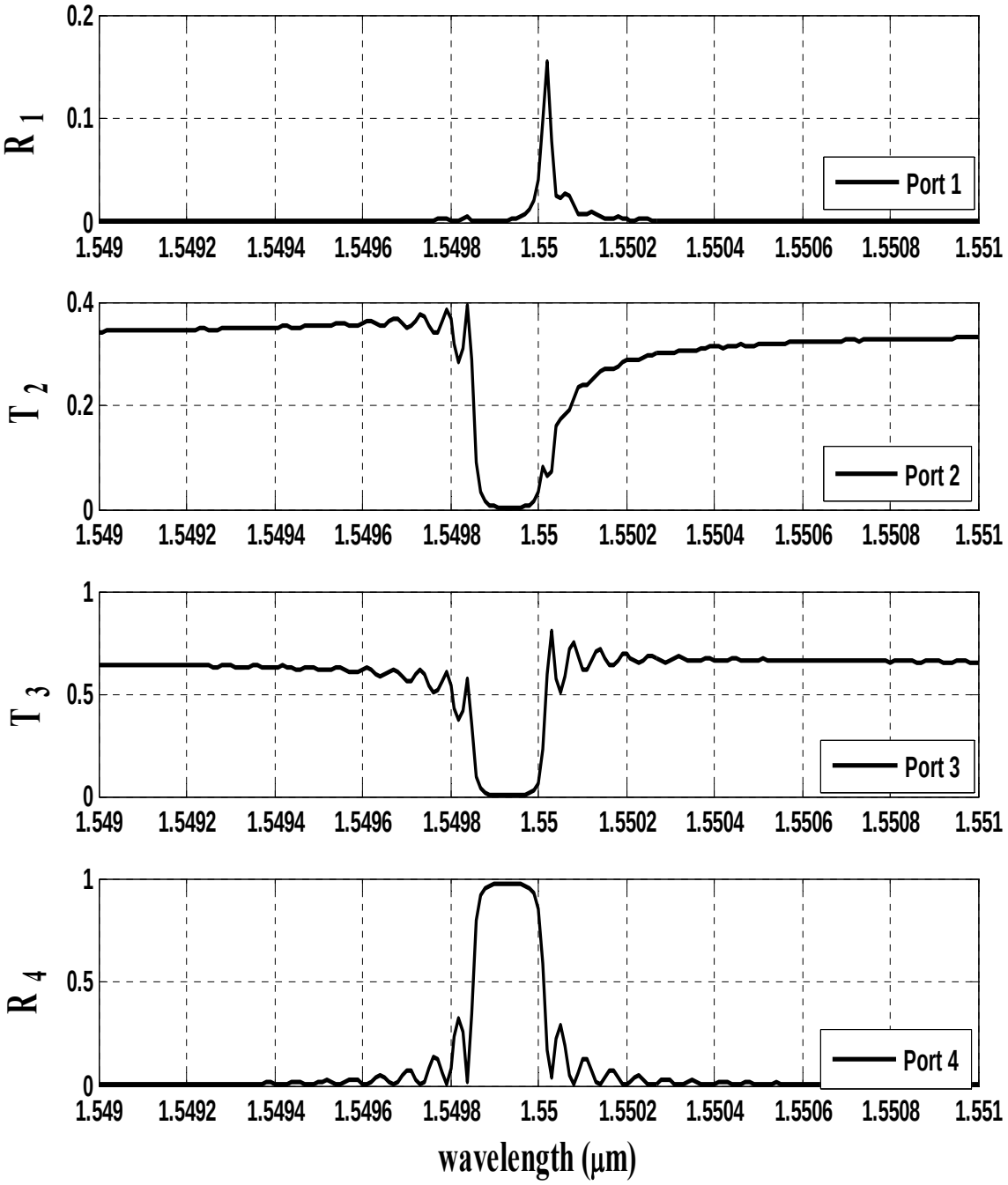

Figure 5.16 Spectral response of all ports of WSDC appended with a 0.5Lc long Directional Coupler section.

5.7 Equal power in ports 2 and 3

Optical power can be equally divided between the ports 2 and 3 when the air groove width is set at 0.1 μm, its length is 1.4 μm, with an added directional coupler section of length $0.5L_c$ to a length $0.25L_c$ of the WSDC. Figure 5.17 shows the spectral response of all the four ports of the resulting structure.

The modal reflectivity R_1 at port 1 is almost negligible with a peak of $\approx 0.6\times10^{-4}$ at the wavelength 1.54994 μm. The modal transmissivity T_2 at port 2, as we move from the left of the spectrum, remains almost constant at ≈0.5, it drops with some ripples to a minimum value of about 0.025 at the wavelength of 1.54985 μm and then it rises back to 0.5 at 1.5499 μm and remains constant at 0.5 throughout the right side of the spectrum. The spectral width of the dip is ≈1 Å.

The modal transmissivity response T_3 at port 3 is very similar to the modal transmissivity response T_2 at port 2. The modal reflectivity R_4 at port 4 acts as a band-pass filter with a peak of ≈0.95 at the resonance wavelength of 1.54985 μm with a spectral width of ≈1 Å. In this case, we can see almost complete drop of the power from port 1 into port 4 within the pass-band. Outside the pass-band, the device acts as equal power divider between ports 2 and 3.

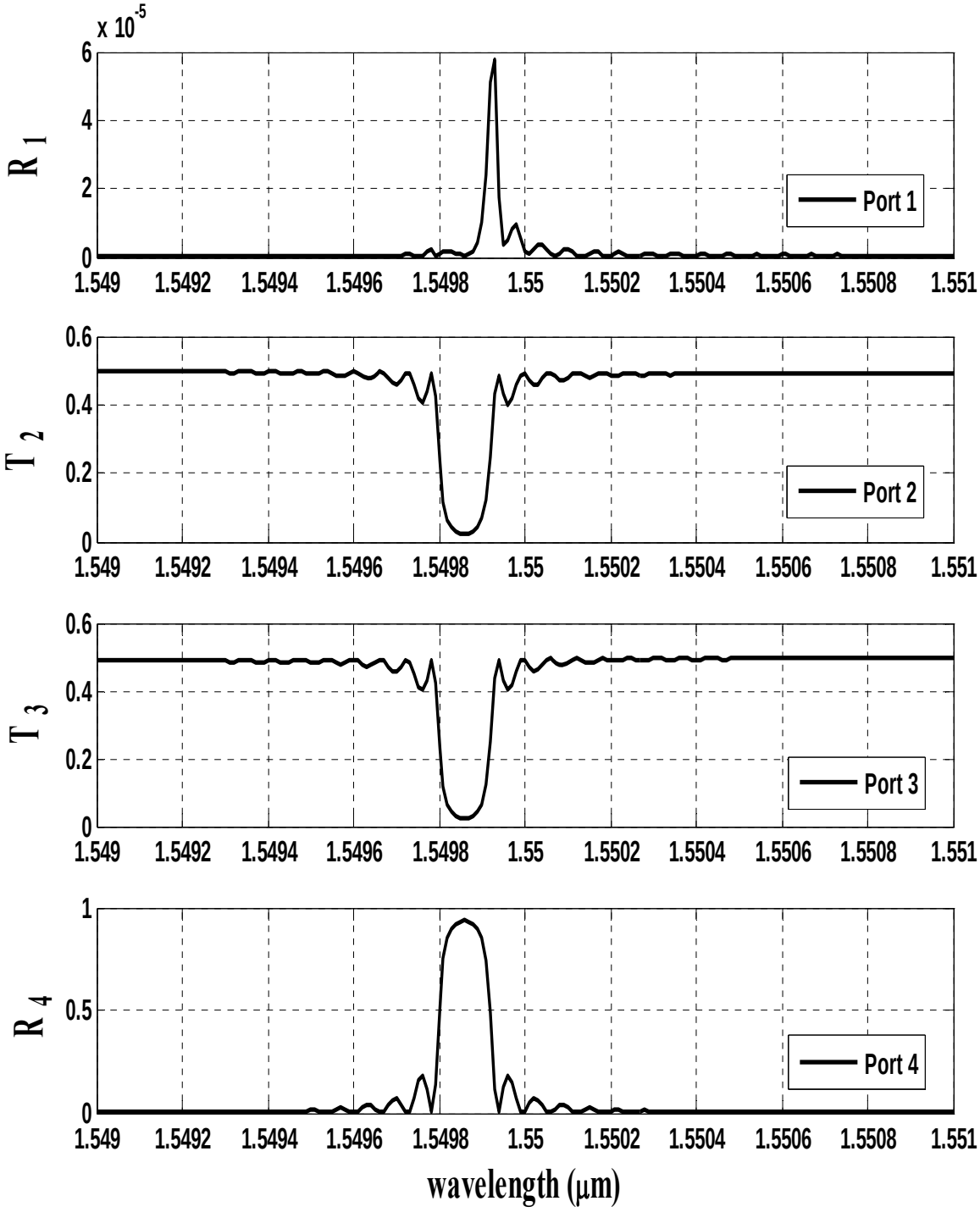

Figure 5.17 Equal powers in ports 2 and 3 of the WSDC with Directional Coupler

5.8 Special case of a sub-Angstrom filter

Consider the WSDC with a 3.2 μm separation between the two slab waveguides. The length of the device is L_c = 5.9898 cm, the air groove width is 0.09 μm and its length is 1.5 μm. The device response was calculated using these specifications. Figure 5.18 illustrates the calculated spectral response of all the four ports in this case.

The modal reflectivity R_1 at port 1 of the WSDC is ≈zero on the left side of the spectrum and it slowly increases with small ripples and attains the maximum of ≈unity at the resonance wavelength of 1.54994 μm, and again drops back to ≈zero with some ripples. The modal transmissivity T_2 at port 2 is the reverse action of the modal reflectivity R_1 at port 1 as can be seen from Figure 5.18. It stays at the maximum of ≈unity with a drop to ≈zero at the wavelength of 1.54994 μm

The modal transmissivity T_3 at port 3 of the WSDC is ≈zero throughout the spectrum but peaks to ≈0.2 at the wavelength of 1.54996 μm. The spectral width of T_3 is ≈0.1 Å. The modal reflectivity R_4 at port 4 of the WSDC is also ≈zero throughout the spectrum but peaks to ≈0.18 at the wavelength of 1.54996 μm and its spectral width is ≈0.1 Å.

Hence the modal transmissivity T_3 at port 3 and the modal reflectivity R_4 at port 4 can be used as sub-Angstrom filters since their spectral width is ≈0.1 Å.

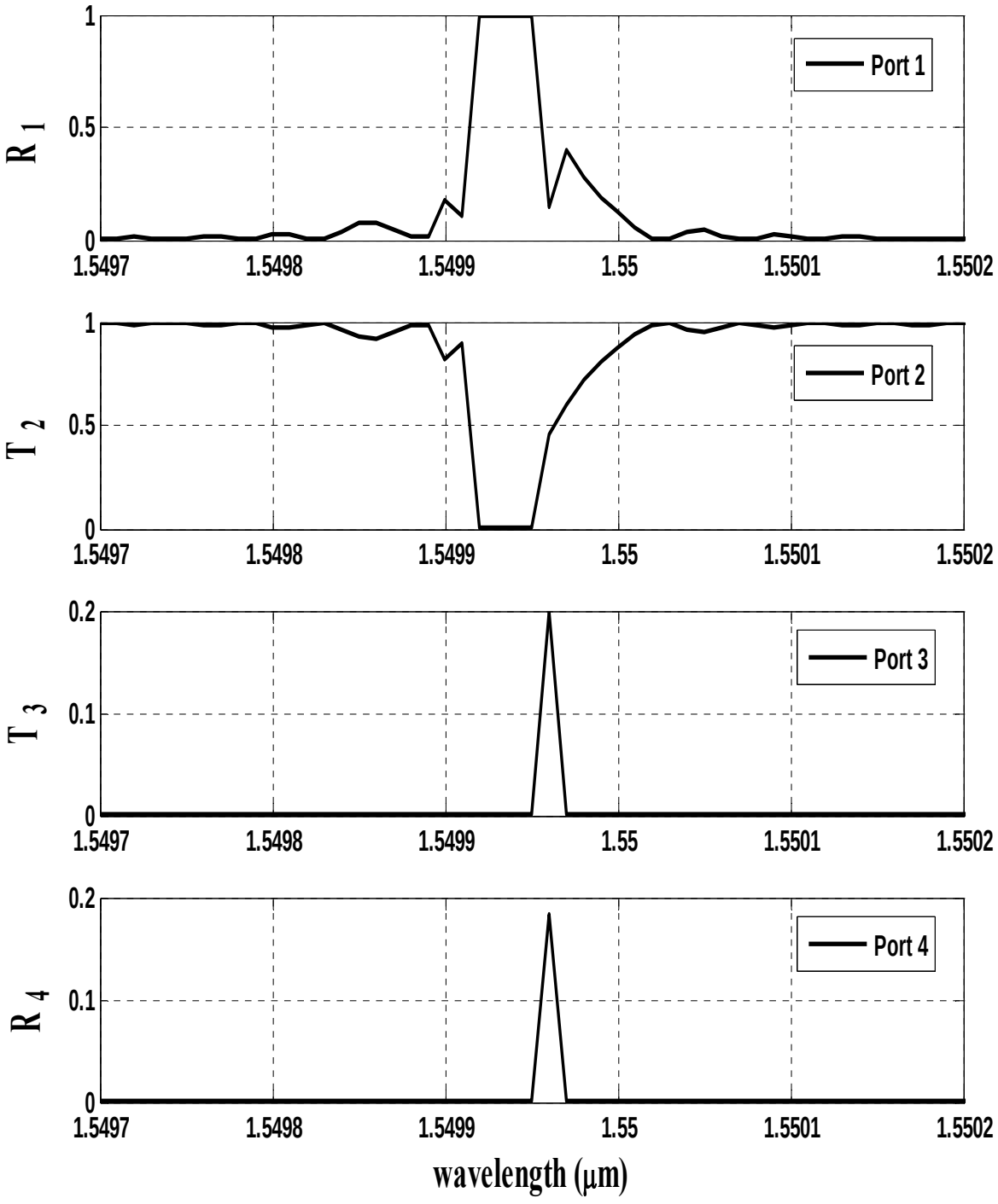

Figure 5.18 Sub-Angstrom filter at ports 3 and 4 of the WSDC

5.9 WSDC with two rows of periodic air grooves

A WSDC with two rows of periodic air grooves is simulated next. A schematic diagram of the structure is shown in Figure 5.19. The waveguides have a refractive index of 3.5. The surrounding media has a refractive index of 3.4. Both waveguide core widths are 0.8 μm. The waveguides are kept 2.8 μm apart. The computational window is 11.4 μm wide and the mesh size along x-axis is set at 50 nm.

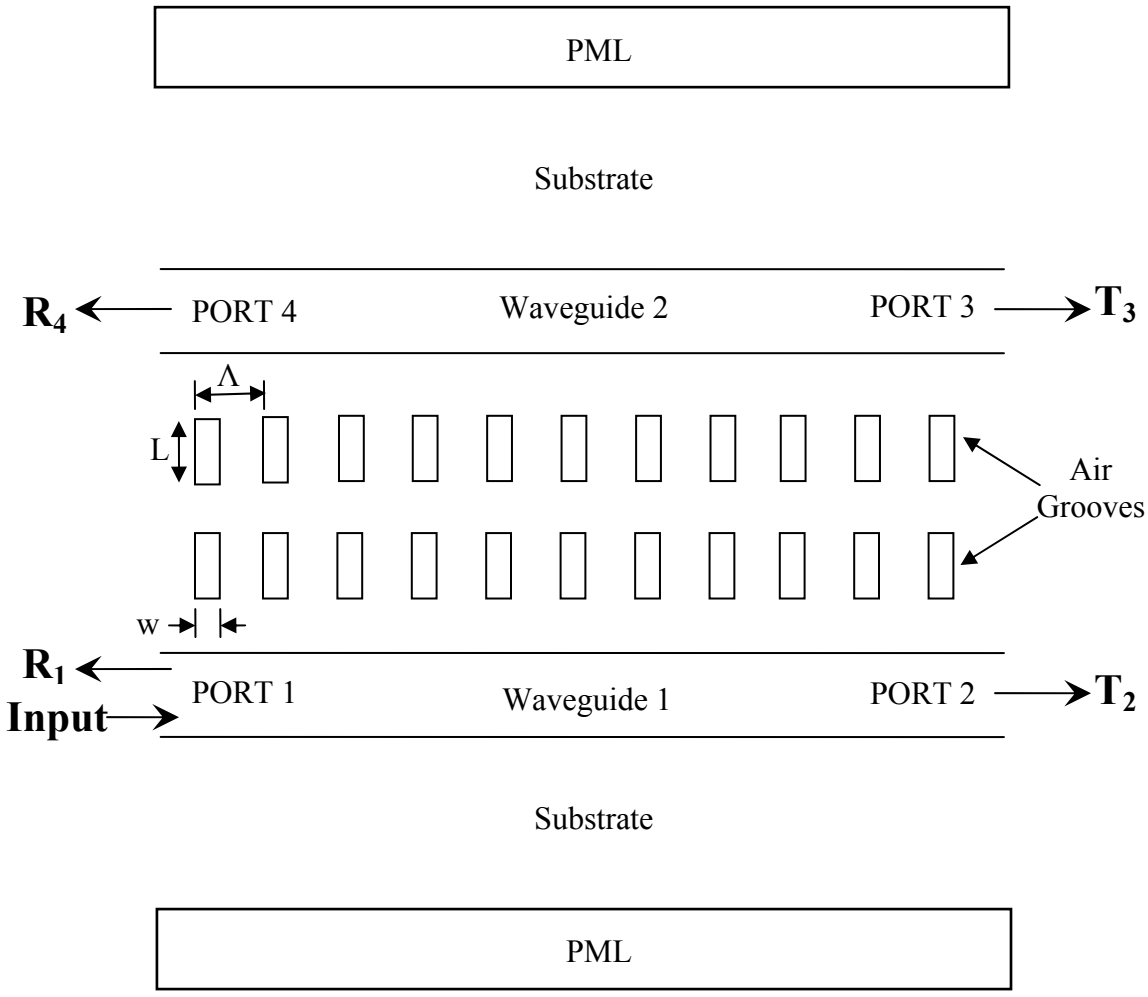

Figure 5.19 WSDC with two rows of periodic air grooves

The length of the WSDC is taken to be $0.25L_c$ which equals 0.537675 cm. The period of the air grooves is 0.224079 μm (calculated using equation 5.1). Thus the number of the air groove periods is 23995. The air groove width (w) considered is 0.03 μm and its height (L) is 0.5 μm.

Figure 5.20 illustrates the spectral response of all four ports of the WSDC with two rows of periodic air grooves. The modal reflectivity R_1 at port 1 is ≈zero at the left side of the spectrum and it slowly increases with small ripples and attains the maximum of ≈unity at the resonance wavelength of 1.5499 μm, and again drops back to ≈zero with some ripples.

The modal transmissivity T_2 at port 2 is ≈0.95 throughout the spectrum except for a spectral width of ≈2.2 Å there is a dip in T_2. The modal transmissivity T_3 remains constant at ≈0.03, it drops to ≈zero at the wavelength of 1.5497 μm and then it starts to increase and a maximum of ≈0.3 occurs at 1.55 μm, and again it drops with some ripples and remains constant at ≈0.03 for the wavelengths greater than 1.5504 μm.The modal reflectivity R_4 is ≈zero through out the spectrum, but has a peak of ≈0.18 at 1.55 μm.

The device responses with two rows and single row of periodic air grooves appear to be similar. The impact of varying air groove width, length and the number of the periods on this device is also similar. For this reason, detail analysis of the device response with two rows of air grooves will not be carried out. It does not appear to us that using two rows of air grooves results in any interesting features.

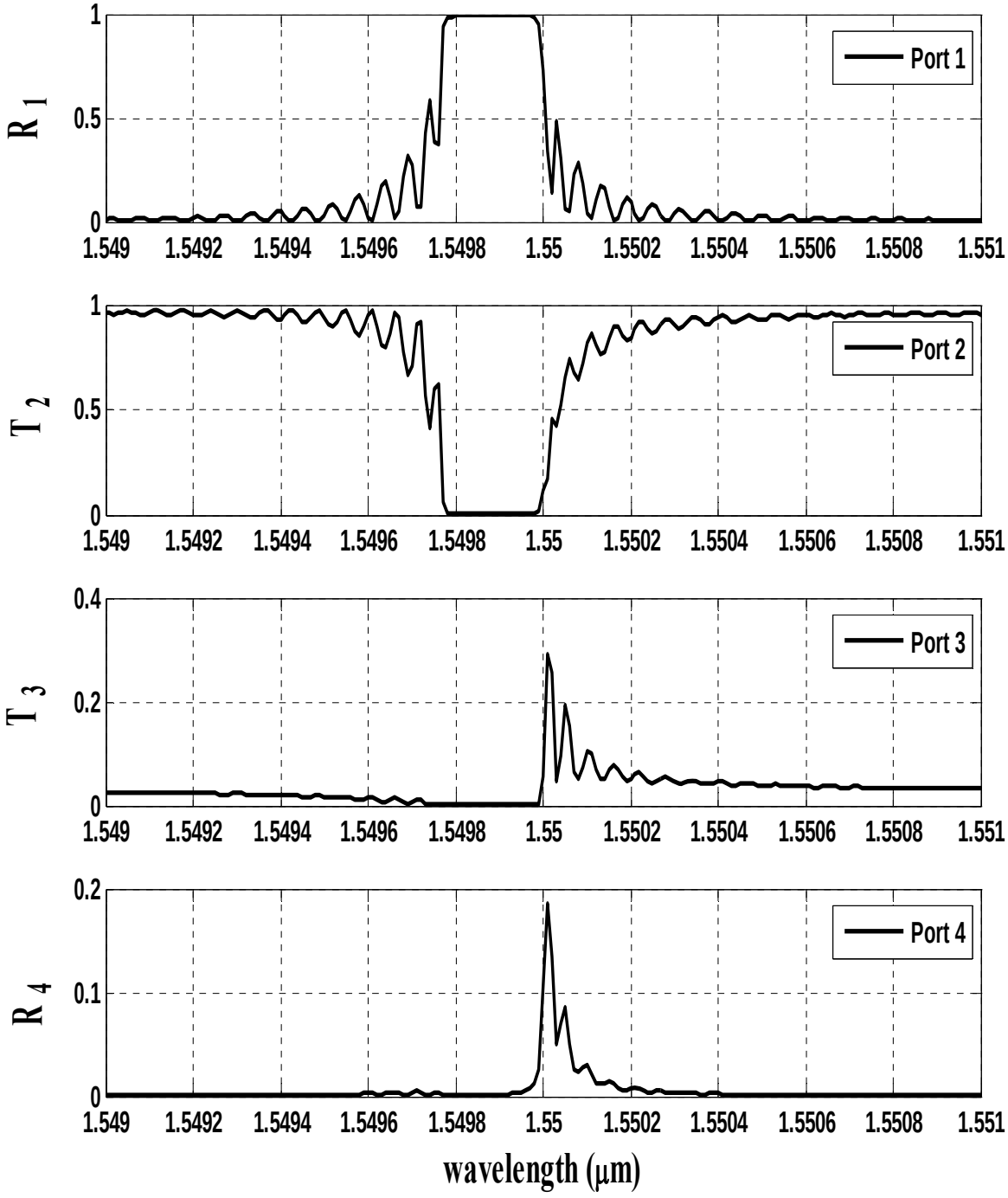

Figure 5.20 Spectral response of all the ports of WSDC with two rows of air grooves

CHAPTER 6

SUMMARY, CONCLUSION AND FUTURE WORK

6.1 Introduction

In this thesis work Method of Lines has been used for the analysis of Wavelength Selective Directional Coupler (WSDC) with air grooves. A three point non-uniform mesh is used in the MOL. The cascading and doubling approach is utilized for this purpose. An absorbing PML layer of tan-profile has also been implemented. In this chapter a brief summary of the work that has been carried out in this thesis is presented followed by conclusions and some suggestions for extension of the work.

6.2 Summary

• An MOL code has been developed and tested. The method utilizes a three point central difference approximation of the transverse second derivative operator with non-uniform discretizations for the analysis of the WSDC.

• A PML with absorbing boundary conditions with a tangent loss profile has been incorporated into the MOL code and tested.

• The cascading and doubling approach was incorporated into the MOL to analyze multiple longitudinal discontinuities. The results of the developed computer program were compared with the literature.

• The WSDC with single and two rows of air grooves have been simulated with the MOL using the cascading and doubling algorithm.

• The spectral response of four ports of the WSDC has been investigated by calculating the modal reflectivities/transmissivities of the ports.

• The influence of the length, width and the number of periodic air grooves on the coupling and filtering characteristics of the WSDC have been highlighted.

6.3 Conclusions

• Simulation results show that it is possible to drop approximately 100% of the power at a certain wavelength from the input waveguide of the WSDC.

• An increase in the width of the air grooves tends to deteriorate the coupling of optical power into port 3 and also reduces the reflection into port 4. In a specific range of the air groove widths almost 100% of the incident optical power is reflected into the input port at a certain wavelength (with a spectral width of ≈1.5 Å), which if required can be transferred to a port in the other waveguide. This can be done by power swapping of the ports on the input side by adding a $0.5L_c$ long directional coupler section without air grooves.

• An increase in the length of the air grooves increases the spectral width of the modal reflectivity R_1 at port 1 and the modal transmissivity T_2 at port 2.

• An increase in the length of the WSDC drops the optical power from port 2 and couples it to port 3.

• An interesting special case of the WSDC with air grooves has been noted. In this special case the ports 3 and 4 of the WSDC can be used as band-pass filters with a spectral width of 0.1 Å.

6.4 Extensions

There is always a room for extension in any research work. We have analyzed the WSDC with air grooves. The two identical and parallel slab waveguides of the WSDC were assumed to be surrounded by a material with refractive index 3.4. In this case the length of our device was 0.537675 cm. For integration purpose the length of the device need to be reduced. It may be possible to decrease the length of this device by replacing the surrounding material with air, and the air grooves with posts of some high index material as shown in Figure 6.1. This new device may yield better reflections into port 4; at the same time the coupling efficiency may also improve, and may result in a shorter device.

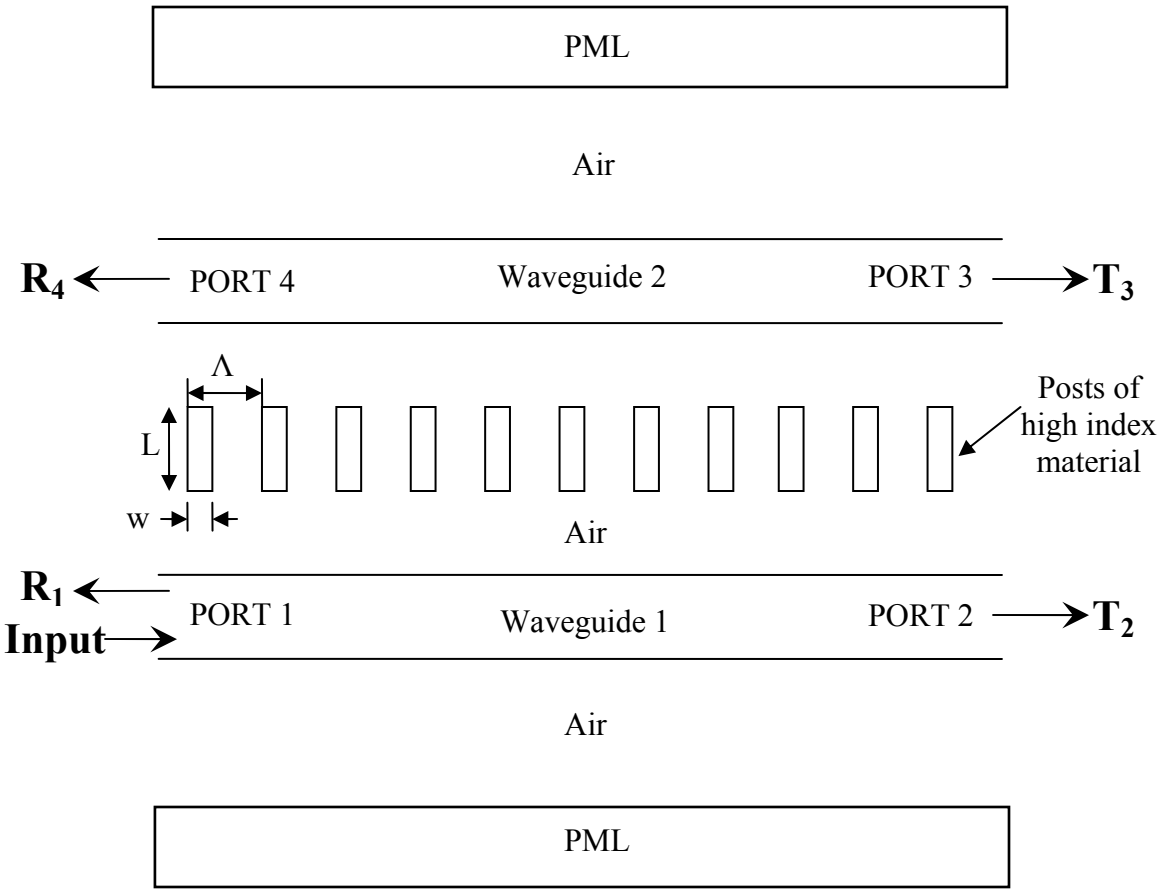

Figure 6.1 WSDC with posts of high index material

BIBLIOGRAPHY

[1]. S. E. Miller, “Light propagation in generalized lens like media,” Bell Syst. Tech. Journal, vol. 44, PP.2017-2064, 1965.

[2]. S. E. Miller, "Integrated optics: An introduction," *Bell Syst. Tech. Journal*, vol. 48, pp. 2059-2069, 1969.

[3]. H. Kogelnik, "An Introduction to Integrated Optics," *Microwave Theory and Techniques, IEEE Transactions on*, vol. 23, pp. 2-16, 1975.

[4]. V. Evtuhov and A. Yariv, "GaAs and GaAlAs Devices for Integrated Optics" *Microwave Theory and Techniques, IEEE Transactions on*, vol. 23, pp. 44-57, 1975.

[5]. J. Farina, "Integrated optics: Theory and technology," *Quantum Electronics, IEEE Journal of*, vol. 19, pp. 770, 1983.

[6]. R. Syms, J. Cozens, “Coupled mode devices,” in *Optical Guided Waves and Devices*, (McGraw-Hill International Ltd., 1992), pp. 1-31.

[7]. Weiping Huang, Brent E. Little and Sujeet K. Chaudhuri, “A New Approach to Grating-Assisted Couplers” *JOURNAL OF LIGHTWAVE TECHNOLOGY, VOL. 9, NO. 6, JUNE 1991*

[8]. Giora Griffel and Amnon Yariv, “Frequency Response and Tunability of Grating-Assisted Directional Couplers” *IEEE JOURNAL OF QUANTUM ELECTRONICS, VOL. 27. NO. 5. MAY 1991*

[9]. Giora Griffel, M. Itzkovich, and Amos A. Hardy, "Coupled Mode Formulation for Directional Couplers with Longitudinal Perturbation" *IEEE JOURNAL OF QUANTUM ELECTRONICS, VOL. 27, NO. 4, APRIL 1991*

[10]. Vittorio M. N. Passaro, "Optimal Design of Grating-Assisted Directional Couplers", *Journal of Lightwave Technology, vol 18, no 7, July 2000.*

[11]. Nai-Hsiang Sun, Jerome K. Butler, Gary A. Evans, Lily Pang, and Phil Congdon, "Analysis of Grating-Assisted Directional Couplers Using the Floquet–Bloch Theory" *Journal of Lightwave Technology, vol 15, no 12, December 1997*

[12]. Goran Z. Masanovic, Vittorio M. N. Passaro, Graham T. Reed, "Dual Grating-Assisted Directional Coupling Between Fibers and Thin Semiconductor Waveguides" *IEEE PHOTONICS TECHNOLOGY LETTERS, VOL. 15, NO. 10, OCTOBER 2003*

[13]. Feng Liu, Harry Hier, and Terrance L. Worchesky, "Dual-Side Processed Demultiplexer Using Grating-Assisted Codirectional Coupler" *IEEE PHOTONICS TECHNOLOGY LETTERS, VOL. 17, NO. 3, MARCH 2005*

[14]. Dug-Bong Kim, Chan-Yong Park, Beom-hoan O, Hong-Man Kim, and Tae-Hoon Yoon, "Fabrication of Sidelobe-Suppressed InP–InGaAsP Vertical Coupler Optical Filter Using Pair Grating Structure" *IEEE PHOTONICS TECHNOLOGY LETTERS, VOL. 10, NO. 11, NOVEMBER 1998.*

[15]. Yu-Heng Jan, Greg A. Fish, Larry A. Coldren, and Steven P. DenBaars, "Demonstration of InP–InGaAsP Vertical Grating- Assisted Codirectional Coupler Filters and Receivers with Tapered Coupling Coefficient Distributions" IEEE PHOTONICS TECHNOLOGY LETTERS, VOL. 9, NO. 7, JULY 1997

[16]. Hajime Sakata and Shinsuke Takeuchi, “Grating Assisted Directional Coupler Filters Using AlGaAs/GaAs MQW Waveguides” IEEE PHOTONICS TECHNOLOGY LETTERS, VOL. 3, NO. 10, OCTOBER 1991

[17]. S. Tanaka, K. Utaka, T. Yamamoto, M. Horita and Y. Matsushima, “Proposal of New Narrow-band Wavelength Filter using Grating-assisted Vertical Contra-directional Coupler” *KDD Research and Development Laboratories*

[18]. Chan-Yong Park, Bug-Bong Kim, Seung-Won Lee, Kwang-Ryong Oh, Hong-Man Kim, and Kwang-Eui Pyun, “High Performance Directional Coupler filter using novel phase-shift pair grating” *ECOC98,20-24 September 1998.*

[19]. Jeong Hwan Song, Jong Hoon Lim, Ryun Kyung Kim, Kyung Shik Lee, Kyoung-Youm Kim, Jaegeol Cho, Dongkyoon Han, Suntae Jung, Yunkyung Oh, and Dong-Hoon Jang, “Bragg Grating-Assisted WDM Filter for Integrated Optical Triplexer Transceivers” *IEEE PHOTONICS TECHNOLOGY LETTERS, VOL. 17, NO. 12, DECEMBER 2005*

[20]. H. M. Masoudi, M. Al-Sunaidi, and J. M. Arnold, “Time-domain finite difference beam propagation method,” IEEE Photonics technology Letters, vol. 11, pp. 1274-1276, Oct. 1999.

[21]. R. Scarmozzino. A. Gopinath, R. Pregla, and S. Helfert, “Numerical techniques for modeling guided-wave photonic devices,” IEEE Journal of selected topics in Quantum Electronics, vol. 6, No. 1, pp. 150-162, Jan. 2000.

[22]. S. T. Chu and S. K. Chaudhuri, "A finite-difference time-domain method for the design and analysis of guided-wave optical structures," *Journal of Lightwave Technology*, vol. 7, pp. 2033-2038, Dec. 1989.

[23]. S. T. Chu, S. K. Chaudhuri, and W. P. Huang, "Analysis of optical guided-wave devices with the finite-difference time-domain method," *Antennas and Propagation Society International Symposium*, vol. 1, pp. 257 - 260, July 1992.

[24]. R. J. Hawkins and R. McLeod, "Finite-difference time-domain simulations of linear integrated photonic devices," *Antennas and Propagation Society International Symposium*, vol. 1, pp. 261, July 1992.

[25]. K. Taneja and A. Sharma, "Reflection characteristics of guided wave bragg gratings using the collection method," *SPIE Proceeding, International conference on fiber optics and photonics,* vol. 3666, pp. 112-119, April 1999.

[26]. Rahman and J. Davies, "Finite-element solution of integrated optical waveguides," *Journal of Lightwave Technology*, vol. 2, pp. 682 - 688, Oct 1984.

[27]. J. P. Webb and J. B. Davies, "Finite Element Analysis of Long Optical structures," presented at Electromagnetic Field Computation, 1992. Digest of the Fifth Biennial IEEE Conference on, 1992.

[28]. N. Mabaya and P. E. Lagasse, "Finite Element Analysis of Optical Waveguides," presented at Microwave Symposium Digest, 1980 MTT-S International, 1980.

[29]. T. P. Young, "Design of integrated optical circuits using finite elements," *Science, Measurement and Technology, IEE Proceedings A*, vol. 135, pp. 135-144, 1988.

[30]. U. Rogge and R. Pregla. "Method of lines for the analysis of strip loaded optical waveguides," *Optical society of America (B)*, vol. 8 pp. 459-463, Feb. 1991.

[31]. J. Geres and R. Pregla, "Beam-propagation algorithm based on the method of lines," *Optical society of America (B),* vol. 8, pp. 389-394, Feb. 1991.

[32]. J J Gerdes “Bidirectional eigen mode propagation analysis of optical waveguides based on method of lines.” *Electronics Letters*, 30(7) 550, March 1994.

[33]. Jose Rodriguez, R. D. Crespo, and S. Fernandez. “Radiation losses on discontinuities in integrated optical waveguides.” *Optical Engineering,* 38(11) 1896-1906, November 1999.

[34]. Al-Bader S. J. and Jamid H. A. “Mode scattering by a non-linear step-discontinuity in dielectric optical waveguides”. *IEEE Transactions on Microwave theory and Techniques*, 44(2) 218-224, February 1996.

[35]. J. Gerdes, B. Lunitz, D. Benish, and R. Pregla, “Analysis of slab waveguide discontinuities including radiation and absorption effects,” *Electronics Letters*, vol. 28, p. 1013, May 1992.

[36]. S. T. Peng and T. Tamir. “TM mode perturbation analysis of dielectric gratings.” *Applied Physics*, 7(35) 35-38, 1975.

[37]. W. D. Yang and R. Pregla, “Method of lines for analysis of waveguide structures with multi-discontinuities,” *Electronics Letters,* vol. 31, p. 892, May 1995.

[38]. R. Pregla and W. Yang, “Method of lines for analysis of multilayered dielectric waveguides with Bragg gratings,” *Electronics Letters*, vol. 29, p. 1962, October 1993.

[39]. R. Pregla and E. Ahlers, “Method of lines for analysis of discontinuities in optical waveguides,” *Electronics Letters*, vol. 29, p. 1845, October 1993.

[40]. W. D. Yang and R. Pregla, “The method of lines for analysis of integrated optical waveguide structures with arbitrary curved interfaces," *Journal of Lightwave Technology,* vol. 14, pp. 879-884, May 1996.

[41]. F. H. Al-Harbi, “Implementation of a full vectorial method of lines analysis in the study of metal clad rib waveguide," *Master's thesis, King Fahd Univeristy of Petroleum and Minerals, Saudi Arabia,* December 2000

[42]. S. J. Al-Badar and H. A. Jamid., “Method of lines applied to non-linear guided waves.” *Electronic letters,* 31(17):79-85, February 1995.

[43]. M. J. Al-Majid, “Method of lines analysis for Gaussian beam coupling of the dielectric slab waveguide,” *Master’s thesis, King Fahd University of Petroleum and Minerals, Saudi Arabia*, Feb. 1994.

[44]. A. Shittu, S. Al-Bader, and H. Jamid, "Mode Reflectivity of Finitely-Periodic Dielectric Waveguides," *Optics Communications*, vol. 114, pp. 242-246, September 1994.

[45]. F. J. Schmuckle and R. Pregla, "The method of lines for the analysis of lossy planar waveguides," *Microwave Theory and Techniques*, vol. 38, pp. 1473 - 1479, Oct. 1990.

[46]. H. Diestel and S. Worm, “Analysis of hybrid field problems by the method of lines with nonequidistant discretization”, *IEEE Trans. Microwave Theory Tech*., vol. MTT-32, no. 6, pp. 633-638, 1984.

[47]. S. J. Al-Badar and H. A. Jamid, “Perfectly matched layer absorbing boundary conditions for the method of lines modeling scheme,” *IEEE Microwave and Guided Wave Letters,* 8(11):357-359, Nov 1998.

[48]. H. A. Jamid, “Frecuency-Domain PML layer based on the complex mapping of space boundary condition treatment,” *IEEE Microwave and Guided Wave Letters,* 10:356-358, Sep. 2000.

[49]. T. de Hoop, P. M. van den Berg, and R. F. Remis, "Absorbing boundary conditions and perfectly matched layers - an analytic time-domain performance analysis," *Magnetics, IEEE Transactions on*, vol. 38, pp. 657-660, 2002.

[50]. Q.-H. Liu and W. C. Chew, "Analysis of discontinuities in planar dielectric waveguides: An eigenmode propagation method", *IEEE Transactions on Microwave Theory and Techniques*, vol. 39, pp. 422-430, Mar. 1991.

[51]. W. D. Yang and R. Pregla, "Method of lines for analysis of waveguide structures with multi-discontinuities", *Electronics Letters*, vol. 31, p. 892, May 1995.

[52]. R. Pregla and W. Yang, "Method of lines for analysis of multilayered dielectric wavegides with bragg gratings", *Electronics Letters*, vol. 29, p. 1962, October 1993.

[53]. M.N. Akram, "Analysis of anti-resonant reflecting optical waveguide (ARROW) grating using the method of lines," Master's thesis, King Fahd University of Petroleum and Minerals, Saudi Arabia, April 2000.

[54]. Y. P. Chiou and H. C. Chang, "Analysis of Optical Waveguide Discontinuities Using the Pade Approximants," *IEEE Photonics Technology Letters*, vol. 9,pp. 964–966, July 1997.

[55]. H. A. Jamid and M. N. Akram, "Analysis of Deep Waveguide Gratings: An efficient Cascading and Doubling Algorithm in the Method of Lines Framework," *Journal of Lightwave Technology*, vol. 20, pp. 1204-1208, July 2002.

[56]. Alexander M. Kenis, Ilya Vorobeichik, Meir Orenstein, and Nimrod Moiseyev, "Non-Evanescent Adiabatic Directional Coupler," *IEEE Journal of Quantum Electronics,* Vol. 37, No. 10, Oct. 2001

[57]. R. Syms and J. Cozens, “Optical Guided Waves and Devices.” Shopenhangers Road, Maidenhead, Bershire, SL6 2QL, England,: McGraw-Hill Book Company Europ, 1992.

[58]. Charles K. Kao, “Optical Fiber Systems: Technology, Design and Applications,” McGraw-Hill, 1982

[59]. M.F. Bracey et al. “Surface-Wave Research in Sheffield” *IRE TRANSACTIONS ON ANTENNAS AND PROPAGATION, AP-7,S219,1959*

[60]. R. Syms, J. Cozens, “Coupled mode devices,” in *Optical Guided Waves and Devices*, (McGraw-Hill International Ltd., 1992), pp. 1-31.

VITAE

Mohammad Sameer

- Born on 1st July'1983 in Kurnool, A.P., India.
- Feb,2006-Jan,2008 M.S. in Electrical Engineering with specialization in Communications at King Fahd University of Petroleum and Minerals, Dhahran, KSA.
    - Full Fee Waiver.
    - Held Research Assistantship during the period of study.
    - GPA 3.6/4.0.
- 2004-2006 Lecturer at G. Pulla Reddy Engineering College, Kurnool, India.
- 2000-2004 B.E. Electronics and Communications Engineering at Jawaharlal Nehru Technological University, Hyderabad, India.
    - First Division with Distinction.